博士論文

Vortex structures created by the Casimir invariants of plasma dynamics

(プラズマの力学におけるカシミール不変量によって生成される渦構造)

江本 伸悟

Table of Contents

List of Figures

Chapter 1

Introduction

1.1 A vortex and its identity

Our world is filled with vortices such as galaxies, typhoons, ocean vortices, and so on. Also, in a plasma, we observe a wide variety of vortices such as a circulating, helical, spiral, or shearing mode of magnetic and flow fields. A vortex is a strange being in that it seems to be a "phenomenon" as well as a "matter". It is primarily a pattern, or a mode, of the motion of something, and therefore, it is a kind of phenomena rather than a matter. However, once it makes its appearance, it often keeps its identity for a long time, and thereby, we sometimes regard the vortex as a matter. In fact, we often gives a name to a vortex (for example, a typhoon is given a name like Katrina).

If a vortex is a matter holding its identity, how can we capture its essential identity? The most common way to capture the identity of some object is decomposing it into its elements, as the atomic theory does so. However, we can not apply this method to a vortex because if it is decomposed, it loses its identity. For example, the identity of a galaxy does not exist in stars, which constitute the galaxy. We have to find an identity of a vortex in its motion and dynamics rather than in its elements or static structure. To deal with this problem from the viewpoint of physics, above all, it is important to consider how we "measure" a vortex and what is "invariant" in a vortex dynamics.

The curl operator [1] is an operator by which we can "measure" vorticity. Thence, a *Beltrami vortex*, an eigenfunction of the curl operator, may be the simplest and most important vortex, by which we can represent and understand the essential characteristics of vortex phenomena. For example, in the single-fluid magnetohydrodynamics (MHD), the energy of the system tends to condensate into a single Beltrami magnetic field and, as a result, there emerges a self-organized, force-free equilibrium — the well-known Taylor relaxed state satisfying $\nabla \times \boldsymbol{B} = \lambda \boldsymbol{B}$[2–4]. In the two-fluid MHD (or Hall MHD), a pair of Beltrami fields[5, 6] (called double-Beltrami fields) is also available to describe a wilder class of equilibria or phenomena, such as coronal structures[7–10], circular polarized Alfvén wave[11, 12], and so on.

Although the interest of physics is lying in motions of things or changes occurring in the world, we often put a focus on "invariants" in motions or changes in order to investigate them. Paradoxically, the identity of the motion is lying in invariants during the motion (*constant of motion*). A non-canonical hamiltonian mechanics[13] gives us a good framework to consider the identity of vortex in terms of its invariants. In this framework, a *Casimir element*, which conserves as a constant of motion, gives a structure to the phase space where the motion of the vortex is described. In other word, the vortex is structured and characterized by Casimir elements.

This introduction is organized as follows: First, in Sec.1.2, we will review a non-canonical Hamiltonian mechanics and prepare the notion of Casimir. Then, in Sec.1.3, we will see how a Beltrami vortex, eigenfunction of the curl operator, is characterized by regular Casimir elements, such as the helicity. Next, in Sec.1.4,

it will be noted that not all equilibrium points, representing long-run vortices, are characterized by Casimir elements. We will introduce the notion of *singular Casimir element* in order to extend the scope of analysis using Casimir elements. Last, in Sec.1.5, we will review the *tearing mode*[14], a typical magnetic vortex observed in many situations. Although the tearing mode can not be characterized only by regular Casimir elements, it can be by invoking a singular Casimir element[15]. Therefore, it is a good example by which we can consider the question — how can we characterize the vortex by Casimir elements? Sec.1.6 is devoted to describing purposes and the outline of the present thesis.

1.2 Non-canonical Hamiltonian mechanics

1.2.1 Hamiltonian equation

We start from a canonical, finite-dimensional Hamiltonian mechanics. The evolution equation is given by

$$\frac{d}{dt}z = J\partial_z H(z), \quad J = \begin{pmatrix} 0 & I \\ -I & 0 \end{pmatrix}, \tag{1.1}$$

where z is a state vector belonging to a phase space $X \in \mathbb{R}^{2m}$, and $H(z)$ is a Hamiltonian (a real function on the phase space X). Obviously, Ker$J = 0$. The poisson bracket, defined by J as $\{F, G\} = (\partial_{z_i} F) J_{ij} (\partial_{z_j} G)$, satisfies the antisymmetry condition

$$\{F, G\} + \{G, F\} = 0, \tag{1.2}$$

and the Jacobi identity

$$\{F, \{G, H\}\} + \{G, \{H, F\}\} + \{H, \{F, G\}\} = 0. \tag{1.3}$$

To consider the non-canonical, infinite-dimensional Hamiltonian mechanics, by which we describe plasma dynamics, we have to generalize the above system in

two directions. First, we generalize the symplectic matrix J to a Poisson operator $\mathcal{J}(z)$ that is a function of the state vector z (or u in the infinite-dimensional case as described below) while its Poisson operator still satisfies the antisymmetric condition (1.2) and the Jacobi identity(1.3). The non-canonical Hamiltonian mechanics allows $\mathcal{J}(z)$ to have non-trivial kernel elements, that is, Ker$\mathcal{J}(z) \neq 0$. Second, we expand the phase space to be an infinite-dimensional function space.

Based on what we mentioned above, we consider an evolution equation

$$\partial_t u = \mathcal{J}(u)\partial_u \mathcal{H}(u), \tag{1.4}$$

where u is a state vector (a member of some Hilbert space X; we denote by $\langle a, b\rangle$ the inner product of X), $\mathcal{H}(u)$ is a Hamiltonian (a real functional on X), and ∂_u is the gradient in X (the functional derivative). The gradient ∂_u is often denoted by $\delta/\delta u$, leaving the exact definition somewhat obscure, but, here, we invoke a rigorously extended definition based on the Clarke gradient [16, 17]. $\mathcal{J}(u)$ denotes a Poisson operator, a linear antisymmetric operator in X that generally depends on u. The corresponding Poisson bracket is given by

$$\{F, G\} = \langle \partial_u F, \mathcal{J}(u)\partial_u G\rangle. \tag{1.5}$$

The Poisson operator $\mathcal{J}(u)$ must be defined so that its Poisson bracket satisfies the antisymmetry condition (1.2) and Jacobi identity (1.3). By using the Poisson bracket, we can describe a time evolution of some functional $\mathcal{F}(u)$ as

$$\frac{d}{dt}F(u) = \langle \partial_u F(u), du/dt\rangle = \langle \partial_u F(u), \mathcal{J}(u)\partial_u \mathcal{H}(u)\rangle = \{F, \mathcal{H}\}. \tag{1.6}$$

Obviously, the Hamiltonian $\mathcal{H}(u)$ is the constant of motion of the system (1.4).

1.2.2 Equilibrium, energy-Casimir functional, and Casimir leaf

In the introduction, we asked the question of what characterizes a vortex as a "matter". In the Hamiltonian framework, a long-existing vortex may be represented as an equilibrium point u_0 of the evolution equation (1.4). Therefore, we consider here what it is that characterizes the equilibrium points in the Hamiltonian framework.

The equilibrium point is a point that satisfies the following equilibrium equation

$$\partial_t u_0 = \mathcal{J}(u_0)\partial_u \mathcal{H}(u_0) = 0. \tag{1.7}$$

In the case of canonical Hamiltonian mechanics, its Poisson operator does not have non-trivial kernel element ($\mathrm{Ker}\mathcal{J}(u_0) = 0$), therefore, equilibria emerge only from extremums of the Hamiltonian $\partial_u \mathcal{H}(u_0) = 0$. In other words, all equilibrium points are characterized only by the structure of Hamiltonian. On the other hand, in the non-canonical case, there also exist equilibria that emerge from the nullspace of the Poisson operator ($\mathrm{Ker}\mathcal{J}(u_0) \neq 0$). Even if $\mathcal{H}(u_0) \neq 0$, the total $\mathcal{J}(u_0)\partial_u \mathcal{H}(u_0)$ can become zero. We may characterize this kind of equilibria by Casimir elements, constants of motion stemming from the Kernel of Poisson operator.

First of all, let us see the definition of Casimir element $C(u)$ (a functional $X \to \mathbb{R}$). It is defined as a nontrivial solution to

$$\mathcal{J}(u)\partial_u C(u) = 0. \tag{1.8}$$

Casimir elements conserve for any Hamiltonian $\mathcal{H}'$, which can be easily verified by the following calculation:

$$\frac{d}{dt}C(u) = \langle \partial_u C(u), \mathcal{J}(u)\partial_u \mathcal{H}'(u)\rangle = -\langle \mathcal{J}(u)\partial_u C(u), \partial_u \mathcal{H}'(u)\rangle = 0, \tag{1.9}$$

where the second equation follows from the antisymmetry of the Poisson operator and the last equation Eq.(1.8). Namely, Casimir elements are constants of motion that depend only on the structure of Poisson operator and are independent from the detail structure of Hamiltonian.

Using a Casimir element $C(u)$, we can transform the Hamiltonian $\mathcal{H}(u)$ to an *energy-Casimir functional*

$$\mathcal{H}_\mu(u) := \mathcal{H}(u) - \mu C(u), \tag{1.10}$$

and rewrite the evolution equation (1.4) as

$$\partial_t u = \mathcal{J}(u)\partial_u \left\{\mathcal{H}(u) - \mu C(u)\right\} = \mathcal{J}(u)\partial_u \mathcal{H}_\mu(u), \tag{1.11}$$

without changing the dynamics (since $\mathcal{J}(u)\partial_u C(u) = 0$). In this expression, we can find a richer set of equilibrium points u_μ given by

$$\partial_u \mathcal{H}_\mu(u_\mu) = 0. \tag{1.12}$$

The parameter μ, which may be regarded as an eigenvalue, is determined by matching $C(u)$ of the solution with some given value c.

In the geometric view, the solution u_μ obtained as described above is an equilibrium point on a *Casimir leaf* $C(u) = c$. As we have already mentioned, a Casimir elements $C(u)$ is a constant of motion, and therefore, the motion $\partial_t u$ is restricted onto a level set of the Casimir element $C(u) = \text{const}$. To be more precise, the gradient of a Casimir element belongs to the kernel of the Poisson operator, i.e. $\partial_u C(u) \in \text{Coker}\mathcal{J}(u)$, which can be easily confirmed as

$$0 = \langle \mathcal{J}(u)\partial_u C(u), v\rangle = -\langle \partial_u C(u), \mathcal{J}(u)v\rangle \quad \text{for all } v \in X. \tag{1.13}$$

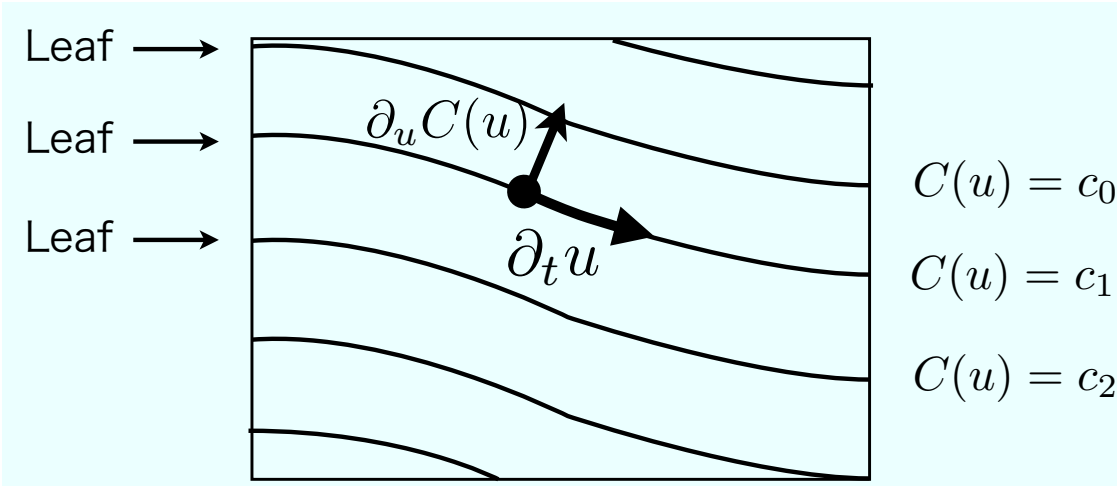

Figure 1.1: Foliation of the phase space.

As a result, the phase space X is foliated by Casimir leaves. Fig.1.1 depicts the Casimir foliation of the phase space X.

In this subsection, we have introduced the notion of a Casimir and have seen how it characterizes equilibrium points of (1.4). However, we have to note that not all equilibrium points are characterized by some Casimir. We will deal with this issue in more detail in Sec.1.4.

1.2.3 Simplest example of Non-canonical Hamiltonian mechanics

We end this section by giving the simplest example of a non-canonical Hamiltonian mechanics with a Hamiltonian

$$H(z_1, z_2, z_3) = \frac{1}{2}(z_1^2 + z_2^2 + z_3^2), \tag{1.14}$$

and a Poisson operator

$$J = \begin{pmatrix} 0 & 1 & 0 \\ -1 & 0 & 0 \\ 0 & 0 & 0 \end{pmatrix}. \tag{1.15}$$

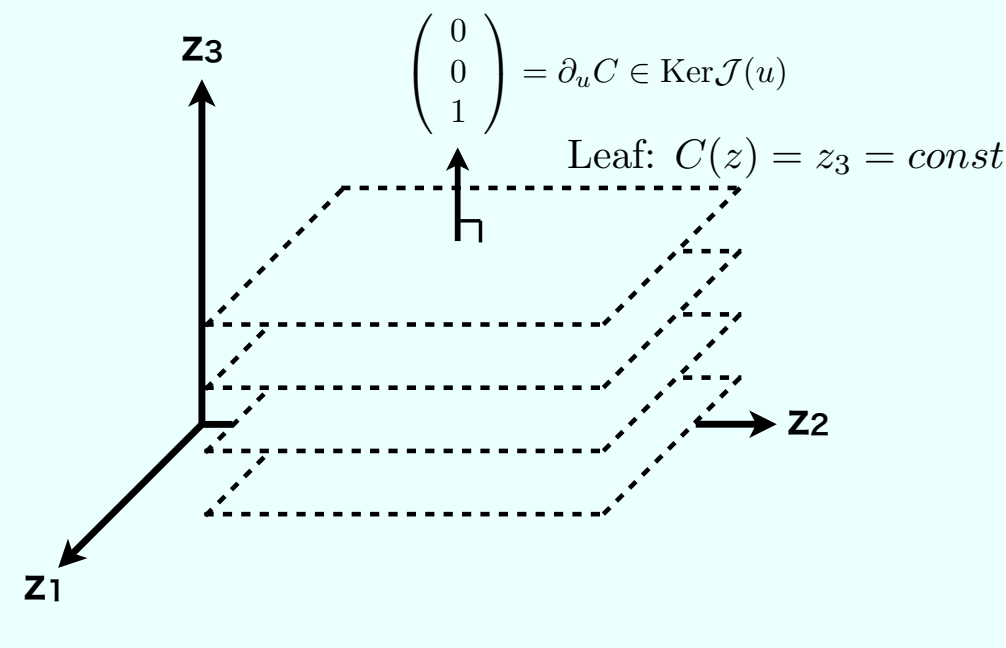

Figure 1.2: The simplest example of a Casimir foliation.

The state variable is $\boldsymbol{z} = {}^t(z_1, z_2, z_3)$. Obviously, ${}^t(0, 0, 1)$ is an element of Ker$J$. By 'integrating' it with respect to the state variable, we obtain a Casimir element $C(\boldsymbol{z}) = z_3$, by which we can construct an energy-Casimir functional

$$H_\mu := \frac{1}{2}(z_1^2 + z_2^2 + z_3^2) - \mu z_3. \tag{1.16}$$

From the extremum of H_μ, we obtain a non-trivial equilibrium point $\boldsymbol{z}_0 = {}^t(0, 0, \mu)$. Fig.1.2 shows the foliation given by the level sets of the Casimir $C(\boldsymbol{z})$.

1.3 Beltrami vortex

In this section, we will review a Beltrami vortex, an eigenfunction of the curl operator[1]. First, we will introduce the non-canonical Hamiltonian formism of the magnetohydrodynamics (MHD), which gives a single-fluid description of the

plasma. Then, we will see that a Beltrami vortex is obtained as an equilibrium point characterized by the helicity, one of the Casimir elements of MHD.

1.3.1 Magnetohydrodynamics

Here, we consider the Hamiltonian formalism of an ideal MHD plasma, which is described by the following equations:

$$\partial_t n = -\nabla \cdot (\boldsymbol{V} n), \tag{1.17}$$

$$\partial_t \boldsymbol{V} = \boldsymbol{V} \times (\nabla \times \boldsymbol{V}) + n^{-1}(\nabla \times \boldsymbol{B}) \times \boldsymbol{B} - \nabla(h + V^2/2), \tag{1.18}$$

$$\partial_t \boldsymbol{B} = \nabla \times (\boldsymbol{V} \times \boldsymbol{B}), \tag{1.19}$$

where n is the density, $\boldsymbol{V}$ is the fluid velocity, $\boldsymbol{B}$ is the magnetic field, and h is the molar enthalpy. The variables are normalized in the standard Alfvén units.

Let us define the state vector $u = {}^t(n, \boldsymbol{V}, \boldsymbol{B})$, a Hamiltonian functional

$$\mathcal{H}(u) = \int_\Omega \left\{ n(\frac{V^2}{2} + \varepsilon(n)) + \frac{B^2}{2} \right\} d\boldsymbol{x}, \quad \partial_u \mathcal{H}(u) = \begin{pmatrix} h + V^2/2 \\ n\boldsymbol{V} \\ \boldsymbol{B} \end{pmatrix}, \tag{1.20}$$

and a Poisson operator

$$\mathcal{J}(u) = \begin{pmatrix} 0 & -\nabla\cdot & 0 \\ -\nabla & n^{-1}(\nabla \times \boldsymbol{V})\times & n^{-1}(\nabla \times \circ) \times \boldsymbol{B} \\ 0 & \nabla \times (\circ \times n^{-1}\boldsymbol{B}) & 0 \end{pmatrix}, \tag{1.21}$$

with which the MHD equations are concisely rewritten in the Hamiltonian form (1.4). $\varepsilon(n)$ in (1.20) is the thermal energy density, which is related to the molar enthalpy by $h(n) = \partial(n\varepsilon(n))/\partial n$.

The Poisson operator (1.21) has three representative Casimir elements:

$$C_1(u) = \int_\Omega \boldsymbol{A} \cdot \boldsymbol{B} d\boldsymbol{x}, \quad \partial_u C_1(u) = \begin{pmatrix} 0 \\ 0 \\ \boldsymbol{A} \end{pmatrix}, \tag{1.22}$$

$$C_2(u) = \int_\Omega \boldsymbol{V} \cdot \boldsymbol{B} d\boldsymbol{x}, \quad \partial_u C_2(u) = \begin{pmatrix} 0 \\ \boldsymbol{B} \\ \boldsymbol{V} \end{pmatrix}, \tag{1.23}$$

$$C_3(u) = \int_\Omega n d\boldsymbol{x}, \quad \partial_u C_3(u) = \begin{pmatrix} 1 \\ 0 \\ 0 \end{pmatrix}, \tag{1.24}$$

which, respectively, represent the magnetic helicity, the cross helicity, and the total particle number.

Note 1. In the presence of magnetic surfaces, we can find 'local Casimir elements' that represents the conservation of surface quantities. Hameiri [18] found the complete set of flux-surface Casimir elements of the MHD plasma with nested magnetic surfaces. Kawazura and Hameiri [19] found that of the Hall MHD plasma. The three Casimir elements (1.22)-(1.24) are invariants that do not require magnetic surfaces and are, therefore, the most robust.

1.3.2 Helicity and Beltrami vortex

Let us consider an equilibrium point characterized by the above three Casimir elements (1.22)-(1.24), i.e. the solution of

$$\partial_u \left(\mathcal{H}(u) - \sum_{i=1}^{3} \mu_i C_i(u) \right) = 0, \tag{1.25}$$

which reads as

$$V^2/2 + h - \mu_3 = 0, \tag{1.26}$$

$$n\boldsymbol{V} - \mu_2 \boldsymbol{B} = 0, \tag{1.27}$$

$$\nabla \times \boldsymbol{B} - \mu_1 \boldsymbol{B} - \mu_2 \nabla \times \boldsymbol{V} = 0, \tag{1.28}$$

in deriving (1.28), we have applied the curl operator. For the sake of simplicity, let us consider a subclass of solutions with $n = 1$. Combining (1.27) and (1.28),

we obtain

$$(1-\mu_2^2)\nabla\times\boldsymbol{B}-\mu_1\boldsymbol{B}=0. \tag{1.29}$$

For $\mu_2\neq\pm1$, by denoting $\mu:=\mu_1/(1-\mu_2^2)$, we can rewrite the above equation as

$$(\mathrm{curl}-\mu)\boldsymbol{B}=0, \tag{1.30}$$

which is nothing but the eigenvalue problem of the curl operator[1]. We call (1.30) as the Beltrami equation (or the single-Beltrami equation when we distinguish it from the double-Beltrami equation). Solving this equation, we obtain the Beltrami vortex, which is characterized by the magnetic helicity C_1 and the cross helicity C_2 through the eigenvalue $\mu=\mu_1/(1-\mu_2^2)$.

Note 2. For $\mu_2=\pm1$, an interesting situation occurs[11]. In this case, $\boldsymbol{B}$ can be arbitrary and $\boldsymbol{V}=\pm\boldsymbol{B}$ (because $\mu_1=0$). By applying the Galilean boost, we can transform this class of stationary solutions to Alfvén waves. Namely, the Alfvén wave turns out to be the Galilean-boosted Beltrami vortex at the singularity ($\mu_2=\pm1$) of the equilibrium equation (1.29).

In Chap.2, we will consider a two-fluid MHD system [19, 20]. In a two-fluid MHD plasma, the canonical helicity conserves as a Casimir element instead of the cross helicity (1.23), and, as a counterpart of the single-Beltrami equation (1.30), we have the double-Beltrami equation

$$(\mathrm{curl}-\mu_1)(\mathrm{curl}-\mu_2)\boldsymbol{B}=0, \tag{1.31}$$

where μ_1 and μ_2 are parameters associated with the magnetic and canonical helicities. A general solution of (1.31) is given by a linear superposition of two Beltrami vortices.

Note 3. In the case of the two-fluid MHD as well, we can obtain the Alfvén wave as the Galilean-boosted Beltrami vortex. An integrable structure in the nonlinear modulation of the Alfvén wave was found in [11] and analyzed in [12].

1.4 Singular Casimir

1.4.1 Singularity and Singular Casimir

In the above sections, we have seen how Casimir elements characterize the equilibrium points of the non-canonical Hamiltonian dynamics. However, as we have already noted, generally there are not enough Casimir elements to characterize all equilibrium points[13]. Namely, an equilibrium point, satisfying (1.7), is not always characterized as an extremum of some energy-Casimir functional.

One reason of this discrepancy lies in the difficulty of constructing a Casimir element by solving (1.8). We may solve (1.8) by two steps. First, we find the kernel of $\mathcal{J}(u)$, i.e., find $v(u)$ such that $\mathcal{J}(u)v(u) = 0$. Then, we 'integrate' $v(u)$ with respect to u to find a functional $C(u)$ such that $v(u) = \partial_u C(u)$. However, this may not always possible. In Subsec.1.2.3, we gave the simplest example of non-canonical Hamilton mechanics. There, we 'integrated' the kernel element ${}^t(0, 0, 1)$ by solving the three-dimensional partial differential equation $\partial_z C(z) = {}^t(0, 0, 1)$. In the case of an infinite-dimensional system, this 'integration', or the total process of obtaining a Casimir element, means solving an infinite-dimensional partial differential equation.

If there is a 'singularity' where the rank of $\mathrm{Ker}\mathcal{J}(u)$ changes, the problem becomes more interesting. In this case, we may obtain singular Casimir elements from the singularity. Let us see the finite-dimensional example of singularity and singular Casimir, given in [17]. We consider a one-dimensional system $X = \mathbb{R}$ with

a Poisson operator $J = ix$ ($x \in \mathbb{R}$). $x = 0$ is a singularity where Rank$J(x)$ drops to 0 from 1, and this point is a singular point of the differential equation $J(x)\partial_x C(x) = 0$. If there were no singularity, $J(x)\partial_x C(x) = 0$ would have only a trivial solution $C(x) = \text{const}$. However, in the presence of singularity, by 'integrating' the kernel element $\delta(x) \in \text{Ker}J(x)$ ($\delta(x)$ is the delta function), we can obtain a non-trivial solution $C(x) = Y(x)$, where $Y(x)$ is the Heaviside step function.

The important points are that, if the Poisson operator $\mathcal{J}(u)$ has singularities, we have to involve singular solutions such as $\delta(x)$, and that we will need to generalize the notion of functional derivative for singular Casimir elements, as we did when we obtained the singular Casimir $C(x) = Y(x)$ from $\delta(x)$. In [17], the above-mentioned problem of the nonequivalence of the sets of equilibrium points and energy-Casimir extremal points is addressed in the context of the Euler equation, and singular Casimir elements stemming from the singularity are unearthed using a generalization of the functional derivative (the gradient ∂_u of an infinite-dimensional system). With singular Casimir elements, we can characterize the wilder class of equilibrium points. In [15, 21], the tearing mode (see Sec.1.5) is characterized by a linear, singular Casimir (called *helical-flux*) stemming from the resonance singularity of the Poisson operator.

Fig.1.3 shows a 2-dimensional cartoon of Casimir foliations of regular(left) and singular(right) Casimir elements (this cartoon is drawn by reference to Fig.1. in [17]). Outside of the singularity, Rank$\mathcal{J}(u)$ is constant, but, at the singularity, Rank$\mathcal{J}(u)$ changes, resulting in a singular Casimir leaf.

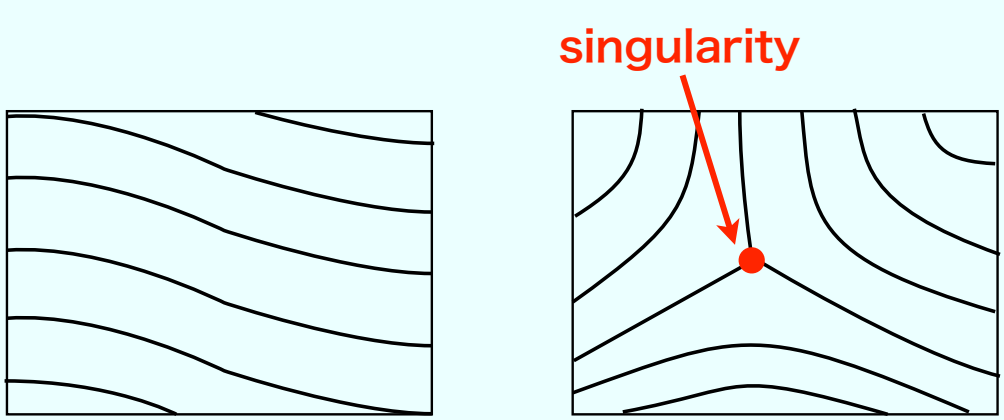

Figure 1.3: Two-dimensional cartoon of Casimir foliations of regular and singular Casimir elements.

1.4.2 Plateau singularity in Vortex equation

Here, let us review the *plateau singularity* of the two-dimensional vorticity equation[17]:

$$\partial_t \omega = [\omega, \phi], \tag{1.32}$$

where ϕ is the stream function, $\omega := -\Delta\phi$ is the z-component of the vorticity, and

$$[a, b] := -\nabla a \times \nabla b \cdot \nabla z \tag{1.33}$$

is the standard Poison bracket. Let the vorticity ω be a state variable. Then, the above vorticity equation can be put into the non-canonical Hamiltonian form

$$\partial_t \omega = \mathcal{J}(\omega)\partial_\omega \mathcal{H}(\omega), \tag{1.34}$$

with a Hamiltonian functional

$$\mathcal{H}(\omega) = \frac{1}{2}\int_\Omega \phi\omega d\boldsymbol{x} \quad , \tag{1.35}$$

and a Poisson operator

$$\mathcal{J}(\omega)\varphi = [\omega, \varphi]. \tag{1.36}$$

Remark 1.4.1. Although here we have naively defined the vorticity equation, it should actually be defined more carefully by using the theories of functional analysis and weak solution, see [17].

First of all, let us consider the regular Casimir elements of the Poisson operator $\mathcal{J}(\omega)$. In order for φ to be a member of $\mathrm{Ker}\mathcal{J}(\omega)$, it must satisfy the condition

$$\nabla\omega \times \nabla\varphi \cdot \nabla z = 0, \tag{1.37}$$

which implies that two vectors $\nabla\omega$ and $\nabla\varphi$ must align almost every where in the region Ω. By invoking a certain scalar $\zeta : \mathbb{R}^2 \to \mathbb{R}$ and certain Lipschitz continuous functions $f, g : \mathbb{R} \to \mathbb{R}$, the above condition may be represented as

$$\omega(\boldsymbol{x}) = f(\zeta(\boldsymbol{x})), \quad \varphi(\boldsymbol{x}) = g(\zeta(\boldsymbol{x})). \tag{1.38}$$

Let us consider the simplest case of $f =$ identity, that is,

$$\varphi(\boldsymbol{x}) = g(\omega(\boldsymbol{x})), \tag{1.39}$$

which can be 'integrated' as

$$C_G(\omega) = \int_\Omega G(\omega(\boldsymbol{x}))d\boldsymbol{x}, \tag{1.40}$$

where $G : \mathbb{R} \to \mathbb{R}$ is the indefinite integral of g, that is, $dG/d\zeta = g$.

Next, let us consider the case that ω has a 'plateau' $\Omega_0 \subseteq \Omega$ where $\omega(\boldsymbol{x}) = \omega_0$ (constant). In such a plateau region, the Poisson operator $\mathcal{J}(\omega)$ trivializes as $\mathcal{J}(\omega) = [\omega_0, \circ] = 0$. Therefore, within Ω_0, $\varphi(\boldsymbol{x})$ can take an arbitrary value. Note that the representation (1.39) restricts $\varphi(\boldsymbol{x})$ to $g(\omega_0)$ in Ω_0 and omits this type of solution. To remove this degeneracy, we allow the function $g(\zeta)$ to have a jump at

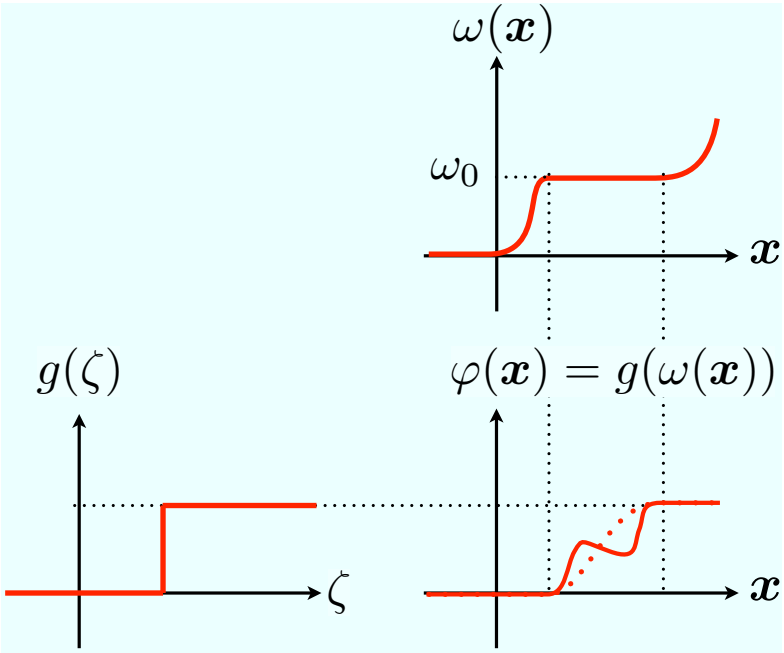

Figure 1.4: The vorticity $\omega(\boldsymbol{x})$ with a plateau, the simplest example of $g(\zeta)$, and the resultant $\varphi(\boldsymbol{x})$.

$\zeta = \omega_0$. Formally, we write

$$g(\zeta) = g_L(\zeta) + \alpha Y(\zeta - \omega_0), \tag{1.41}$$

where g_L is a Lipschitz continuous function, $Y(\zeta - \omega_0)$ is the 'filled' step function, and α is a constant representing the width of the jump. The term "filled" means that the step function $Y(\zeta - \omega_0)$ is multi-valued at $\zeta = \omega_0$ and can take an arbitrary value in the range of $[0, \alpha]$. Fig.1.4 shows the vorticity ω with a plateau, the simplest example of $g(\zeta) = Y(\zeta - \omega_0)$, and the resultant $\varphi(\boldsymbol{x}) = g(\omega(\boldsymbol{x})) = Y(\omega(\boldsymbol{x}))$. In the plateau region Ω_0, φ can take an arbitrary form. This arbitrary property is represented by the filled (multi-valued) step function.

In [17], the Clarke gradient[16] is invoked to 'integrate' the singular kernel element (1.41). The Clarke gradient is a generalized gradient for Lipschitz contin-

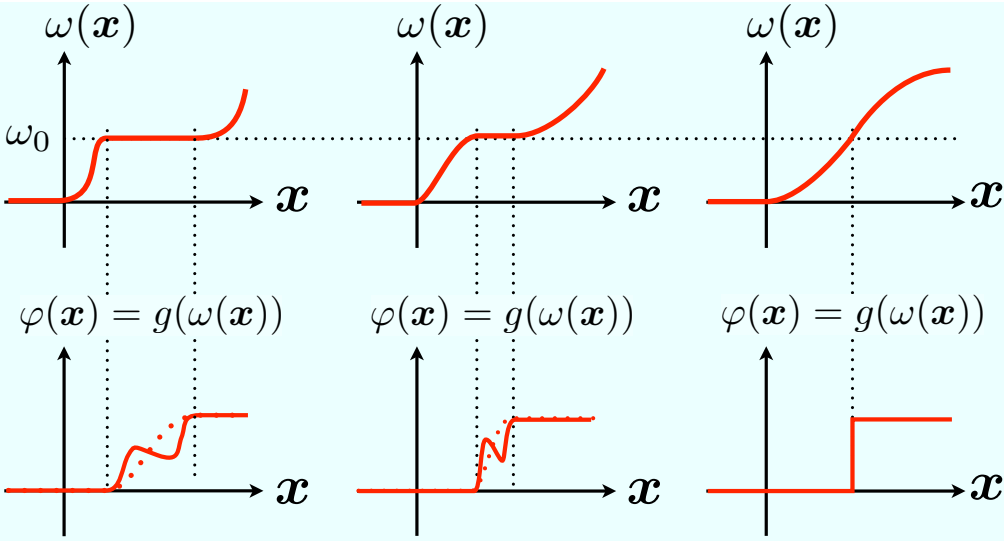

Figure 1.5: Singular $\varphi(\omega(\boldsymbol{x}))$ that emerges when the plateau of ω shrinks and disappears.

uous functions (or functionals). Specifically, for $F : \mathbb{R} \to \mathbb{R}$, the Clarke gradient of F at x (we denote it by $\tilde{\partial}_x F(x)$ is defined to be the convex full of the set of limit points of the form

$$\lim_{j\to\infty} \partial_x F(x + \delta_j) \quad \text{with} \quad \lim_{j\to\infty} \delta_j = 0. \tag{1.42}$$

Evidently, if $F(x)$ is continuously differentiable in the neighborhood of x, $\tilde{\partial}_x F(x)$ is equivalent to the classical gradient. On the other hand, if $F(x)$ kinks at x (the left and right derivatives differ from each other), $\tilde{\partial}_x F(x)$ becomes multi-valued. Using the Clarke gradient, we define $G(\zeta)$ such that

$$\tilde{\partial}_\zeta G(\zeta) = g(\zeta) = g_L(\zeta) + \alpha Y(\zeta - \omega_0). \tag{1.43}$$

Then, we obtain a singular Casimir element

$$C_G(\omega) = \int_\Omega G(\omega(\boldsymbol{x}))d\boldsymbol{x}, \tag{1.44}$$

which gives a multi-valued gradient $\tilde{\partial}_\omega C_G = g(\omega(\boldsymbol{x})) \in \mathrm{Ker}\mathcal{J}(\omega)$.

As we have seen, when ω has a plateau, the degree of freedom of the kernel element $\varphi = g(\omega)$ increases infinitely. This means that ω with plateaus is a singularity where the rank of $\mathrm{Ker}\mathcal{J}(\omega)$ changes. At a singularity, there is an increased number of directions to which the motion $\partial_t\omega$ can not proceed. This increase is represented by the multi-valued gradient defined by using the Clarke gradient.

Remark 1.4.2. Although $g(\zeta)$ defined above is not a continuous function, the resultant, composed function $g(\omega(\boldsymbol{x})) : \mathbb{R}^2 \to \mathbb{R}$ is continuous on the plateau region. We have to carefully distinguish these $g(\zeta)$ and $g(\omega(\boldsymbol{x})$. The interesting situation occurs when the plateau of ω shrinks and disappears. In this case, the resultant $\varphi(\omega(\boldsymbol{x}))$ takes the form of step function, as shown in 1.5. Such a singular $\varphi(\boldsymbol{x}))$ is still a "hyperfunction solution" of (1.37), see [17] (Remark 3.3) and Appendix A.

1.5 Tearing mode

In the previous section, we have seen the existence of equilibrium points that are characterized by singular Casimir elements, and can not only by regular Casimir elements. A physically important example of such structures is the tearing mode[15], a typical vortex structure of magnetic field that emerges in the presence of magnetic shear.

Here, we first review the conventional studies of the tearing mode: (1) what the tearing mode is and (2) how plasma flow affects the tearing mode. We should note that our motivation is different from the conventional one. While conventional studies focus their interest on "the tearing mode itself" and therefore consider specific plasma configulations, we are interested in "how we can characterize a vortex by Casimir invariants", and the tearing mode is just a good example of a

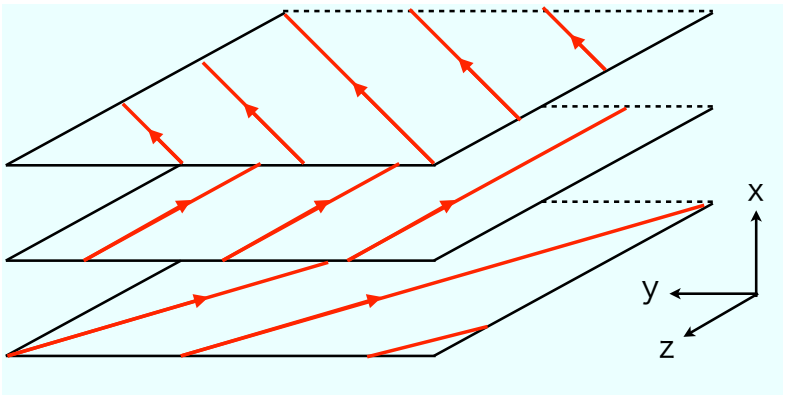

Figure 1.6: Schematic drawing of a sheared magnetic field.

general vortex observed in a plasma. With this motivation, in Subsec.1.5.3, we will see (3) how the tearing mode theory is located in the non-canonical hamiltonian theory.

1.5.1 Tearing mode and Magnetic reconnection

The term "tearing mode"[14] refers to a spontaneous reconnection process[22] that occurs in the presence of a sheared magnetic field. Fig.1.6 and Fig.1.7 show a schematic drawing of a sheared magnetic field and its projection onto $x-y$ plane, respectively. As a result of the reconnection, the tearing mode changes the topology of magnetic field as shown in Fig.1.8. It can be seen that the magnetic field, which was just sheared before the reconnection, is rotating in magnetic islands (regions surrounded by the separatrix) after the reconnection.

The magnetic reconnection often takes place in order for magnetic field to release its excess energy stored on its global structure[15, 23]. Let us consider the plasma in an equilibrium state. When some external force is applied to the plasma, the equilibrium state gradually changes to a new equilibrium state while plasma pa-

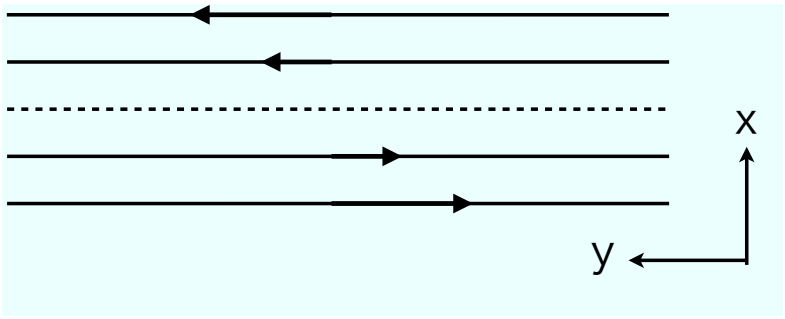

Figure 1.7: Projection of a sheared magnetic field onto $x - y$ plane.

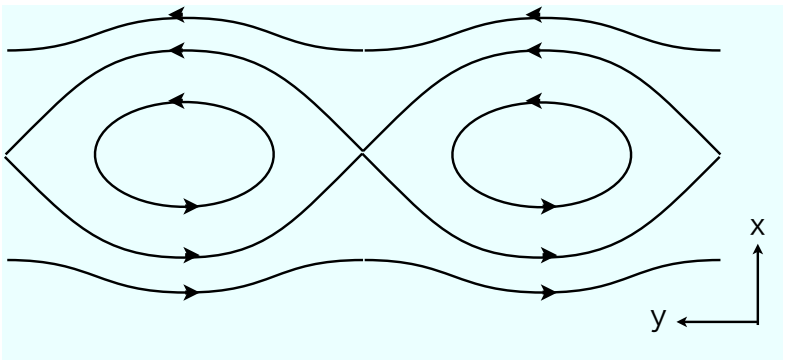

Figure 1.8: Topology of the tearing mode (reconnected magnetic field).

rameters slowly adjust. When this new state becomes unstable compared to some other stable states, the plasma may self-organize itself to a new stable equilibrium state, through forming current sheets, reconnecting the magnetic field lines, and changing the magnetic topology. Such self-organizing phenomena through the magnetic reconnection can be observed in many places like solar flares, the magnetosphere, or fusion plasmas[23].

Let us see the basic theory of the tearing mode[14, 22, 24]. The tearing mode is usually analyzed by using the resistive, incompressible MHD:

$$\partial_t \boldsymbol{\Omega} = \nabla \times (\boldsymbol{V} \times \boldsymbol{\Omega}) + \nabla \times \{(\nabla \times \boldsymbol{B}) \times \boldsymbol{B}\}\,, \tag{1.45}$$

$$\partial_t \boldsymbol{B} = \nabla \times (\boldsymbol{V} \times \boldsymbol{B}) - \nabla \times (\eta \nabla \times \boldsymbol{B}), \tag{1.46}$$

where $\boldsymbol{\Omega} := \nabla \times \boldsymbol{V}$ is the vorticity of the fluid and η is the magnetic resistivity. Eq.(1.45) is obtained from the curl of (1.18) and Eq.(1.46) is obtained by adding the resistive term $\nabla \times (\eta \nabla \times \boldsymbol{B})$ to Eq.(1.19). Let us consider the tearing mode without equilibrium flow ($\boldsymbol{V}_0 = 0$). We assume that the ambient magnetic field has the form

$$\boldsymbol{B}_0 = \nabla \psi_0(x) \times \nabla z + B_z \nabla z, \tag{1.47}$$

and perturbations of magnetic and flow fields can be written in the following form:

$$\tilde{\boldsymbol{V}} = \nabla \tilde{\phi}(x, y, t) \times \nabla z, \quad \tilde{\boldsymbol{B}} = \nabla \tilde{\psi}(x, y, t) \times \nabla z, \tag{1.48}$$

where $\tilde{\phi}$ and $\tilde{\psi}$ is the stream and magnetic flux functions. Such a class of perturbation fields is appropriate in a plasma embedded in a strong uniform external magnetic field, viz. the plasma in a fusion device like the tokamak. Substituting $\boldsymbol{V} = \tilde{\boldsymbol{V}}$ and $\boldsymbol{B} = \boldsymbol{B}_0 + \tilde{\boldsymbol{B}}$ into Eq.(1.45) and the curl^{-1} of (1.46), we obtain

$$\partial_t \tilde{\psi} = \boldsymbol{B}_0 \cdot \nabla \tilde{\phi} + \eta \Delta \tilde{\psi}, \tag{1.49}$$

$$\partial_t \tilde{\omega}_z = \boldsymbol{B}_0 \cdot \nabla \tilde{j}_z + \tilde{\boldsymbol{B}} \cdot \nabla j_{z0}, \tag{1.50}$$

where $\tilde{\omega}_z := -\Delta \tilde{\phi}$, $\tilde{j}_z := -\Delta \tilde{\psi}$, and $j_{z0} := -\Delta \psi_0$ are the z-component of the vorticity of flow perturbation, the current of magnetic field perturbation, and the current of the ambient magnetic field, respectively.

Since the magnetic resistivity η and the growth rate of the tearing mode are small (to be precise, we focus on a slowly growing mode), inertia and resistivity terms in Eqs.(1.49) and (1.50) can be neglected in most parts of the region (called the ideal region or the outer region). These terms, however, become important

in a narrow layer (called the resistive region of the inner region) around the resonance line $x = x_r$, where $\boldsymbol{B}_0(x_r) \cdot \nabla = \boldsymbol{B}_0(x_r) \cdot \boldsymbol{k} = 0$ ($\boldsymbol{k}$ is the wave number of perturbations). Thus, when one solves Eqs.(1.49) and (1.50), one starts by finding solutions separately in the ideal region, where equations are simplified, and in the resistive region, where the geometry is simplified. Then, one fabricate the entire solution by assembling solutions obtained in each region.

The magnetic perturbation solution $\tilde{\psi}$, obtained in the outer region, is continuous in the entire region but its derivative $\tilde{\psi}'$ $(= \partial_x \tilde{\psi})$ exhibits a jump characterized by the quantity Δ'

$$\Delta' := \lim_{\epsilon \downarrow 0} \left[\tilde{\psi}'(x_r + \epsilon) - \tilde{\psi}'(x_r - \epsilon) \right] / \tilde{\psi}(x_r). \tag{1.51}$$

This quantity Δ' is used when one evaluate the growth rate of the tearing mode by matching both inner and outer solutions asymptotically. Thus, Δ' is an important index for the tearing instability and gives the necessary condition for the tearing mode to grow and self-organize itself. In fact, it can be shown that the tearing mode is unstable if and only if $\Delta' > 0$, in the incompressible MHD plasma without equilibrium flow[14].

When the tearing mode grows and its island width exceeds the resistive layer width, the tearing mode enters the nonlinear regime, where the growth of the mode is drastically slowed, i.e. the exponential growth is replaced by a slower algebraic growth[25]. Finally, the mode converges to the saturated state. The time evolution of the island width (we denote it by w) is given by the following equation[26]:

$$\frac{dw}{dt} = \alpha\eta(\Delta'(w) - \beta w). \tag{1.52}$$

where α and β are positive constants. $\Delta'(w)$ is the finite-island-width generalization of the linear quantity $\Delta' = \Delta'(0)$, which is determined by the outer region solutions. It can be seen, from (1.52), that if and only if $\Delta' > 0$ the island emerges, as we have already seen. Moreover, the width of the saturated island is determined by $\Delta'(w)$, which is, therefore, important not only for the growth rate but also for the final saturated state.

The Hahm-Kulsrud-Taylor mode, developed by Hahm and Kulsrud[27] following a suggestion by J.B. Taylor, follows through the onset of the tearing instability to the formation of magnetic islands and to the final asymptotic approach to the saturated state with islands. They considered a simple plasma in a slab geometry, i.e. the plasma contained between two infinitely conducting wall at $x = \pm a$, associated with a linearly varying magnetic field $B_y = B_0 x/a$ in the y-direction and a uniform ambient magnetic field $B_z = B_0$ in the z-direction. They analytically examined the response of the plasma to the boundary deformation $x = \pm(a - \delta \cos ky)$. They found two exact MHD equilibrium solutions: the first one with a singular current sheet on the resonance surface and no islands, and the second one with magnetic islands and no current sheet. After the deformation, the plasma first approaches the current layer solution, until the layer is thin enough that reconnection occurs by the resistiviy $\eta \nabla \times \tilde{\boldsymbol{B}}$. Then, the plasma changes direction toward the second solution with islands and no singular current.

In terms of the Alfvén wave theory, the tearing mode is regarded as the mode for which the "zero-frequency resonance" occurs[24]. An important point for us is that the tearing mode is virtually obtained by solving the equilibrium equation in the outer region. In fact, a sequence of equilibrium solutions, which may contin-

uously connecting the two solutions of the Hahm-Kulsrud-Taylor model[27], have recently been found[28]. Moreover, the singular Casimir characterizing the linear tearing mode as an equilibrium have been found in [15], which will be discussed in more detail later. Before that, in the next subsection, let us see the flow effect on the tearing mode.

1.5.2 Flow effect on Tearing instability

Although we have seen the tearing mode without flow in the previous subsection, a plasma is generally accompanied by a flow. Since, in the absence of resistivity the magnetic fields is frozen into the flow, the tearing mode is greatly influenced by the flow. Therefore, there is a rich literature of flow effects on the tearing mode. There is a wide variety of viewpoint: (1) Linear theory (stability and growth rate) or Nonlinear theory (saturation and island width), (2) Flow strength; small, sub-Alfvénic, or super-Alfvénic flow, (3) Flow type; toroidal, poloidal, parallel, or antiparallel flow, (4) Geometry; slab, cylindrical, or toroidal, (5) Method; analytical, numerical, or experimental, and so on. Here, let us review how the flow affects the tearing mode.

Chen and Morrison[29] analytically investigated the linear stability of the tearing mode in a slab geometry and found that the value of the tearing instability criterion Δ', obtained from the outer region solution, is drastically changed by the flow shear at the resonance surface. From the inner region analysis, it was found that, when the flow shear is smaller than the magnetic field shear, the growth rate of the tearing mode varies intricately depending on the details of the profiles of the magnetic and flow fields. On the other hand, in the case of super-Alfvénic flow shear, the flow freezes the magnetic field and the tearing mode is

completely stabilized. Ofman et al.[30] numerically analyzed the sub-Alfvénic flow effect on the nonlinear saturation of the tearing mode. It was found that the shear flow slows down the nonlinear saturation development and reduces the saturated magnetic island width. Li and Ma[31] focused on not only the flow amplitude but also the flow thickness (shear parameter) and numerically found that the shear flow has both stabilizing and destabilizing effects depending on the flow thickness. Chandra[32] focused on the small, toroidal flow effect (in tokamaks, the observed flows are primarily toroidal) and numerically analyzed its effect. It was concluded that the flow itself has the stabilizing effect but, on the other hand, the flow shear has the destabilizing effect.

Because the magnetic field is frozen into the electron flow rather than the ion flow, the Hall effect, which distinguishes the electron flow from the ion flow, is also important for the tearing mode. The Hall effect is known to enhance the growth rate of the tearing mode[33, 34]. The viscosity also influences the tearing instability[35]. It is observed that the flow that has destabilizing effect in the low-viscosity regime can have the stabilizing effect in the high-viscosity regime[36]. Sen and Chandra[37] focused on the curvature effect. They analytically estimated the small, toroidal flow effects both in a toroidal geometry and in a cylindrical geometry and compared them. It was found that the destabilizing effect of the flow in the toroidal geometry is less than that of cylindrical case, and it was concluded that the curvature of geometry acts in the stabilizing direction. While analytical and numerical methods often predict the destabilizing effect of the small, poloidal, shear flow, experimental results suggest that flow shear at the resonance surface makes the tearing stability index Δ' more negative and has the stabilizing effect[38].

When the flow shear is larger than the magnetic field shear, the tearing mode is completely stabilized and disappears, and then, instead, the Kelvin-Helmholtz instability appears[29, 35]. Hu and Liu[39] suggested that the Kelvin-Helmholtz instability may twist the magnetic field lines and lead to the formation of the magnetic islands, which is called the *vortex-induces magnetic reconnection*. The numerical results of the incompressible plasma model[40, 41] suggested that super-Alfvénic shear flows always brings the Kelvin-Helmholtz instability. When the plasma compressibility is included, the Kelvin-Helmholtz instability may become either stable or unstable depending on the amplitude of the super-Alfvénic shear flow[42].

These literatures show that the small, sub-Alfvénic flow effects are very complicated and depending on the specific details of magnetic and flow configurations, flow amplitude, flow thicknesses, geometry, and so on. It should be noted that our interest is not in a specific behavior of the tearing mode depending on a specific situation, but in a little more universal property of the tearing mode. One important thing for us is that, in the presence of the super-Alfvénic shear flow, the tearing instability disappears and, instead, the Kelvin-Helmholtz instability appears as a dominant instability mode.

1.5.3 Singular Casimir and Linear tearing mode

As we have seen, the tearing mode itself is obtained actually as a equilibrium point of the ideal MHD. Although the detailed information about the growth rate needs the resistive layer analysis, we can use the quantity Δ', which is obtained from the outer region solution (ideal solution), as the criterion of the tearing mode instability, especially in the no-flow case. These things raise a question: Can we

characterize the tearing mode and analyze its stability by some Casimir elements? Certainly a general tearing mode shows a complicated behavior and might not be the object of the ideal, hamiltonian theory. However, the tearing mode of Beltrami fields can be analyzed in the framework of the non-canonical hamiltonian framework. The reason of this is as follows: For a perturbed Beltrami equilibrium $u = u_\mu + \tilde{u}$, where u_μ is a Beltrami equilibrium and $\tilde{u}$ is a perturbation, we can linearize Eq.(1.11) as

$$\partial_t \tilde{u} = \mathcal{J}(u_\mu)\widetilde{\partial_u \mathcal{H}_\mu(u)} + \widetilde{\mathcal{J}(u)}\partial_u \mathcal{H}_\mu(u_\mu) = \mathcal{J}(u_\mu)\widetilde{\partial_u \mathcal{H}_\mu(u)}, \tag{1.53}$$

the second equality follows from (1.12). It can be seen in the above linearized equation that the perturbation energy $\widetilde{\partial_u \mathcal{H}_\mu(u)}$ is tidily defined in terms of the energy-Casimir functional, which greatly simplifies the linear analysis.

Recently, Yoshida and Dewar[15] have formulated the bifurcation theory of the Beltrami field in the non-canonical Hamiltonian framework, with the magnetic flux as the fixed parameter and the magnetic helicity as the control parameter. In this framework, a Beltrami field may be viewed as the minimum-energy state on a certain level set of the helicity. As the helicity value increases, the energy norm on the corresponding level set surface is distorted, thereby, equilibrium points may bifurcate to produce helical relaxed states in addition to symmetric relaxed states. They revealed the relation between the helical relaxed state and the tearing mode. The linear tearing mode, which resembles the helical relaxed state, is shown to be a perturbed, singular equilibrium state characterized by a new-found Casimir element (named *helical-flux*) pertinent to a 'resonant singularity' of the linearized poisson operator $\mathcal{J}(u_\mu)$. This helical-flux Casimir gives an additional foliation on the phase space and its leaves separates the bifurcated helical and symmetric

equilibria on the same helicity leaf.

Thereby, the linear tearing mode can be viewed as an equilibrium point on the intersection of helicity and helical-flux leaves, which may exist between a helical equilibrium (a saturated tearing mode with an island) and a symmetric equilibrium (a sheared magnetic field without islands). Although, in this ideal (no-resistive) model, the tearing mode is forbidden to grow, it might do so in the presence of dissipation violating the conservation of helical-flux Casimir. The standard criterion Δ' for linear tearing instability of Beltrami equilibria is shown to be directly related to the energy-Casimir (magnetic helicity) functional and the spectrum of the curl operator.

Remark 1.5.1. Note that, although we are obtaining the equilibrium equation as an Euler-Lagrange equation by minimizing the Hamiltonian, this Euler-Lagrange equation is different from the Newcomb equation, which is often used in a plasma analysis. The Newcomb equation is an Euler-Lagrange equation involving only the radial coordinate, which is obtained by minimizing the energy integral of the ideal MHD with respect to the "Lagrangian displacement vector field"[43]. We are considering the MHD in terms of the "Euler variables".

1.6 Purposes and Outline

As mentioned in the opening section, we are interested in the question: How can we capture the identity of the vortex as a matter? In the framework of the non-canonical Hamiltonian mechanics, we can rephrase this somewhat abstract question as: What Casimir element characterizes the vortex? To concretely deal with this question, we put the problem in the context of the tearing mode, a typical

magnetic vortex emerging in the presence of any magnetic shear.

As we have seen, if there is no ambient flow, the tearing mode can be characterized by the helical-flux Casimir and its stability criterion Δ' is directly related to the magnetic helicity Casimir and the smallest eigenvalue of the curl operator. On the other hand, in the presence of an ambient flow, it is still unclear whether or not the tearing mode can be characterized by some Casimir elements, because the ambient flow shear has a significant influence on the tearing mode.

Hence, the first purpose of the present thesis is to see if the tearing mode with flow can be characterized by some Casimir elements. More concretely, we will first see if there is a Casimir element by which the tearing mode can be characterized as an equilibrium point. If such a Casimir element exists and the tearing mode as an equilibrium is obtained, then, we will examine what Casimir element determines its stability. We should describe a plasma associated with flow by the two-fluid MHD (or Hall MHD) rather than the one-fluid MHD, because the latter can not distinguish between ion and electron flows and, moreover, overlooks the scale hierarchy created by the flow through singular perturbation of the Hall term[44]. Therefore, before we deal with the problem of the tearing mode with flow, we have to prepare the bifurcation theory of double-Beltrami fields in the two-fluid MHD(cf. in [15], the tearing mode theory is based on the bifurcation theory of single-Beltrami fields in the MHD).

It should be noted that our result of the stability analysis may be difficult to be compared with those of the traditional studies. It is because, although the traditional researches examine how the tearing stability responses to the change in some few parameters while fixing other parameters, the parameters of double-Beltrami

fields, our ambient fields, are organically linked to each other, and therefore, we can not change only particular parameters artificially. However, this is not the problem because our primary interest is not in the detailed property of the tearing instability depending on a specific situation (magnetic and flow configuration, flow amplitude and thickness, geometry, and so on) but in a little more universal property of the tearing mode. For us, the boundary between sub- and super-Alfvénic flow shear may be important, because when the flow shear becomes super-Alfvénic, the tearing instability disappears and, instead, the Kelvin-Helmholtz instability appears as a dominant instability mode, as we have seen in Subsec.1.5.2.

The second purpose of the present thesis is developing the nonlinear theory of the tearing mode without flow. The linear tearing-mode eigenfunction, obtained in [15], provides a somewhat strange structure of the island, that is, the magnetic surface "kinks" at the resonance surface. This may be because the linear theory neglects the second-order $\tilde{\boldsymbol{J}} \times \tilde{\boldsymbol{B}}$ force despite the existence of singular current $\tilde{\boldsymbol{J}}$ described by the delta function, which violates the smallness of the corresponding force and may bring the strange kinks of the magnetic surface.

As we will show in Sec.4.3, the resonance singularity ($\boldsymbol{B}_0 \cdot \boldsymbol{k} = 0$), which causes the tearing mode, is related to the extremal of the magnetic flux function $\nabla\psi = 0$. On the other hand, in [17, 21], the singular Casimir is unearthed from the "plateau" singularity stemming from the plateau of the stream function $\nabla\phi = 0$. The plateau becomes the "extremal line" when its width shrinks to zero. Therefore, it is natural to expect that, by extending the notion of plateau singularity to *extremal singularity*, we can obtain a proper Casimir that characterizes the nonlinear tearing mode.

This paper is organized as follows: In Chap.2, we will start by preparing the bifurcation theory of double-Beltrami fields and then, by using it, we will deal with the problem of the tearing mode with flow. In Sec. 2.1, we will formulate a bifurcation theory of double-Beltrami fields in the framework of a non-canonical Hamiltonian mechanics, and will show a existence theorem of bifurcation. In Sec. 2.2, we will give a concrete example of bifurcation in a slab geometry. In Sec. 3.1, we will analyze a linear dynamics in the vicinity of a double-Beltrami field, an equilibrium point of the energy-Casimir (magnetic and canonical helicities) functional. The tearing modes will be formulated as equilibrium points of the energy-Casimir (helical-flux) functional. In Sec.3.2, the stability of the tearing mode will be analyzed. In Chap.4, we develop the notion of extremal singularity and the nonlinear tearing mode theory. In Sec.4.1, we will review the linear tearing mode theory of the ideal MHD[15]. Then, in Sec.4.2, we will formulate, by using stream and magnetic flux functions, the Hamiltonian formalism of the incompressible MHD with two independent variables and three dimensional vector fields. With this formulation, in Sec.4.3, we will rewrite the linear tearing mode theory and reveal the relation between the resonance singularity and the linear, extremal singularity. Lastly, in Sec.4.4, we will develop a singular Casimir of the extremal singularity and apply it to the nonlinear tearing mode theory.

Chapter 2

Bifurcation theory of Double-Beltrami fields

In this chapter, we develop the bifurcation theory of double-Beltrami fields. The magnetic helicity and the canonical helicity play the role of control parameters and the magnetic fluxes and canonical fluxes are set as the fixed parameters.

2.1 Bifurcation theory

2.1.1 An incompressible, two-fluid MHD

An incompressible, two-fluid MHD[45] is given by

$$\partial_t \boldsymbol{P} = \boldsymbol{V} \times (\nabla \times \boldsymbol{P}) - \delta_i \nabla \left(p_i + V^2/2 \right), \tag{2.1}$$

$$\partial_t \boldsymbol{A} = \boldsymbol{V}_e \times (\nabla \times \boldsymbol{A}), \tag{2.2}$$

where $\boldsymbol{P} := \delta_i \boldsymbol{V} + \boldsymbol{A}$ is the ion canonical momentum, $\boldsymbol{V}$ is the ion flow field, $\boldsymbol{A}$ is the vector potential of the magnetic field $\boldsymbol{B}$, $\boldsymbol{V}_e := \boldsymbol{V} - \delta_i \nabla \times \boldsymbol{B}$ is the electron flow field, p_i is the ion pressure, and δ_i is the ratio of the ion-skin length to the scale length. They are normalized in the standard Alfvén units. We denote the ion canonical vorticity by $\boldsymbol{\Omega} := \nabla \times \boldsymbol{P}$. We assume that $\Omega \in \mathbb{R}^3$ is a smooth bounded domain, and the vector fields $\boldsymbol{V}$, $\boldsymbol{V}_e$, $\boldsymbol{\Omega}$ and $\boldsymbol{B}$ are confined in Ω, i.e. we impose boundary conditions (denoting by $\boldsymbol{n}$ the unit normal vector onto the boundary $\partial\Omega$)

$$\boldsymbol{n} \cdot \boldsymbol{V} = 0, \quad \boldsymbol{n} \cdot \boldsymbol{V}_e = 0, \quad \boldsymbol{n} \cdot \boldsymbol{\Omega} = 0, \quad \boldsymbol{n} \cdot \boldsymbol{B} = 0, \tag{2.3}$$

which are equivalent to

$$\boldsymbol{n}\cdot\boldsymbol{V}=0,\quad \boldsymbol{n}\cdot\boldsymbol{B}=0,\quad \boldsymbol{n}\cdot\nabla\times\boldsymbol{V}=0,\quad \boldsymbol{n}\cdot\nabla\times\boldsymbol{B}=0. \tag{2.4}$$

2.1.2 Flux condition: decomposition of harmonic fields

We can make a multiply connected domain Ω into a simply connected domain Ω_0 by inserting cuts Σ_l across each handle of Ω: $\Omega_0 := \Omega \setminus (\cup_{l=1}^{\nu}\Sigma_l)$, where ν is termed the genus of Ω. The fluxes of $\boldsymbol{B}$ and $\boldsymbol{\Omega}$, given by

$$\Phi_l(\boldsymbol{B}) := \int_{\Sigma_l}\boldsymbol{B}\cdot d\sigma,\quad \Phi_l(\boldsymbol{\Omega}) := \int_{\Sigma_l}\boldsymbol{\Omega}\cdot d\sigma, \tag{2.5}$$

can be shown to be constants of motion, where $d\sigma$ is the surface element on Σ_l. To separate these fixed degrees of freedom, we introduce a self-adjoint curl operator $\mathcal{S}$, a non-self-adjoint curl operator $\mathcal{T}$, and basic function spaces, by drawing on [1] (which is summarized also in [15]). We denote by $L^2(\Omega)$ the Hilbert space of Lebesgue-measurable, square-integrable real vector functions of Ω, which is endowed with the standard inner product $\langle \boldsymbol{a},\boldsymbol{b}\rangle := \int_\Omega \boldsymbol{a}\cdot\boldsymbol{b}\; d\boldsymbol{x}$ and the norm $\|\boldsymbol{a}\| := \langle \boldsymbol{a},\boldsymbol{a}\rangle^{1/2}$. We will use the same notation of L^2-norm and inner product regardless of the dimensions of independent and dependent variables. We define

$$L^2_\sigma(\Omega) := \{\, \boldsymbol{u}\in L^2(\Omega);\ \nabla\cdot\boldsymbol{u}=0, \boldsymbol{n}\cdot\boldsymbol{u}=0\,\}, \tag{2.6}$$

$$L^2_\Sigma(\Omega) := \{\, \boldsymbol{u}\in L^2(\Omega);\ \nabla\cdot\boldsymbol{u}=0,\ \boldsymbol{n}\cdot\boldsymbol{u}=0,\ \Phi_l(\boldsymbol{u})=0\ (\forall l)\,\}, \tag{2.7}$$

$$L^2_H(\Omega) := \{\, \boldsymbol{u}\in L^2(\Omega);\ \nabla\times\boldsymbol{u}=0,\ \nabla\cdot\boldsymbol{u}=0,\ \boldsymbol{n}\cdot\boldsymbol{u}=0\,\}, \tag{2.8}$$

$$H^1_{\Sigma\Sigma}(\Omega) := \{\, \boldsymbol{u}\in L^2_\Sigma(\Omega)\cap H^1(\Omega);\ \nabla\times\boldsymbol{u}\in L^2_\Sigma(\Omega)\,\}, \tag{2.9}$$

$$H^1_{\Sigma\sigma}(\Omega) := \{\, \boldsymbol{u}\in L^2_\Sigma(\Omega)\cap H^1(\Omega);\ \nabla\times\boldsymbol{u}\in L^2_\sigma(\Omega)\,\}. \tag{2.10}$$

The space $L^2_\sigma(\Omega)$ is the totality of magnetic fields $\boldsymbol{B}$ and canonical vortices $\boldsymbol{\Omega}$ that satisfy the boundary conditions (2.3). The dimension of $L^2_H(\Omega)$, the space

of harmonic fields (or cohomologies), is equal to the genus ν of Ω. $H^1_{\Sigma\Sigma}(\Omega)$ is densely included in $L^2_\Sigma(\Omega)$. The self-adjoint curl operator (which we denote by $\mathcal{S}$) is such that $\mathcal{S}\boldsymbol{u} = \nabla \times \boldsymbol{u}$ for every $\boldsymbol{u}$ in the operator domain

$$D(\mathcal{S}) = H^1_{\Sigma\Sigma}(\Omega). \tag{2.11}$$

The inverse map $\mathcal{S}^{-1} : L^2_\Sigma(\Omega) \to H^1_{\Sigma\Sigma}(\Omega)$ is a compact operator. We denote by $\sigma_p(\Omega)$ the point spectrum (the set of eigenvalues) of $\mathcal{S}$. Evidently, $0 \notin \sigma_p(\mathcal{S})$. By the compactness of $\mathcal{S}^{-1}$, $\sigma_p(\mathcal{S})$ is a discrete set on $\Re$. The eigenvalues of $\mathcal{S}$ are unbounded in both positive and negative directions. The eigenfunctions of $\mathcal{S}$ constitute a complete orthogonal basis of the Hilbert space $L^2_\Sigma(\Omega)$. When Ω is a multiply-connected smoothly bounded domain, $L^2_H(\Omega)$ has a finite dimension. For each $\boldsymbol{B}_H \in L^2_H(\Omega)$, there is a vector potential $\boldsymbol{A}^H \in L^2_\Sigma(\Omega)$, i.e $\boldsymbol{B}_H = \nabla \times \boldsymbol{A}^H$. Extending the range of curl to include all such $\boldsymbol{B}_H$, and its domain to include the corresponding $\boldsymbol{A}^H$, we extend $\mathcal{S}$ to an operator $\mathcal{T}$ (which we call the non-self-adjoint curl operator) such that $\mathcal{T}\boldsymbol{u} = \nabla \times \boldsymbol{u}$ for every $\boldsymbol{u}$ in the operator domain

$$D(\mathcal{T}) = H^1_{\Sigma\sigma}(\Omega). \tag{2.12}$$

By the orthogonal Hodge-Kodaira decomposition

$$L^2_\sigma(\Omega) = L^2_\Sigma(\Omega) \oplus L^2_H(\Omega), \tag{2.13}$$

we can decompose the total $\boldsymbol{B}, \boldsymbol{\Omega} \in L^2_\sigma(\Omega)$ into the fixed harmonic fields $\boldsymbol{B}_H, \boldsymbol{\Omega}_H \in L^2_H(\Omega)$ (which carry the given fluxes $\Phi_1, \ldots, \Phi_\nu$) and residual components $\boldsymbol{B}_\Sigma, \boldsymbol{\Omega}_\Sigma$:

$$\boldsymbol{B} = \boldsymbol{B}_\Sigma + \boldsymbol{B}_H, \quad [\boldsymbol{B}_\Sigma := \mathcal{P}_\Sigma \boldsymbol{B} \in L^2_\Sigma(\Omega),\ \boldsymbol{B}_H \in L^2_H(\Omega)], \tag{2.14}$$

$$\boldsymbol{\Omega} = \boldsymbol{\Omega}_\Sigma + \boldsymbol{\Omega}_H, \quad [\boldsymbol{\Omega}_\Sigma := \mathcal{P}_\Sigma \boldsymbol{\Omega} \in L^2_\Sigma(\Omega),\ \boldsymbol{\Omega}_H \in L^2_H(\Omega)], \tag{2.15}$$

where $\mathcal{P}_\Sigma$ denotes the orthogonal projector from $L^2(\Omega)$ onto $L^2_\Sigma(\Omega)$.

The current field $\boldsymbol{J} := \nabla \times \boldsymbol{B}$ satisfying the boundary condition (2.4) belongs to the functional space $L^2_\sigma(\Omega)$. Therefore, we can decompose the total $\boldsymbol{J}$ into the harmonic field $\boldsymbol{J}_H \in L^2_H(\Omega)$, which is not fixed differently from $\boldsymbol{B}_H$ and $\boldsymbol{\Omega}_H$, and the residual component $\boldsymbol{J}_\Sigma$

$$\boldsymbol{J} = \boldsymbol{J}_\Sigma + \boldsymbol{J}_H = \nabla \times \boldsymbol{B}^\Sigma + \nabla \times \boldsymbol{B}^H, \quad [\boldsymbol{J}_\Sigma \in L^2_\Sigma(\Omega),\, \boldsymbol{J}_H \in L^2_H(\Omega)], \tag{2.16}$$

where $\boldsymbol{B}^\Sigma := \mathcal{S}^{-1}\boldsymbol{J}_\Sigma \in H^1_{\Sigma\Sigma}(\Omega)$ and $\boldsymbol{B}^H := \mathcal{T}^{-1}\boldsymbol{J}_H \in H^1_{\Sigma\sigma}(\Omega)$. In terms of $\boldsymbol{B}^\Sigma$ and $\boldsymbol{B}^H$, the magnetic field $\boldsymbol{B}$ (or $\boldsymbol{B}_\Sigma$) can be decomposed as

$$\boldsymbol{B} = \boldsymbol{B}_\Sigma + \boldsymbol{B}_H = \boldsymbol{B}^\Sigma + \boldsymbol{B}^H + \boldsymbol{B}_H, \quad [\boldsymbol{B}^\Sigma \in H^1_{\Sigma\Sigma}(\Omega),\, \boldsymbol{B}^H \in H^1_{\Sigma\sigma}(\Omega),\, \boldsymbol{B}_H \in L^2_H(\Omega)]. \tag{2.17}$$

Note that $\boldsymbol{B}^\Sigma$ and $\boldsymbol{B}^H$ are not orthogonal each other in general, that is, $\langle \boldsymbol{B}^\Sigma, \boldsymbol{B}^H \rangle \neq 0$.

2.1.3 Hamiltonian formalism

Subtracting the static components $\boldsymbol{A}^H := \mathcal{T}^{-1}\boldsymbol{B}_H$ and $\boldsymbol{P}^H := \mathcal{T}^{-1}\boldsymbol{\Omega}_H$, we define dynamical components of the variables $\boldsymbol{A}' := \boldsymbol{A} - \boldsymbol{A}^H$ and $\boldsymbol{P}' := \boldsymbol{P} - \boldsymbol{P}^H$. Replacing the variables from $\boldsymbol{P}$ and $\boldsymbol{A}$ to $\boldsymbol{P}'$ and $\boldsymbol{A}'$, and then operating a projector $\mathcal{P}_\sigma$ from $L^2(\Omega)$ to $L^2_\sigma(\Omega)$ on (2.1), we obtain an incompressible, two-fluid MHD

$$\partial_t \boldsymbol{P}'_\sigma = \mathcal{P}_\sigma \boldsymbol{V} \times (\nabla \times \boldsymbol{P}'_\sigma + \boldsymbol{\Omega}_H)\,, \tag{2.18}$$

$$\partial_t \boldsymbol{A}' = \boldsymbol{V}_e \times (\nabla \times \boldsymbol{A}' + \boldsymbol{B}_H)\,, \tag{2.19}$$

where $\boldsymbol{P}'_\sigma := \mathcal{P}_\sigma \boldsymbol{P}'$ and the gauge of $\boldsymbol{A}'$ is such that $\boldsymbol{n} \times \boldsymbol{A}' = 0$. (2.18) and (2.19) are concisely written in the Hamiltonian form

$$\partial_t u = \mathcal{J}(u)\partial_u \mathcal{H}(u), \tag{2.20}$$

with a state vector $u = {}^t(\boldsymbol{P}'_\sigma, \boldsymbol{A}')$, a Poisson operator

$$\mathcal{J}(u) := \delta_i \begin{pmatrix} -\mathcal{P}_\sigma(\nabla \times \boldsymbol{P}'_\sigma + \boldsymbol{\Omega}_H)\times & 0 \\ 0 & (\nabla \times \boldsymbol{A}' + \boldsymbol{B}_H)\times \end{pmatrix}, \tag{2.21}$$

and a Hamiltonian functional

$$\mathcal{H}(u) := \frac{1}{2}\int_\Omega \left\{ \left| \frac{\delta_i \boldsymbol{V}^H + \boldsymbol{P}'_\sigma - \mathcal{P}_\sigma \boldsymbol{A}'}{\delta_i} \right|^2 + \frac{1}{2}\left|\nabla \times \boldsymbol{A}'\right|^2 \right\} d\boldsymbol{x}, \tag{2.22}$$

where $\boldsymbol{V}^H := (\boldsymbol{P}^H - \boldsymbol{A}^H)/\delta_i$ and ∂_u denotes the functional derivative based on the Clarke gradient [16, 17].

The operator $\mathcal{J}(u)$ has two independent Casimir elements:

$$C_1(u) := \frac{1}{2}\langle \boldsymbol{A}', \nabla \times \boldsymbol{A}' \rangle + \langle \boldsymbol{A}', \boldsymbol{B}_H \rangle, \tag{2.23}$$

$$C_2(u) := \frac{1}{2}\langle \boldsymbol{P}'_\sigma, \nabla \times \boldsymbol{P}'_\sigma \rangle + \langle \boldsymbol{P}'_\sigma, \boldsymbol{\Omega}_H \rangle, \tag{2.24}$$

which, respectively, represent the magnetic helicity and the ion canonical helicity.

The equation of motion (2.20) is invariant against the transformation $\mathcal{H}(u) \mapsto \mathcal{H}_\nu(u) := \mathcal{H}(u) - \Sigma \nu_j C_j(u)$ (each ν_j is a constant number playing a role as 'Lagrange multiplier'); we have an equivalent representation of the equation of motion

$$\partial_t u = \mathcal{J}(u)\partial_u \mathcal{H}_\nu(u). \tag{2.25}$$

The transformed Hamiltonian $\mathcal{H}_\nu(u)$ is called an energy-Casimir functional. The 'Beltrami equilibrium' is an equilibrium point of the energy-Casimir functional, i.e. the solution of

$$\partial_u \left(\mathcal{H}(u) - \sum_{j=1}^{2} \nu_j C_j(u) \right) = 0, \tag{2.26}$$

which reads

$$\nabla \times \boldsymbol{B} - \boldsymbol{V}/\delta_i - \nu_1 \boldsymbol{B} = 0, \tag{2.27}$$

$$\boldsymbol{V}/\delta_i - \nu_2 \nabla \times \boldsymbol{P} = 0. \tag{2.28}$$

From (2.27) and (2.28), we obtain

$$\nabla \times \boldsymbol{B} = \nu_1 \boldsymbol{B} + \nu_2 \nabla \times \boldsymbol{P}, \tag{2.29}$$

$$\boldsymbol{V} = \delta_i \left(\nabla \times \boldsymbol{B} - \nu_1 \boldsymbol{B} \right), \tag{2.30}$$

the last of which determines $\boldsymbol{V}$ (and $\boldsymbol{P}$) as the function of $\boldsymbol{B}$. Inserting (2.30) into (2.29) yields

$$\nabla \times \nabla \times \boldsymbol{B} - \left(\nu_1 + \frac{1}{\delta_i^2 \nu_2} \right) \nabla \times \boldsymbol{B} + \frac{1}{\delta_i^2} \left(1 + \frac{\nu_1}{\nu_2} \right) \boldsymbol{B} = 0, \tag{2.31}$$

which may be rewritten as

$$(\mathrm{curl} - \mu_1)(\mathrm{curl} - \mu_2)\boldsymbol{B} = 0, \tag{2.32}$$

where μ_1 and μ_2 are constants (we call them Beltrami parameters) related to the Lagrange multipliers ν_1 and ν_2 as

$$\mu_1 + \mu_2 = \nu_1 + \frac{1}{\delta_i^2 \nu_2}, \quad \mu_1 \mu_2 = \frac{1}{\delta_i^2} \left(1 + \frac{\nu_1}{\nu_2} \right). \tag{2.33}$$

We call (2.31) and (2.32) the double-Beltrami equation[5, 6], the solution of which is given by a combination of two Beltrami vortices[1]. Lagrange multipliers ν_1 and ν_2 can be given as explicit functions of Beltrami parameters μ_1 and μ_2 as follows:

$$\delta_i \nu_1 = \frac{\delta_i \left(\mu_1 + \mu_2 \right) \pm \sqrt{\delta_i^2 \left(\mu_1 - \mu_2 \right)^2 + 4}}{2}, \quad \delta_i \nu_2 = \frac{2}{\delta_i \left(\mu_1 + \mu_2 \right) \mp \sqrt{\delta_i^2 \left(\mu_1 - \mu_2 \right)^2 + 4}}. \tag{2.34}$$

We write down here useful relations connecting them:

$$\nu_1 + \nu_2 = \delta_i^2 \mu_1 \mu_2 \nu_2, \tag{2.35}$$

$$\delta_i^2 (\nu_1 - \mu_1)(\nu_1 - \mu_2) = \left(\frac{1}{\delta_i \nu_2} - \delta_i \mu_1 \right) \left(\frac{1}{\delta_i \nu_2} - \delta_i \mu_2 \right) = 1. \tag{2.36}$$

2.1.4 Inhomogeneous double Beltrami equation

While the double-Beltrami equation (2.32) together with the homogeneous boundary condition (2.4) are seemingly homogeneous equations, there is a hidden inhomogeneity stemming from the fixed harmonic field $\boldsymbol{\Omega}_H$ and $\boldsymbol{B}_H$ ($\boldsymbol{P}^H$ and $\boldsymbol{A}^H$) when Ω is multiply connected.

The equilibrium equation (2.29) implies that the harmonic component $\boldsymbol{J}_H$ of the current field is determined by $\boldsymbol{B}_H$ and $\boldsymbol{\Omega}_H$ as $\boldsymbol{J}_H := \nu_1 \boldsymbol{B}_H + \nu_2 \boldsymbol{\Omega}_H$. Inserting (2.17) into (2.32) and transposing the fixed fields $\boldsymbol{B}^H$ and $\boldsymbol{B}_H$ to right-hand side, we obtain the inhomogeneous, double-Beltrami equation

$$(\mathrm{curl} - \mu_1)(\mathrm{curl} - \mu_2)\boldsymbol{B}^\Sigma = (\mu_1 + \mu_2)\nabla \times \boldsymbol{B}^H - \mu_1\mu_2(\boldsymbol{B}^H + \boldsymbol{B}_H). \tag{2.37}$$

When $\boldsymbol{B}^H, \boldsymbol{B}_H, \mu_1$ and μ_2 are given, we solve (2.37) for $\boldsymbol{B}^\Sigma$ to obtain double-Beltrami field $\boldsymbol{B}_{\mu_1,\mu_2} = \boldsymbol{B}^\Sigma + \boldsymbol{B}^H + \boldsymbol{B}_H$ and $\boldsymbol{P}_{\mu_1,\mu_2}$. As we have already noted, $\boldsymbol{B}^H$ and $\boldsymbol{B}_H$ are uniquely determined by the fluxes. We must also give the parameters μ_1 and μ_2 by some physical condition; here, we determine them by matching the magnetic and canonical helicities of $\boldsymbol{B}_{\mu_1,\mu_2}$ and $\boldsymbol{P}_{\mu_1,\mu_2}$ to prescribed values c_1 of C_1 and c_2 of C_2. But the relation between the Beltrami parameters μ_1 and μ_2 and the helicity-values c_1 and c_1 is somewhat involved and may not be unique; this is the root of the bifurcation problem. In the next subsection, we will see how bifurcations occur in the helicity-matching process.

2.1.5 Helicity matching

The helicity-matching problem may have solutions under the following four different situations.

(A) If the inhomogeneous equation (2.37) determines a unique $\boldsymbol{B}^{\Sigma}$ for given $\boldsymbol{B}^{H}$ and $\boldsymbol{B}_{H}$ and some set of μ_1 and μ_2, then (2.23) and (2.24) evaluates the magnetic helicity and canonical momentum helicity respectively as functions of μ_1 and μ_2, which we denote by $\mathcal{C}_{1A}(\mu_1, \mu_2)$ and $\mathcal{C}_{2A}(\mu_1, \mu_2)$. For a given values c_1 of the helicity C_1 and c_2 of the canonical momentum helicity C_2, we must choose an appropriate μ_1 and μ_2 to satisfy $c_1 = \mathcal{C}_{1A}(\mu_1, \mu_2)$ and $c_2 = \mathcal{C}_{2A}(\mu_1, \mu_2)$.

The homogeneous part of (2.37) may have a nontrivial solution for some special (μ_1, μ_2).

(B) If one of μ_1 or μ_2, here let it be μ_1, equals to an eigenvalue λ_i of the self-adjoint curl operator $\mathcal{S}$ and the inhomogeneous equation (2.37) still has a particular solution (let us denote it by $\boldsymbol{G}$), then the general solution of (2.37) is given by

$$\boldsymbol{B}^{\Sigma} = \alpha_i \boldsymbol{\omega}_i + \boldsymbol{G}, \tag{2.38}$$

where α_i is an arbitrary real number and $\boldsymbol{\omega}_i$ is the eigenfunction corresponding to λ_i, i.e. $(\mathrm{curl} - \lambda_i)\boldsymbol{\omega}_i = 0$. Substituting this $\boldsymbol{B}^{\Sigma}$, we evaluate the helicities (2.23) and (2.24) as functions of α_i and μ_2 (here, μ_1 is fixed at an eigenvalue λ_i), which we denote by $\mathcal{C}_{1B}(\alpha_i, \mu_2; \lambda_i)$ and $\mathcal{C}_{1B}(\alpha_i, \mu_2; \lambda_i)$. The helicity matching $c_1 = \mathcal{C}_{1B}(\alpha_i, \mu_2; \lambda_i)$ and $c_2 = \mathcal{C}_{2B}(\alpha_i, \mu_2; \lambda_i)$ selects an appropriate amplitude α_i and μ_2.

(C) If μ_1 equals to an eigenvalue λ_i and μ_2 equals to another eigenvalue $\lambda_j (\neq \lambda_i)$ of $\mathcal{S}$, and the inhomogeneous equation (2.37) still has a particular solution

$\boldsymbol{G}$, then the general solution of (2.37) is given by

$$\boldsymbol{B}^{\Sigma} = \alpha_i \boldsymbol{\omega}_i + \alpha_j \boldsymbol{\omega}_j + \boldsymbol{G}, \tag{2.39}$$

where α_i (α_j) is an arbitrary real number and $\boldsymbol{\omega}_i$ ($\boldsymbol{\omega}_j$) is the eigenfunction corresponding to λ_i (λ_j). Substituting this $\boldsymbol{B}^{\Sigma}$, we evaluate the helicities (2.23) and (2.24) as functions of α_i and α_j (here, μ_1 and μ_2 are fixed at eigenvalues λ_i and λ_j), which we denote by $\mathcal{C}_{1C}(\alpha_i, \alpha_j; \lambda_i, \lambda_j)$ and $\mathcal{C}_{2C}(\alpha_i, \alpha_j; \lambda_i, \lambda_j)$. The helicity matching $c_1 = \mathcal{C}_{1C}(\alpha_i, \alpha_j; \lambda_i, \lambda_j)$ and $c_2 = \mathcal{C}_{2C}(\alpha_i, \alpha_j; \lambda_i, \lambda_j)$ selects appropriate amplitudes α_i and α_j.

(D) In the case that μ_1 and μ_2 both equal to an same eigenvalues $\lambda := \lambda_i = \lambda_j$ of $\mathcal{S}$, the eigenfunctions $\boldsymbol{\omega}_i$ and $\boldsymbol{\omega}_j$ degenerate into the same function $\boldsymbol{\omega}$. If there exists a 'generalized eigenfunction' $\boldsymbol{\omega'}$ such that $(\mathrm{curl} - \lambda)^2 \boldsymbol{\omega'} = 0$, and the inhomogeneous equation (2.37) still has a particular solution $\boldsymbol{G}$, then the general solution of (2.37) may be given by

$$\boldsymbol{B}^{\Sigma} = \alpha \boldsymbol{\omega} + \alpha' \boldsymbol{\omega}' + \boldsymbol{G}, \tag{2.40}$$

where α and α' are arbitrary real numbers. Substituting this $\boldsymbol{B}^{\Sigma}$, we evaluatethe helicities (2.23) and (2.24) as functions of α and α' (here, μ_1 and μ_2 are fixed at an eigenvalue λ), which we denote by $\mathcal{C}_{1D}(\alpha, \alpha'; \lambda)$ and $\mathcal{C}_{2D}(\alpha, \alpha'; \lambda)$. In this case, the helicity matching $c_1 = \mathcal{C}_{1D}(\alpha, \alpha'; \lambda)$ and $c_2 = \mathcal{C}_{2D}(\alpha, \alpha'; \lambda)$ selects appropriate amplitudes α and α'.

In the case (B), (C), and (D), if there are multiple eigenfunctions belonging to the same eigenvalue λ, we may consider a linear combination $\Sigma_s \alpha_s \boldsymbol{\omega}_s$, or if there exists twofold degeneracy, we may take $\boldsymbol{\omega}$ and α to be complex, and write $\Re(\alpha \boldsymbol{\omega})$; see Section 2.2.

We note that the branches (B)-(D) can appear only if at least one of μ_1 and μ_2 is an eigenvalue of the self-adjoint curl operator, and moreover, if the inhomogeneous equation (2.37) has a particular solution $\boldsymbol{G}$. As is to be shown, the latter condition does not always apply, i.e. at some eigenvalues the equation (2.37) may be solvable only for some special $\boldsymbol{B}^H$ and $\boldsymbol{B}_H$ like $\boldsymbol{B}^H = \boldsymbol{B}_H = 0$.

We have developed complicated decompositions of the double-Beltrami magnetic field. For the convenience of forthcoming discussions, we summarize the notions.

- $\boldsymbol{B}_{\mu_1,\mu_2}$ is a finite-flux double-Beltrami magnetic field, such that

$$(\mathrm{curl} - \mu_1)(\mathrm{curl} - \mu_2)\boldsymbol{B}_{\mu_1,\mu_2} = 0. \tag{2.41}$$

- $\boldsymbol{B}_{\mu_1,\mu_2} = \boldsymbol{B}^\Sigma + \boldsymbol{B}^H + \boldsymbol{B}_H$ ($\boldsymbol{B}^\Sigma \in H^1_{\Sigma\Sigma}(\Omega), \boldsymbol{B}^H \in H^1_{\Sigma\sigma}(\Omega), \boldsymbol{B}_H \in L^2_H(\Omega)$) so that

$$(\mathrm{curl} - \mu_1)(\mathrm{curl} - \mu_2)\boldsymbol{B}^\Sigma = (\mu_1 + \mu_2)\nabla \times \boldsymbol{B}^H - \mu_1\mu_2(\boldsymbol{B}^H + \boldsymbol{B}_H). \tag{2.42}$$

- On the branches (B), (C) and (D), $\boldsymbol{B}^\Sigma$ is obtained, like (2.38), (2.39) and (2.40), by superposition of homogeneous solutions $\boldsymbol{\omega}$ and a particular solution $\boldsymbol{G}$ such that

$$(\mathrm{curl} - \mu_1)(\mathrm{curl} - \mu_2)\boldsymbol{G} = (\mu_1 + \mu_2)\nabla \times \boldsymbol{B}^H - \mu_1\mu_2(\boldsymbol{B}^H + \boldsymbol{B}_H). \tag{2.43}$$

In the next subsection, we will study the condition for a particular solution $\boldsymbol{G}$ to exist.

2.1.6 Bifurcation of Beltrami equilibrium

We have already briefly introduced the self-adjoint curl operator $\mathcal{S}$ and the non-self-adjoint curl operator $\mathcal{T}$ needed to elucidate the mathematical structure around the bifurcation point. We start by reviewing the property of the operator $\mathcal{T}$ proven in [1]:

Proposition 1. For every $\mu \notin \sigma_p(\mathcal{S})$, the inhomogeneous equation

$$(\mathcal{T} - \mu)\boldsymbol{B}_\Sigma = \boldsymbol{b} \in L^2_\sigma(\Omega) \tag{2.44}$$

has a unique solution $\boldsymbol{B}_\Sigma = (\mathcal{T} - \mu)^{-1}\boldsymbol{b} \in L^2_\Sigma(\Omega)$.

Using this proposition, we can readily obtain the following theorem:

Theorem 1. Let $\mu_1, \mu_2 \notin \sigma_p(\mathcal{S})$. The inhomogeneous equation

$$(\mathcal{T} - \mu_1)(\mathcal{S} - \mu_2)\boldsymbol{B}^\Sigma = (\mu_1 + \mu_2)\nabla \times \boldsymbol{B}^H - \mu_1\mu_2(\boldsymbol{B}^H + \boldsymbol{B}_H) \tag{2.45}$$

has a unique solution

$$\boldsymbol{B}^\Sigma = (\mathcal{S}-\mu_2)^{-1}(\mathcal{T}-\mu_1)^{-1}\left\{(\mu_1 + \mu_2)\nabla \times \boldsymbol{B}^H - \mu_1\mu_2(\boldsymbol{B}^H + \boldsymbol{B}_H)\right\} \quad (\in H^1_{\Sigma\Sigma}(\Omega)), \tag{2.46}$$

implying that (2.37) has a unique solution.

In the case that at least one of μ_1 or μ_2 belongs to $\sigma_p(\mathcal{S})$, we have nontrivial solution $\boldsymbol{\omega}$ of the homogeneous part of the double-Beltrami equation (2.37). We are ready to study the existence of a particular solution $\boldsymbol{G}$ of (2.37) for given $\boldsymbol{B}^H$ and $\boldsymbol{B}_H$. As mentioned above, a nontrivial particular solution $\boldsymbol{G}$ becomes the trunk from which the branches (B), (C) and (D) solutions bifurcate. We have the following two theorems.

Theorem 2. Let $\mu_1 = \lambda_i \in \sigma_p(\mathcal{S})$ and $\mathcal{S}\boldsymbol{\omega}_i = \lambda_i \boldsymbol{\omega}_i$, and $\mu_2 \notin \sigma_p(\mathcal{S})$. Iff

$$\langle \boldsymbol{B}^H - \mu_2 \boldsymbol{A}^H, \boldsymbol{\omega}_i \rangle = 0, \tag{2.47}$$

the inhomogeneous double Beltrami equation

$$(\mathcal{T} - \lambda_i)(\mathcal{S} - \mu_2)\boldsymbol{G} = (\lambda_i + \mu_2)\nabla \times \boldsymbol{B}^H - \lambda_i \mu_2 (\boldsymbol{B}^H + \boldsymbol{B}_H) \tag{2.48}$$

has a solution $\boldsymbol{G} \in H^1_{\Sigma\Sigma}(\Omega)$.

Proof. Let V_i be the eigenspace corresponding to λ_i. We define $L^2_{\Sigma\perp}(\Omega) := L^2_\Sigma(\Omega)/V_i$ and $H^1_{\Sigma\Sigma\perp}(\Omega) := H^1_{\Sigma\Sigma}(\Omega)/V_i$. The restriction of $\mathcal{S}$ on $H^1_{\Sigma\Sigma\perp}(\Omega)$ will be denoted by $\mathcal{S}_\perp$. Obviously

$$\mathrm{Coker}(\mathcal{S}_\perp - \lambda_i) = V_i. \tag{2.49}$$

If the orthogonality condition (2.47) holds, $\boldsymbol{B}^H - \mu_2 \boldsymbol{A}^H \in L^2_{\Sigma\perp}(\Omega)$. Let us write

$$(\mathcal{S} - \mu_2)\boldsymbol{G} = \boldsymbol{W} + (\lambda_i + \mu_2)\boldsymbol{B}^H - \lambda_i \mu_2 \boldsymbol{A}^H \quad (\in L^2_\Sigma(\Omega)). \tag{2.50}$$

Inserting this into (2.48) yields

$$(\mathcal{T} - \lambda_i)\boldsymbol{W} = \lambda_i^2 \left(\boldsymbol{B}^H - \mu_2 \boldsymbol{A}^H\right) \quad (\in L^2_{\Sigma\perp}(\Omega)), \tag{2.51}$$

which can be solved by

$$\boldsymbol{W} = (\mathcal{S}_\perp - \lambda_i)^{-1} \lambda_i^2 \left(\boldsymbol{B}^H - \mu_2 \boldsymbol{A}^H\right) \quad (\in H^1_{\Sigma\Sigma\perp}(\Omega)). \tag{2.52}$$

Thus, the solution of (2.45) is given by

$$\boldsymbol{G} = (\mathcal{S} - \mu_2)^{-1} \left\{ (\mathcal{S}_\perp - \lambda_i)^{-1} \mu_1^2 \left(\boldsymbol{B}^H - \mu_2 \boldsymbol{A}^H\right) + (\lambda_i + \mu_2)\boldsymbol{B}^H - \lambda_i \mu_2 \boldsymbol{A}^H \right\}. \tag{2.53}$$

Next, we show that $\langle \boldsymbol{B}^H - \mu_2 \boldsymbol{A}^H, \boldsymbol{\omega}_j \rangle \neq 0$ is in contradiction with the solvability of (2.48). It suffices to assume that V_j is one dimensional. Projecting both sides of (2.51) onto V_j, we obtain

$$\langle (T-\lambda_i)\boldsymbol{W}, \boldsymbol{\omega}_i \rangle = \langle (T-\lambda_i)\boldsymbol{W}_\perp, \boldsymbol{\omega}_i \rangle = \langle T\boldsymbol{W}_\perp, \boldsymbol{\omega}_i \rangle = \lambda_i^2 \langle \boldsymbol{B}^H - \mu_2 \boldsymbol{A}^H, \boldsymbol{\omega}_j \rangle, \quad (2.54)$$

where $\boldsymbol{W}_\perp$ is the projection of $\boldsymbol{W}$ onto $L^2_{\Sigma\perp}$. For this relation to hold, there must be an element $\boldsymbol{w} \in L^2_{\Sigma\perp}(\Omega)$ such that $\mathcal{T}\boldsymbol{w} = c\boldsymbol{\omega}_j$ ($c \neq 0$). Substituting $c\boldsymbol{\omega}_j = (c/\lambda_j)\mathcal{T}\boldsymbol{\omega}_j$, we obtain $\mathcal{T}[\boldsymbol{w} - (c/\lambda_j)\boldsymbol{\omega}_j] = 0$. Since $\mathrm{Ker}(\mathcal{T}) = \{0\}$, we deduce $\boldsymbol{w} = (c/\lambda_j)\boldsymbol{\omega}_j$, which contradicts the assumption $\boldsymbol{w} \in L^2_{\Sigma\perp}(\Omega)$. Therefore, if $\langle \boldsymbol{B}^H - \mu_2 \boldsymbol{A}^H, \boldsymbol{\omega}_j \rangle \neq 0$, (2.48) cannot have a solution. □

Note that the particular solution $\boldsymbol{G}$ obtained here does not necessarily satisfy $\langle \boldsymbol{G}, \boldsymbol{\omega}_i \rangle = 0$ because, although $\boldsymbol{W} + \lambda_i \left(\boldsymbol{B}^H - \mu_2 \boldsymbol{A}^H \right) \in L^2_{\Sigma\perp}$, $\langle \boldsymbol{B}^H, \boldsymbol{\omega}_i \rangle$ may have finite value. If, instead of (2.50), we use

$$(\mathcal{S} - \mu_2)\boldsymbol{G} = \boldsymbol{W} + (\lambda_i + \mu_2)\boldsymbol{B}^H - \lambda_i \mu_2 \boldsymbol{A}^H - \mu_2 \langle \boldsymbol{B}^H, \boldsymbol{\omega}_i \rangle \boldsymbol{\omega}_i \in H^1_{\Sigma\sigma}/V_i, \quad (2.55)$$

the, we can obtain a particular solution $\boldsymbol{G}$ such that $\boldsymbol{G} \in H^1_{\Sigma\Sigma}(\Omega)$ and $\langle \boldsymbol{G}, \boldsymbol{\omega}_i \rangle = 0$.

Theorem 3. Let $\lambda_i, \lambda_j \in \sigma_p(\mathcal{S})$, $\mathcal{S}\boldsymbol{\omega}_i = \lambda_i \boldsymbol{\omega}_i$ and $\mathcal{S}\boldsymbol{\omega}_j = \lambda_j \boldsymbol{\omega}_j$. Iff

$$\langle \boldsymbol{B}^H - \lambda_j \boldsymbol{A}^H, \boldsymbol{\omega}_i \rangle = \langle \boldsymbol{B}^H - \lambda_i \boldsymbol{A}^H, \boldsymbol{\omega}_j \rangle = 0, \quad (2.56)$$

the inhomogeneous double Beltrami equation

$$(\mathcal{T} - \lambda_i)(\mathcal{S} - \lambda_j)\boldsymbol{G} = (\lambda_i + \lambda_j)\nabla \times \boldsymbol{B}^H - \lambda_i \lambda_j (\boldsymbol{B}^H + \boldsymbol{B}_H) \quad (2.57)$$

has a solution.

Proof. Let V_k be the eigenspace corresponding to λ_k $(k = i, j)$. The restriction of $\mathcal{S}$ on $H^1_{\Sigma\Sigma}(\Omega)/V_k$ will be denoted by $\mathcal{S}_{\perp k}$ $(k = i, j)$. Obiously

$$\mathrm{Coker}(\mathcal{S}_{\perp k} - \lambda_k) = V_k \quad (k = i, j). \tag{2.58}$$

If the orthogonality conditions (2.56) hold, $\boldsymbol{B}^H - \lambda_j \boldsymbol{A}^H \in L^2_\Sigma(\Omega)/V_i$ and $\boldsymbol{B}^H - \lambda_i \boldsymbol{A}^H \in L^2_\Sigma(\Omega)/V_j$. Let us write

$$(S - \lambda_j)\boldsymbol{G} = \boldsymbol{W} + (\lambda_i + \lambda_j)\boldsymbol{B}^H - \lambda_i\lambda_j \boldsymbol{A}^H. \tag{2.59}$$

Inserting this into (2.57) yields

$$(T - \lambda_i)\boldsymbol{W} = \lambda_i^2 \left(\boldsymbol{B}^H - \lambda_j \boldsymbol{A}^H\right) \quad (\in L^2_\Sigma(\Omega)/V_i). \tag{2.60}$$

We can solve (2.60) by $\boldsymbol{W} = (\mathcal{S}_{\perp i} - \lambda_i)^{-1}\lambda_i^2(\boldsymbol{B}^H - \lambda_j \boldsymbol{A}^H)$, with which the right-hand side of (2.59) is shown to belong to $L^2_\Sigma(\Omega)/V_j$ as follows:

$$\begin{aligned}
& \langle (\mathcal{S}_{\perp i} - \lambda_i)^{-1} \lambda_i^2 \left(\boldsymbol{B}^H - \lambda_j \boldsymbol{A}^H\right) + (\lambda_i + \lambda_j)\boldsymbol{B}^H - \lambda_i\lambda_j \boldsymbol{A}^H, \boldsymbol{\omega}_j \rangle \\
= \; & \langle (\mathcal{S}_{\perp i} - \lambda_i)^{-1} \lambda_i^2 \left(\boldsymbol{B}^H - \lambda_j \boldsymbol{A}^H\right) + \lambda_i \boldsymbol{B}^H, \boldsymbol{\omega}_j \rangle \\
= \; & \frac{\lambda_i^2}{\lambda_j - \lambda_i} \langle (\mathcal{S}_{\perp i} - \lambda_i)^{-1} \left(\boldsymbol{B}^H - \lambda_j \boldsymbol{A}^H\right), (\mathcal{S}_{\perp i} - \lambda_i)\, \boldsymbol{\omega}_j \rangle + \lambda_i \langle \boldsymbol{B}^H, \boldsymbol{\omega}_j \rangle \\
= \; & \frac{\lambda_i^2}{\lambda_j - \lambda_i} \langle \boldsymbol{B}^H - \lambda_j \boldsymbol{A}^H, \boldsymbol{\omega}_j \rangle + \lambda_i \langle \boldsymbol{B}^H, \boldsymbol{\omega}_j \rangle \\
= \; & -\lambda_i^2 \langle \boldsymbol{A}^H, \boldsymbol{\omega}_j \rangle + \lambda_i^2 \langle \boldsymbol{A}^H, \boldsymbol{\omega}_j \rangle \\
= \; & 0,
\end{aligned} \tag{2.61}$$

where the first and fourth equalities follow from $\langle \boldsymbol{B}^H - \lambda_i \boldsymbol{A}^H, \boldsymbol{\omega}_j \rangle$. Thereby, we can solve (2.59) by

$$\boldsymbol{G} = (\mathcal{S}_{\perp j} - \lambda_j)^{-1} \left\{ (\mathcal{S}_{\perp i} - \lambda_i)^{-1} \lambda_i^2 (\boldsymbol{B}^H - \lambda_j \boldsymbol{A}^H) + (\lambda_i + \lambda_j)\boldsymbol{B}^H - \lambda_i\lambda_j \boldsymbol{A}^H \right\}. \tag{2.62}$$

Applying the same method of theorem 3, we can show that $\langle \boldsymbol{B}^H - \lambda_j \boldsymbol{A}^H, \boldsymbol{\omega}_i \rangle \neq 0$ is in contradiction with the solvability of (2.57). Because of the symmetry between λ_i and λ_j in the equation (2.57), $\langle \boldsymbol{B}^H - \lambda_i \boldsymbol{A}^H, \boldsymbol{\omega}_j \rangle \neq 0$ is also in contradiction with the solvability of (2.57). □

Although $\boldsymbol{B}^H$ and $\boldsymbol{A}^H$ belong to $L^2_\Sigma(\Omega)$, they are not elements of $H^1_{\Sigma\Sigma}$. Hence, for example, $\langle \boldsymbol{A}_H, \boldsymbol{\omega}_i \rangle = \lambda_i^{-1} \langle \boldsymbol{A}_H, \mathcal{S}\boldsymbol{\omega}_i \rangle$ is not equal to $\lambda_i^{-1} \langle \nabla \times \boldsymbol{A}_H, \boldsymbol{\omega}_i \rangle = \lambda_i^{-1} \langle \boldsymbol{B}_H, \boldsymbol{\omega}_i \rangle = 0$. Therefore, the orthogonality conditions (2.47) and (2.56) are not trivial conditions. As is shown in the subsection 2.5 of [15], they pertain to the symmetry of Ω. In the next section, we will consider a concrete example of slab geometry.

2.2 Helical Bifurcation in Slab geometry

In this section, we concretely examine the bifurcation of the double-Beltrami equilibrium in a Slab geometry. Let the domain be $\Omega = \{ (x, y, z);\ 0 < x < 1,\ 0 \leq y < L_y,\ 0 \leq z < L_z \}$, where $y = 0$ and L_y, as well as $z = 0$ and L_z are periodic boundaries. At $x = 0$ and 1, we impose the boundary condition (2.4).

2.2.1 Eigenfunction

In this domain Ω, every eigenfunctions of $\mathcal{S}$ is given by the slab-geometry version of the CK function[46, 47]:

$$\boldsymbol{\omega}_i = \nabla \times (\Psi_i \nabla z + \nabla \Psi_i \times \nabla z / \lambda_i) \tag{2.63}$$

where Ψ_i is determined by

$$-\Delta \Psi_i = \lambda_i^2 \Psi_i \qquad \text{in } \Omega. \tag{2.64}$$

Taking into account the boundary conditions, we put

$$\Psi_i = \psi_l(x) \Re e^{i(k_y y + k_z z + \chi)} \tag{2.65}$$

where χ is a real number determining the phase angle,

$$k_y = m\frac{2\pi}{L_y}, \quad k_z = n\frac{2\pi}{L_y} \quad (m, n = 0, 1, 2, \ldots) \tag{2.66}$$

and

$$\psi_l(x) = \sin(k_x x + \theta) \quad (k_x := l\pi;\ l = 1, 2, \ldots). \tag{2.67}$$

Without loss of generality, we assume $k_x > 0$. We can easily verify that $\nabla \times \boldsymbol{\omega}_i = \lambda_i \boldsymbol{\omega}_i$.

Then, we have

$$\begin{aligned} \boldsymbol{\omega}_i &= \Re e^{i(k_y y + k_z z + \phi)} \begin{pmatrix} ik_x k_z \cos(k_x x + \theta)/\lambda_i + ik_y \sin(k_x x + \theta) \\ -k_y k_z \sin(k_x x + \theta)/\lambda_i - k_x \cos(k_x x + \theta) \\ \left(k_x^2 + k_y^2\right) \sin(k_x x + \theta)/\lambda_i \end{pmatrix} \\ &= \begin{pmatrix} -\left\{(k_x k_z/\lambda_i)\cos(k_x x + \theta) + k_y \sin(k_x x + \theta)\right\} \sin(k_y y + k_z z + \chi) \\ -\left\{(k_y k_z/\lambda_i)\sin(k_x x + \theta) + k_x \cos(k_x x + \theta)\right\} \cos(k_y y + k_z z + \chi) \\ \left\{(k_x^2/\lambda_i) + (k_y^2/\lambda_i)\right\} \sin(k_x x + \theta) \cos(k_y y + k_z z + \chi) \end{pmatrix} \end{aligned} \tag{2.68}$$

the eigenvalue of which is

$$\lambda_i = \pm\sqrt{k_x^2 + k_y^2 + k_z^2} = \pm\pi\sqrt{l^2 + (2m/L_y)^2 + (2n/L_z)^2}. \tag{2.69}$$

The boundary condition $\boldsymbol{n} \cdot \boldsymbol{\omega}_i = 0$ and the zero-flux conditions $\Phi_y(\boldsymbol{\omega}_i) = \Phi_z(\boldsymbol{\omega}_i) = 0$ read, respectively

$$(k_x k_z/\lambda_i)\cos(k_x x + \theta) + k_y \sin(k_x x + \theta) = 0 \qquad (\text{on } x = 0, 1), \tag{2.70}$$

$$\Phi_y(\boldsymbol{\omega}_i) = \delta_{n0} L_z \cos(k_y y + \chi) \left\{\sin\theta - \sin(k_x + \theta)\right\}, \tag{2.71}$$

$$\Phi_z(\boldsymbol{\omega}_i) = \delta_{m0} L_y \frac{k_x}{\lambda_i} \cos(k_z z + \chi) \left\{\cos\theta - \cos(k_x + \theta)\right\}, \tag{2.72}$$

where δ_{st} denotes Kronecker's delta, by which the eigenvalue λ_i of (2.64) is discretized.

In order to provide a full description of the spectrum, we here regard j as a multi-index $\{m, n, l\}$. Iff $m = n = 0$, the boundary condition (2.70) trivial, whereas the zefo-flux conditions (2.71) and (2.72) are then nontrivial and are used to determine l. Otherwise, the boundary condition (2.70) determines l. Thus,

$$\text{if } m = n = 0, \quad k_x = 2l'\pi, \quad i = \{0, 0, 2l'\}, \qquad \text{otherwise}, \quad k_x = l\pi, \quad i = \{m, n, l\}. \tag{2.73}$$

If we remove the zero-flux condition (2.71) and (2.72) on the $m = n = 0$ CK eigenfunction, we obtain a finite-flux Beltrami field $\boldsymbol{B}_\mu$, such that $\nabla \times \boldsymbol{B}_\mu = \mu \boldsymbol{B}_\mu$ for every real μ (the non-self-adjoint curl operator $\mathcal{T}$ has a continuous point spectrum [1]):

$$\boldsymbol{B}_\mu = B_\mu \begin{pmatrix} 0 \\ -\cos(\mu x + \theta) \\ \sin(\mu x + \theta) \end{pmatrix}, \tag{2.74}$$

where B_μ is a positive real number denoting its amplitude.The poloidal flux $\Phi_y(\boldsymbol{B}_\mu)$ and the toroidal flux $\Phi_z(\boldsymbol{B}_\mu)$ are calculated as

$$\Phi_y(\boldsymbol{B}_\mu) = B_\mu \frac{L_z}{\mu} \left\{ \sin\theta - \sin(\mu + \theta) \right\}, \quad \Phi_z(\boldsymbol{B}_\mu) = B_\mu \frac{L_y}{\mu} \left\{ \cos\theta - \cos(\mu + \theta) \right\}. \tag{2.75}$$

2.2.2 Trunk solution

Here, we consider the trunk solution $\boldsymbol{G}_{\mu_1,\mu_2} + \boldsymbol{B}^H + \boldsymbol{B}_H$, which is in charge of the fluxes of the total solution. In the slab geometory, the magnetic and vortical harmonic fields with fluxes $\Phi_{my}, \Phi_{mz}, \Phi_{cy}$ and Φ_{cz} are given by

$$\boldsymbol{B}_H = \frac{\Phi_{my}}{L_z} \nabla y + \frac{\Phi_{mz}}{L_y} \nabla z, \quad \boldsymbol{\Omega}_H = \frac{\Phi_{cy}}{L_z} \nabla y + \frac{\Phi_{cz}}{L_y} \nabla z. \tag{2.76}$$

The vector potentials of them are

$$\boldsymbol{A}^H = -\frac{\Phi_{my}}{L_z}\left(x-\frac{1}{2}\right)\nabla z + \frac{\Phi_{mz}}{L_y}\left(x-\frac{1}{2}\right)\nabla y, \tag{2.77}$$

$$\boldsymbol{P}^H = -\frac{\Phi_{cy}}{L_z}\left(x-\frac{1}{2}\right)\nabla z + \frac{\Phi_{cz}}{L_y}\left(x-\frac{1}{2}\right)\nabla y, \tag{2.78}$$

which are unique in $H^1_{\Sigma\sigma}(\Omega)$.

The trunk solution $\boldsymbol{G}_{\mu_1,\mu_2} + \boldsymbol{B}^H + \boldsymbol{B}_H$ of the double-Beltrami equilibrium is given by superposition of two finite-flux Beltrami fields as

$$\boldsymbol{G}_{\mu_1,\mu_2} + \boldsymbol{B}^H + \boldsymbol{B}_H = \boldsymbol{B}_{\mu_1} + \boldsymbol{B}_{\mu_2}. \tag{2.79}$$

We have to determine the amplitudes B_{μ_1}, B_{μ_2} and the phases θ_1, θ_2 by given values of fluxes $\Phi_{my}, \Phi_{mz}, \Phi_{cy}$ and Φ_{cz}, through the following equations:

$$\Phi_y\left(\boldsymbol{B}_{\mu_1} + \boldsymbol{B}_{\mu_2}\right) = \Phi_y(\boldsymbol{B}_H) = \Phi_{my}, \tag{2.80}$$

$$\Phi_z\left(\boldsymbol{B}_{\mu_1} + \boldsymbol{B}_{\mu_2}\right) = \Phi_z(\boldsymbol{B}_H) = \Phi_{mz}, \tag{2.81}$$

$$\Phi_y\left(\mu_1\boldsymbol{B}_{\mu_1} + \mu_2\boldsymbol{B}_{\mu_2}\right) = \Phi_y(\nabla\times\boldsymbol{B}^H) = \nu_1\Phi_{my} + \nu_2\Phi_{cy}, \tag{2.82}$$

$$\Phi_z\left(\mu_1\boldsymbol{B}_{\mu_1} + \mu_2\boldsymbol{B}_{\mu_2}\right) = \Phi_z(\nabla\times\boldsymbol{B}^H) = \nu_1\Phi_{mz} + \nu_2\Phi_{cz}, \tag{2.83}$$

the second equalities of (2.82) and (2.83) follow from (**??**). Here, let us introduce new abbreviations to increase readability of the following calculations:

$$\phi_{my} := \frac{\Phi_{my}}{L_z}, \quad \phi_{mz} := \frac{\Phi_{mz}}{L_y}, \quad \phi_{cy} := \frac{\Phi_{cy}}{L_z}, \quad \phi_{cz} := \frac{\Phi_{cz}}{L_y}, \tag{2.84}$$

$$Q_{1y} := (\nu_1-\mu_1)\,\phi_{my} + \nu_2\phi_{cy}, \quad Q_{1z} := (\nu_1-\mu_1)\,\phi_{mz} + \nu_2\phi_{cz}, \tag{2.85}$$

$$Q_{2y} := (\nu_1-\mu_2)\,\phi_{my} + \nu_2\phi_{cy}, \quad Q_{2z} := (\nu_1-\mu_2)\,\phi_{mz} + \nu_2\phi_{cz}. \tag{2.86}$$

For μ_1 and μ_2 such that $\mu_1 \neq \mu_2$, $\mu_1 \neq \lambda_{0,0,2l'}$ and $\mu_2 \neq \lambda_{0,0,2l'}$, we can solve (2.80) - (2.83) and obtain

$$B_{\mu_1}\cos(\theta_1+\frac{\mu_1}{2}) = -\frac{1}{2\sin\mu_1/2}\frac{\mu_1}{\mu_1-\mu_2}Q_{2y}, \quad B_{\mu_1}\sin(\theta_1+\frac{\mu_1}{2}) = \frac{1}{2\sin\mu_1/2}\frac{\mu_1}{\mu_1-\mu_2}Q_{2z}, \tag{2.87}$$

$$B_{\mu_2}\cos(\theta_2+\frac{\mu_2}{2}) = -\frac{1}{2\sin\mu_2/2}\frac{\mu_2}{\mu_2-\mu_1}Q_{1y}, \quad B_{\mu_2}\sin(\theta_2+\frac{\mu_2}{2}) = \frac{1}{2\sin\mu_2/2}\frac{\mu_2}{\mu_2-\mu_1}Q_{1z}. \tag{2.88}$$

Then, we finally obtain

$$\boldsymbol{B}_{\mu_1} = \frac{1}{\mu_1-\mu_2}\frac{\mu_1/2}{\sin(\mu_1/2)}\begin{pmatrix} 0 \\ Q_{2y}\cos\mu_1(x-\frac{1}{2}) + Q_{2z}\sin\mu_1(x-\frac{1}{2}) \\ -Q_{2y}\sin\mu_1(x-\frac{1}{2}) + Q_{2z}\cos\mu_1(x-\frac{1}{2}) \end{pmatrix}, \tag{2.89}$$

$$\boldsymbol{B}_{\mu_2} = \frac{1}{\mu_2-\mu_1}\frac{\mu_2/2}{\sin(\mu_2/2)}\begin{pmatrix} 0 \\ Q_{1y}\cos\mu_2(x-\frac{1}{2}) + Q_{1z}\sin\mu_2(x-\frac{1}{2}) \\ -Q_{1y}\sin\mu_2(x-\frac{1}{2}) + Q_{1z}\cos\mu_2(x-\frac{1}{2}) \end{pmatrix}. \tag{2.90}$$

The reason why we can not solve (2.80)-(2.83) at $\mu_1 = \lambda_{0,0,2l'}$ or $\mu_2 = \lambda_{0,0,2l'}$ may be viewed as a consequence of the violation of the orthogonality conditions (2.47) and (2.56) at these eigenvalues. By easy calculation, we observe

$$\langle (x-\frac{1}{2})\nabla y, \boldsymbol{\omega}_i\rangle = \delta_{m0}\delta_{n0}L_yL_z\cos\chi\sin\theta, \tag{2.91}$$

$$\langle (x-\frac{1}{2})\nabla z, \boldsymbol{\omega}_i\rangle = \mp\delta_{m0}\delta_{n0}L_yL_z\cos\chi\cos\theta. \tag{2.92}$$

At least one of them has a finite value for $i = \{0, 0, 2l'\}$, which violates the orthogonality conditions (2.47) and (2.56).

In the case of $\mu_1 = \mu_2$, two finite-flux Beltrami fields $\boldsymbol{B}_{\mu_1}$ and $\boldsymbol{B}_{\mu_2}$ degenerate into the same field, therefore, we can not solve (2.80) - (2.83) because of the shortage of fields in charge of fluxes $\Phi_{my}, \Phi_{mz}, \Phi_{cy}$ and Φ_{cz} . In this instance, we have to introduce the "generalized" eigenfunction such that $(\mathrm{curl}-\mu)^2\boldsymbol{\omega} = 0$.

2.2.3 Helical bifurcation

Here, we consider the bifurcated branches (B) and (C) obtained by superposing eigenfunctions $\boldsymbol{\omega}_{m,n,l}$ with a non-zero m or n on the trunk solution $\boldsymbol{B}_{\mu_1} + \boldsymbol{B}_{\mu_2}$.

In what follows, we consider μ_1 and μ_2 such that $\mu_1, \mu_2 \neq \lambda_{0,0,2l'}$. Using (2.91) and (2.92), we can easily confirm that eigenfunctions $\boldsymbol{\omega}_{m,n,l}$ with a non-zero m or n satisfy the orthogonality conditions (2.47) and (2.56), therefore, on the line $\mu_1 = \lambda_i \neq \lambda_{0,0,2l'}$ (as well as $\mu_2 = \lambda_j \neq \lambda_{0,0,2l'}$), there exist both the trunk solution $\boldsymbol{B}_{\mu_1} + \boldsymbol{B}_{\mu_2}$ and the homogeneous solution $\boldsymbol{\omega}_i$ ($\boldsymbol{\omega}_j$), which are linearly independent each other. Thus, we can construct a continuous family of bifurcated states by superposing $\boldsymbol{\omega}_i$ or $\boldsymbol{\omega}_j$ on the trunk solution with complex amplitudes α_i and α_j. In the case (B), i.e. $\mu_1 = \lambda_i \neq \lambda_{0,0,2l'}$ and $\mu_1 \neq \lambda_j$, we obtain

$$\text{(B)} \quad \boldsymbol{B}_{\lambda_i,\mu_2,\alpha_i} = \alpha_i \boldsymbol{\omega}_i + \boldsymbol{B}_{\mu_1} + \boldsymbol{B}_{\mu_2}, \tag{2.93}$$

and in the case (C), i.e. $\mu_1 = \lambda_i \neq \lambda_{0,0,2l'}$ and $\mu_2 = \lambda_j \neq \lambda_{0,0,2l'}$, we obtain

$$\text{(C)} \quad \boldsymbol{B}_{\lambda_i,\lambda_j,\alpha_i,\alpha_j} = \alpha_i \boldsymbol{\omega}_i + \alpha_j \boldsymbol{\omega}_j + \boldsymbol{B}_{\mu_1} + \boldsymbol{B}_{\mu_2}. \tag{2.94}$$

The amplitudes $|\alpha_i|$ and $|\alpha_j|$ are determined, as we have noted in the subsection 2.1.5, by using the magnetic helicity value c_1 and the canonical helicity value c_2 as bifurcation parameters, where the phase of α_i and α_j still are arbitrary.

The bifurcated branch-(B) solution (2.93) and branch-(C) solution (2.94), composed of the symmetric function ($\boldsymbol{B}_{\mu_1} + \boldsymbol{B}_{\mu_2}$) and the helical CK functions ($\boldsymbol{\omega}_i$ and $\boldsymbol{\omega}_i$), are fully three dimensional. And yet, we can always define a "helical flux function" φ_B of (2.93) by which we can integrate the magnetic filed lines of the branch-(B) solution. Moreover, when the Fourier coefficient vectors (wavenumber

vectors) of $\boldsymbol{\omega}_i$ and $\boldsymbol{\omega}_j$ are parallel to each other, we can also define a helical flux function φ_C of the branch-(C) solution (2.94). Let k_y and k_z be the Fourier coefficients of $\boldsymbol{\omega}_i$. We denote

$$\bar{k}_y := k_y/\sqrt{k_y^2 + k_z^2}, \quad \bar{k}_z := k_z/\sqrt{k_y^2 + k_z^2}, \tag{2.95}$$

and define

$$\eta := \bar{k}_y y + \bar{k}_z z, \quad \zeta := -\bar{k}_z y + \bar{k}_y z, \tag{2.96}$$

from which we obtain the normalized wavenumber vector $\nabla\eta$ and its normal vector $\nabla\zeta$. Putting

$$\varphi_i := \left\{\bar{k}_y \sin(k_x x + \theta) + (k_x \bar{k}_z/\lambda_j)\cos(k_x x + \theta)\right\} e^{i(k_y y + k_z z + \chi)}, \tag{2.97}$$

we may rewrite $\boldsymbol{\omega}_i$ as

$$\boldsymbol{\omega}_i = \Re\left[\nabla\varphi_i \times \nabla\zeta + \lambda_i \varphi_i \nabla\zeta\right]. \tag{2.98}$$

When the Fourier coefficients vector of $\boldsymbol{\omega}_j$ is parallel to that of $\boldsymbol{\omega}_i$, using the same normal vector $\nabla\zeta$, we can also rewrite $\boldsymbol{\omega}_j$ as

$$\boldsymbol{\omega}_j = \Re\left[\nabla\varphi_j \times \nabla\zeta + \lambda_j \varphi_j \nabla\zeta\right]. \tag{2.99}$$

The ambient, finite-flux Beltrami fields $\boldsymbol{B}_{\mu_1}$ and $\boldsymbol{B}_{\mu_2}$ can be also cast into a similar form. Putting

$$\varphi_{\mu_s} = (B_{\mu_s}/\mu_s)\cos\left\{\mu_s x + \theta - \tan^{-1}(\bar{k}_y/\bar{k}_z)\right\} \quad (s = 1, 2), \tag{2.100}$$

we may write

$$\boldsymbol{B}_{\mu_s} = \nabla\varphi_{\mu_s} \times \nabla\zeta + \mu_s \varphi_{\mu_s} \nabla\zeta \qquad (s = 1, 2). \tag{2.101}$$

Combining φ_i, φ_j, φ_{μ_1} and φ_{μ_2}, we obtain the helical flux functions $\varphi_B := \alpha_i\varphi_i + \varphi_{\mu_1} + \varphi_{\mu_2}$ and $\varphi_C := \alpha_i\varphi_i + \alpha_j\varphi_j + \varphi_{\mu_1} + \varphi_{\mu_2}$, by which we may write

$$\boldsymbol{B}_{\lambda_i,\mu_2,\alpha_i} = \Re\left[\nabla\varphi_B \times \nabla\zeta + (\alpha_i\lambda_i\varphi_i + \mu_1\varphi_{\mu_1} + \mu_2\varphi_{\mu_2})\nabla\zeta\right], \tag{2.102}$$

$$\boldsymbol{B}_{\lambda_i,\lambda_j,\alpha_i,\alpha_j} = \Re\left[\nabla\varphi_C \times \nabla\zeta + (\alpha_i\lambda_i\varphi_i + \alpha_j\lambda_j\varphi_j + \mu_1\varphi_{\mu_1} + \mu_2\varphi_{\mu_2})\nabla\zeta\right]. \tag{2.103}$$

Hence, the level sets of the helical flux functions φ_B and φ_C give the magnetic surfaces of $\boldsymbol{B}_{\lambda_i,\mu_2,\alpha_i}$ and $\boldsymbol{B}_{\lambda_i,\lambda_j,\alpha_i,\alpha_j}$, respectively.

2.2.4 Helicity leaves

Now we can concretely calculate values of the magnetic helicity (2.23) and the canonical helicity (2.24) as functions of μ_1, μ_2, α_i and α_j by using (2.76), (2.89), (2.90), (2.93), and (2.94). In the subsection 2.1.5, we introduced helicity-value functions $\mathcal{C}_{sA}(\mu_1,\mu_2)$, $\mathcal{C}_{sB}(\alpha_i,\mu_2;\lambda_i)$ and $\mathcal{C}_{sC}(\alpha_i,\alpha_j;\lambda_i,\lambda_j)$ $(s=1,2)$. For sake of simplicity, we denote collectively these functions by $\mathcal{C}_s(\alpha_i,\alpha_j,\mu_1,\mu_2)$. Then, we obtain

$$\begin{aligned}
&\mathcal{C}_1(\alpha_i,\alpha_j,\mu_1,\mu_2)\\
=\;& \frac{\alpha_i^2}{2\lambda_i}\|\boldsymbol{\omega}_i\|^2 + \frac{\alpha_j^2}{2\lambda_j}\|\boldsymbol{\omega}_j\|^2\\
&+\frac{L_yL_z}{8}\left\{\frac{1}{\sin^2(\mu_1/2)}\frac{\mu_1}{(\mu_1-\mu_2)^2}\left(Q_{2y}^2+Q_{2z}^2\right)\right.\\
&+\frac{1}{\sin^2(\mu_2/2)}\frac{\mu_2}{(\mu_2-\mu_1)^2}\left(Q_{1y}^2+Q_{1z}^2\right)\\
&-2\frac{1}{\sin(\mu_1/2)\sin(\mu_2/2)}\sin\left(\frac{\mu_1-\mu_2}{2}\right)\frac{\mu_1+\mu_2}{(\mu_1-\mu_2)^3}(Q_{1y}Q_{2y}+Q_{1z}Q_{2z})\\
&-\frac{1}{\sin^2(\mu_1/2)}\frac{\sin\mu_1}{\mu_1-\mu_2}\left(\phi_{my}Q_{2y}+\phi_{mz}Q_{2z}\right)\\
&\left.-\frac{1}{\sin^2(\mu_2/2)}\frac{\sin\mu_2}{\mu_2-\mu_1}\left(\phi_{my}Q_{1y}+\phi_{mz}Q_{1z}\right)\right\},
\end{aligned} \tag{2.104}$$

$$
\begin{aligned}
& \mathcal{C}_2(\alpha_i, \alpha_j, \mu_1, \mu_2) \\
= \; & \frac{\alpha_i^2 \left(\lambda_i - \nu_1\right)^2}{2\lambda_i \nu_2^2} \|\boldsymbol{\omega}_i\|^2 + \frac{\alpha_j^2 \left(\lambda_j - \nu_1\right)^2}{2\lambda_j \nu_2^2} \|\boldsymbol{\omega}_j\|^2 \\
& + \frac{L_y L_z}{8} \left\{ \frac{1}{\sin^2(\mu_1/2)} \frac{\mu_1 (\nu_1 - \mu_1)^2}{\nu_2^2 (\mu_1 - \mu_2)^2} \left(Q_{2y}^2 + Q_{2z}^2\right) \right. \\
& + \frac{1}{\sin^2(\mu_2/2)} \frac{\mu_2 (\nu_1 - \mu_2)^2}{\nu_2^2 (\mu_2 - \mu_1)^2} \left(Q_{1y}^2 + Q_{1z}^2\right) \\
& - 2 \frac{1}{\sin(\mu_1/2) \sin(\mu_2/2)} \sin\left(\frac{\mu_1 - \mu_2}{2}\right) \frac{\mu_1 + \mu_2}{\delta_i^2 \nu_2^2 (\mu_1 - \mu_2)^3} (Q_{1y} Q_{2y} + Q_{1z} Q_{2z}) \\
& - 2 \frac{1}{\sin^2(\mu_1/2)} \left(1 + \frac{\nu_1 - \mu_1}{2\nu_2}\right) \frac{\sin \mu_1}{\mu_1 - \mu_2} \left(\phi_{cy} Q_{2y} + \phi_{cz} Q_{2z}\right) \\
& \left. - 2 \frac{1}{\sin^2(\mu_2/2)} \left(1 + \frac{\nu_1 - \mu_2}{2\nu_2}\right) \frac{\sin \mu_2}{\mu_2 - \mu_1} \left(\phi_{cy} Q_{1y} + \phi_{cz} Q_{1z}\right) \right\}. \qquad (2.105)
\end{aligned}
$$

The terms pertinent to $\boldsymbol{\omega}_i$ and $\boldsymbol{\omega}_j$ appears only in the bifurcation cases (B) and (C).

We obtain double-Beltrami equilibria with given helicity values c_1 and c_2 from μ_1 and μ_2 satisfying the helicity matching conditions $\mathcal{C}_1(\alpha_i, \alpha_j, \mu_1, \mu_2) = c_1$ and $\mathcal{C}_2(\alpha_i, \alpha_j, \mu_1, \mu_2) = c_2$. Fig.2.1 shows the contour plots of $\mathcal{C}_1(\alpha_i, \alpha_j, \mu_1, \mu_2)$ and $\mathcal{C}_2(\alpha_i, \alpha_j, \mu_1, \mu_2)$ projected onto the μ_1-μ_2 plane. We can regard these contour plots as the projection of helicity leaves onto the μ_1-μ_2 plane. It can be seen that the helicity values diverge on lines $\mu_1 = \lambda_{0,0,2} = 2\pi$ and $\mu_2 = -\lambda_{0,0,2} = -2\pi$, and the helicity leaves split. This divergence implies the non-existence of equilibrium at $\mu_1 = \lambda_{0,0,2}$ or $\mu_2 = -\lambda_{0,0,2}$ because of the violation of the orthogonality condition (2.47) at these eigenvalues.

Let us focus on a line $\mu_1 + \mu_2 = 0$, where we can collectively denote Beltrami parameters by $\mu := \mu_1 = -\mu_2$. (Lyapunov stability of double-Beltrami fields with such parameters is studied in [48]. We will develop this study in Appendix B.) Fig.2.2 shows the magnetic helicity value $\mathcal{C}_2$ on the line $\mu_1 + \mu_2 = 0$, as a function of

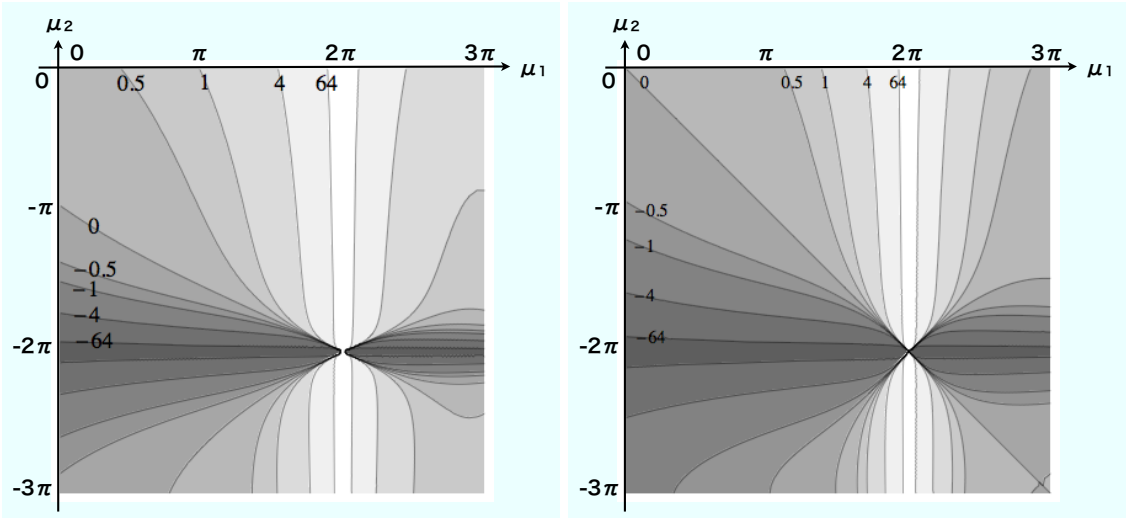

Figure 2.1: Contour plots of the magnetic helicity value $\mathcal{C}_1(0,0,\mu_1,\mu_2)$ (left) and the canonical helicity value $\mathcal{C}_1(0,0,\mu_1,\mu_2)$ (right) projected onto μ_1-μ_2 plane ($0 < \mu_1 < 3\pi, -3\pi < \mu_2 < 0$). Ion-skin length and flux parameters are as follows: $\delta_i = 1/5\pi$, $\phi_{mz} = \sqrt{\delta_i}$, $\phi_{my} = \phi_{cy} = \phi_{cz} = 0$. Geometry parameters are as follows: $L_y = L_z = 2$. In this geometry, $\lambda_{0,0,2} = 2\pi$.

μ. At $\mu = \sqrt{2}\pi = \lambda_{1,0,1}$, where the orthogonality condition (2.56) holds, the helical branch-(C) bifurcates. At $\mu = 2\pi = \lambda_{0,0,2}$, where the orthogonality condition (2.56) breaks, the helicity value diverges. It can be seen that for a small magnetic helicity value , there only exists branch-(A) solution (symmetric double-Beltrami field), on the other hand, for a large value, branch-(C) solution (helical double-Beltrami field) bifurcates. In Fig.2.3, we plot the contours of a helical-flux function φ_C of the branch-(C) solution bifurcated from $\mu_1 = -\mu_2 = \sqrt{2}\pi$.

2.3 Summary and Discussion

We have formulated the bifurcation theory of double-Beltrami fields with the magnetic and canonical fluxes as the fixed parameters and the magnetic and canonical helicities as control parameters. This bifurcation theory can be viewed

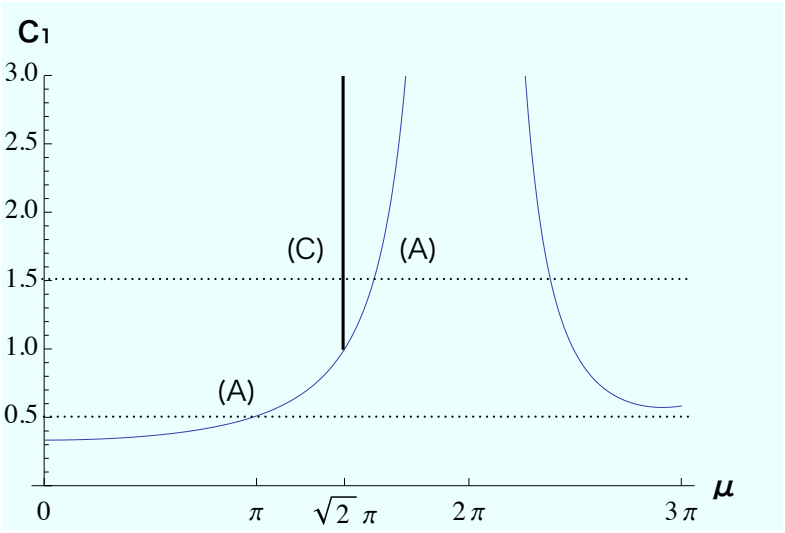

Figure 2.2: Magnetic helicity value $\mathcal{C}_1(0, 0, \mu, -\mu)$ on the line $\mu_1 + \mu_2 = 0$.

as the problem of the existence and uniqueness of solutions of the inhomogeneous double-Beltrami equation (2.37). It is the fixed magnetic and canonical fluxes that give the inhomogeneous part to (2.37). The particular solution of (2.37) becomes the trunk of the bifurcation. As the values of the magnetic and canonical helicities change, Beltrami parameters μ_1 and μ_2 in (2.37) also change. When μ_1 or μ_2 is equal to the eigenfunction of the self-adjoint curl operator $\mathcal{S}$, the homogeneous part of (2.37) has non-trivial solutions (eigenfunctions of $\mathcal{S}$) and the uniqueness of solutions of (2.37) breaks, in other words, bifurcation occurs. Namely, in our bifurcation theory, bifurcation solutions are represented by superposition of homogeneous and particular solutions. It should be noted that the simultaneous existence of homogeneous and particular solutions is non-trivial and, therefore, the existence of bifurcation solutions is also non-trivial. On this issue, we have proved the sufficient and necessary condition of bifurcation (Theorem 2 and Theorem 3), by which we can know what eigenvalues of $\mathcal{S}$ brings the bifurcation.

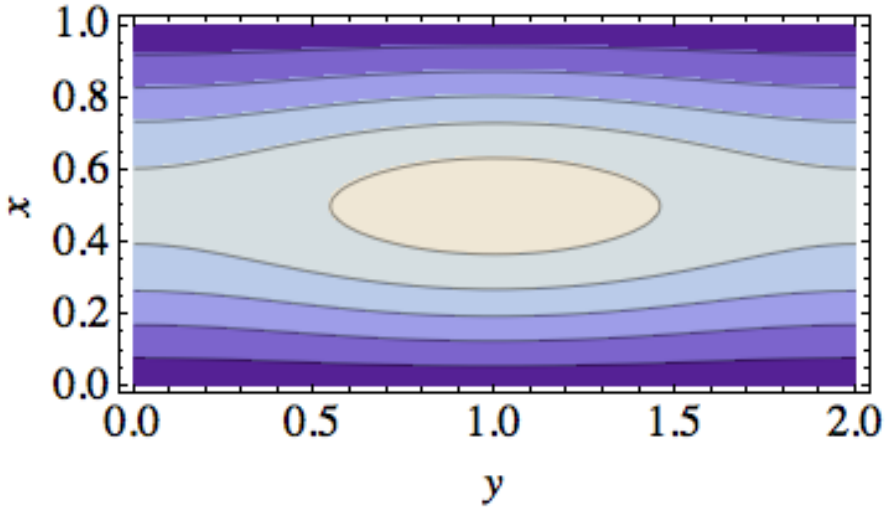

Figure 2.3: Contours of a helical-flux function φ_C on a cross-section of the slab domain.

We have presented a concrete example of bifurcation in a slab geometry. In Fig.2.1, it can be seen that the magnetic and canonical helicity leaves projected onto μ_1-μ_2 plane are ripped apart due to the fixed fluxes. On the rips in leaves, the helicity values diverge, which means the non-existence of the particular solution on these rips. This can be viewed as a consequence of the violation of the orthogonality condition given in Theorem 2 or Theorem 3. In this geometry, the symmetric doubl-Beltrami field gives the trunk solution, which is helically deformed (shown in Fig.2.3) by superposition of homogeneous solutions emerging from bifurcation points.

Chapter 3

Linear tearing mode theory of Double-Beltrami fields

3.1 Linear analysis of Tearing mode

In this section, we analyze the relation between the helical bifurcation and the tearing mode. As in the case of single-Beltrami field[15], also in the case of double-Beltrami field, the tearing mode is viewed as a perturbed, singular equilibrium state characterized by the singular Casimir element (helical-flux) stemming from the resonant singularity of the linearized poisson operator. However, there is a difference between the cases of single-Beltrami and double-Beltrami fields. In the single-Beltrami case, the tearing mode was similar to the branch-(B) helical relaxed state given by superposition of a Beltrami eigenfunction $\boldsymbol{\omega}_i$ on the trunk symmetric Beltrami field. On the other hand, in the double-Beltrami case, the tearing mode is similar to the branch-(C) solution given by two Beltrami eigenfunctions $\boldsymbol{\omega}_i$ and $\boldsymbol{\omega}_j$ rather than the branch-(B) solution. We need two eigenfunctions to obtain the tearing mode with an appropriate flow $\tilde{\boldsymbol{V}} \in H^1(\Omega)$.

3.1.1 Linearized equation around the Beltrami equilibrium

Here, we consider perturbations $\tilde{u} = {}^t(\tilde{\boldsymbol{P}}_\sigma, \tilde{\boldsymbol{A}})$ around the double-Beltrami field u_{μ_1,μ_2}. We assume that perturbations do not change the canonical and magnetic fluxes, that is, $\nabla \times \tilde{\boldsymbol{A}}, \nabla \times \tilde{\boldsymbol{P}}_\sigma \in L^2_\Sigma(\Omega)$. The Hamiltonian form of the linearized equation is is given by

$$\partial_t \tilde{u} = \mathcal{J}_{\mu_1,\mu_2} \partial_{\tilde{u}} U_{\mu_1,\mu_2}(\tilde{u}) \tag{3.1}$$

where $\mathcal{J}_{\mu_1,\mu_2}$ is the Poisson operator (2.21) evaluated at the equilibrium point u_{μ_1,μ_2}, that is,

$$\mathcal{J}_{\mu_1,\mu_2} := \mathcal{J}(u_{\mu_1,\mu_2}) = \delta_i \begin{pmatrix} -\mathcal{P}_\sigma \boldsymbol{\Omega}_{\mu_1,\mu_2} \times & 0 \\ 0 & \boldsymbol{B}_{\mu_1,\mu_2} \times \end{pmatrix}, \tag{3.2}$$

and U_{μ_1,μ_2} is the linearized energy-Casimir functional defined as

$$\begin{aligned} U_{\mu_1,\mu_2}(\tilde{\boldsymbol{P}}_\sigma, \tilde{\boldsymbol{A}}) &:= \mathcal{H}_\nu(u_{\mu_1,\mu_2} + \tilde{u}) - \mathcal{H}_\nu(u_{\mu_1,\mu_2}) \\ &= \frac{1}{2}\int_\Omega \left\{ \left| \frac{\tilde{\boldsymbol{P}}_\sigma - \mathcal{P}_\sigma \tilde{\boldsymbol{A}}}{\delta_i} \right|^2 + \left| \nabla \times \tilde{\boldsymbol{A}} \right|^2 \right. \\ &\qquad \left. -\nu_1 \tilde{\boldsymbol{A}} \cdot (\nabla \times \tilde{\boldsymbol{A}}) - \nu_2 \tilde{\boldsymbol{P}}_\sigma \cdot (\nabla \times \tilde{\boldsymbol{P}}_\sigma) \right\} d\boldsymbol{x}. \end{aligned} \tag{3.3}$$

Let us decompose the member of $\mathrm{Ker}\mathcal{J}_{\mu_1,\mu_2}$ into the following independent classes

$$\begin{pmatrix} \boldsymbol{\omega} \\ 0 \end{pmatrix}, \quad \begin{pmatrix} 0 \\ \boldsymbol{j} \end{pmatrix}, \tag{3.4}$$

where $\boldsymbol{\omega}$ and $\boldsymbol{j}$ are such that

$$\mathcal{P}_\sigma \boldsymbol{\Omega}_{\mu_1,\mu_2} \times \boldsymbol{\omega} = 0, \quad \boldsymbol{B}_{\mu_1,\mu_2} \times \boldsymbol{j} = 0. \tag{3.5}$$

Integrating them, we obtain the following independent Casimir elements

$$C_\omega(\tilde{u}) := \int_\Omega \boldsymbol{\omega} \cdot \tilde{\boldsymbol{P}}_\sigma d\boldsymbol{x}, \quad C_j(\tilde{u}) := \int_\Omega \boldsymbol{j} \cdot \tilde{\boldsymbol{A}} d\boldsymbol{x}. \tag{3.6}$$

3.1.2 Resonance singularity and helical-flux Casimir elements

In what follows, we consider the slab geometry introduced in the beginning of Sec.2.2, in which we can write

$$\boldsymbol{\Omega}_{\mu_1,\mu_2} = \begin{pmatrix} 0 \\ \Omega_y(x) \\ \Omega_z(x) \end{pmatrix}, \quad \boldsymbol{B}_{\mu_1,\mu_2} = \begin{pmatrix} 0 \\ B_y(x) \\ B_z(x) \end{pmatrix}. \tag{3.7}$$

Here, we consider 'singular' Casimir elements stemming from the resonance singularity of the poisson operator $\mathcal{J}_{\mu_1,\mu_2}$. Let us consider

$$\boldsymbol{\omega} = \partial_x\hat{\theta}(x)\begin{pmatrix} 0 \\ -\hat{k}_z \\ \hat{k}_y \end{pmatrix}\Re e^{i(\hat{k}_y y+\hat{k}_z z+\hat{\chi})}, \quad \boldsymbol{j} = \partial_x\theta(x)\begin{pmatrix} 0 \\ -k_z \\ k_y \end{pmatrix}\Re e^{i(k_y y+k_z z+\chi)}. \tag{3.8}$$

Notice that the prime $'$ here does not mean any derivative but it just distinguishes the variable of $\boldsymbol{\omega}$ from $\boldsymbol{b}$. Putting them into (3.5) yields

$$(\hat{k}_y\Omega_y(x)+\hat{k}_z\Omega_z(x))\partial_x\hat{\theta}(x)=0, \quad (k_yB_y(x)+k_zB_z(x))\partial_x\theta(x)=0, \tag{3.9}$$

which have singular solutions

$$\partial_x\hat{\theta}(x)=\delta(x-\hat{x}_r), \quad \partial_x\theta(x)=\delta(x-x_r) \tag{3.10}$$

if there exist $\hat{x}_r$ and x_r satisfying the resonance condition

$$\hat{k}_y\Omega_y(\hat{x}_r)+\hat{k}_z\Omega_z(\hat{x}_r)=0, \quad k_y\Omega_y(x_r)+k_z\Omega_z(x_r)=0. \tag{3.11}$$

Putting (3.8) with (3.10) into (3.6), we obtain Singular Casimir elements

$$C_\omega = \int_\Omega \delta(x-\hat{x}_r)\Re e^{i(\hat{k}_y y+\hat{k}_z z+\hat{\chi})}\begin{pmatrix} 0 \\ -\hat{k}_z \\ \hat{k}_y \end{pmatrix}\cdot\tilde{\boldsymbol{P}}_\sigma d\boldsymbol{x}, \tag{3.12}$$

$$C_j = \int_\Omega \delta(x-x_r)\Re e^{i(k_y y+k_z z+\chi)}\begin{pmatrix} 0 \\ -k_z \\ k_y \end{pmatrix}\cdot\tilde{\boldsymbol{A}} d\boldsymbol{x}. \tag{3.13}$$

The second Casimir C_j is nothing but the helical-flux Casimir, which has been found in [15], and the first one C_ω is the counterpart of ion canonical momentum $\tilde{\boldsymbol{P}}_\sigma$ to the electron canonical momentum $\tilde{\boldsymbol{A}}$. We may rewrite them in the following form:

$$C_\omega = \int_\Omega \delta(x-\hat{x}_r)\nabla x\times\nabla\sin(\hat{k}_y y+\hat{k}_z z+\hat{\chi})\cdot\tilde{\boldsymbol{P}}_\sigma d\boldsymbol{x} = \int_{\hat{\Gamma}_r}\nabla x\times\nabla\sin(\hat{k}_y y+\hat{k}_z z+\hat{\chi})\cdot\tilde{\boldsymbol{P}}_\sigma d\boldsymbol{x}, \tag{3.14}$$

$$C_j = \int_\Omega \delta(x-x_r)\nabla x\times\nabla \sin(k_y y+k_z z+\chi)\cdot\tilde{\boldsymbol{A}}d\boldsymbol{x} = \int_{\Gamma_r} \nabla x\times\nabla \sin(k_y y+k_z z+\chi)\cdot\tilde{\boldsymbol{A}}d\boldsymbol{x}, \tag{3.15}$$

where $\hat{\Gamma}_r$ and Γ_r are the resonant surfaces of $x = \hat{x}_r$ and $x = x_r$. The resonant Fourier component of $\tilde{\boldsymbol{P}}_\sigma$ and $\tilde{\boldsymbol{A}}$, i.e. the parts proportional to $\Re e^{i(\hat{k}_y y+\hat{k}_z z+\hat{\chi})}$ and $\Re e^{i(k_y y+k_z z+\chi)}$, make these integral non-zero and hence are forbidden to change.

3.1.3 Linear Tearing mode

By invoking the helical-flux Casimir C_j, we can obtain 'tearing mode' as a singular equilibrium state. Let us consider an energy-Casimir functional

$$\mathcal{F}_{\mu_1,\mu_2,\beta} := U_{\mu_1,\mu_2}(\tilde{u}) - \beta C_j(\tilde{u}), \tag{3.16}$$

where β is a Lagrange multiplier. Because C_j is the surface integral on the resonant surface Γ_r ($x = x_r$), it is convenient to represent the linearized energy-Casimir functional U_{μ_1,μ_2} as follows:

$$\begin{aligned} U_{\mu_1,\mu_2}(\tilde{u}) \;=\; & \frac{1}{2}\int_{\Omega\backslash\Gamma_r} \left\{ \left| \frac{\tilde{\boldsymbol{P}}_\sigma - \mathcal{P}_\sigma\tilde{\boldsymbol{A}}}{\delta_i} \right|^2 + \left(\nabla\times\tilde{\boldsymbol{B}} - \nu_1\tilde{\boldsymbol{B}}\right)\cdot\tilde{\boldsymbol{A}} \right. \\ & \left. -\nu_2\nabla\times\tilde{\boldsymbol{P}}_\sigma\cdot\tilde{\boldsymbol{P}}_\sigma \right\} d\boldsymbol{x} + \frac{1}{2}\int_{\Gamma_r} [[\nabla x\times\tilde{\boldsymbol{B}}\cdot\tilde{\boldsymbol{A}}]]_{x_r} dydz \end{aligned} \tag{3.17}$$

where $[[f]]_{x_r}$ is the jump across $x = x_r$:

$$[[f]]_{x_r} := \lim_{\epsilon\downarrow 0}\{f(x_r+\epsilon) - f(x_r-\epsilon)\} \tag{3.18}$$

We can find equilibrium points by

$$\partial_{\tilde{u}}\mathcal{F}_{\mu_1,\mu_2,\beta} := \partial_{\tilde{u}}\left[U_{\mu_1,\mu_2}(\tilde{u}) - \beta C_j(\tilde{u})\right] = 0, \tag{3.19}$$

the Euler-Lagrange equation of which is

$$\frac{\tilde{\boldsymbol{P}}_\sigma - \mathcal{P}_\sigma\tilde{\boldsymbol{A}}}{\delta_i^2} = \nabla\times\tilde{\boldsymbol{B}} - \nu_1\tilde{\boldsymbol{B}} \quad (\text{in } \Omega\backslash\Gamma_r), \tag{3.20}$$

$$\frac{\tilde{\boldsymbol{P}}_\sigma - \mathcal{P}_\sigma \tilde{\boldsymbol{A}}}{\delta_i^2} = \nu_2 \nabla \times \tilde{\boldsymbol{P}} \quad (\text{in } \Omega \backslash \Gamma_r), \tag{3.21}$$

$$[[\nabla x \times \tilde{\boldsymbol{B}}]]_{x_r} = \beta \nabla x \times \nabla \sin(k_y y + k_z z + \chi). \tag{3.22}$$

Combining (3.20) and (3.21), we obtain the "double Beltrami equation"

$$\nabla \times \nabla \times \tilde{\boldsymbol{B}} - \left(\nu_1 + \frac{1}{\delta_i^2 \nu_2}\right) \nabla \times \tilde{\boldsymbol{B}} + \frac{1}{\delta_i^2}\left(1 + \frac{\nu_1}{\nu_2}\right) \tilde{\boldsymbol{B}} = 0, \tag{3.23}$$

which may be rewritten as

$$(\text{curl} - \mu_1)(\text{curl} - \mu_2)\tilde{\boldsymbol{B}} = 0. \tag{3.24}$$

The ion-flow field $\tilde{\boldsymbol{V}} = (\tilde{\boldsymbol{P}}_\sigma - \mathcal{P}_\sigma \tilde{\boldsymbol{A}})/\delta_i$ is determined by $\tilde{\boldsymbol{B}}$ through (3.20) as

$$\tilde{\boldsymbol{V}} = \delta_i \left(\nabla \times \tilde{\boldsymbol{B}} - \nu_1 \tilde{\boldsymbol{B}}\right). \tag{3.25}$$

We separate the domain at $x = x_r$ and solve (3.24) in each sub-domain with assuming a form

$$\tilde{\boldsymbol{B}} = \alpha_1 \tilde{\boldsymbol{\omega}}_1 + \alpha_2 \tilde{\boldsymbol{\omega}}_2, \tag{3.26}$$

where

$$\tilde{\boldsymbol{\omega}}_i = \nabla \tilde{\Psi}_i \times \nabla \zeta + \mu_i \tilde{\Psi}_i \nabla \zeta, \quad \tilde{\Psi}_i := \tilde{\psi}_i(x) \Re e^{i(k_y y + k_z z + \chi)} \quad (i = 1, 2). \tag{3.27}$$

The solution is given by

$$\tilde{\psi}_i = \begin{cases} \sin \tilde{k}_i x / \sin \tilde{k}_i x_r & (0 < x < x_r), \\ \sin \tilde{k}_i (1 - x) / \sin \tilde{k}_i (1 - x_r) & (x_r < x < 1), \end{cases} \tag{3.28}$$

where

$$\tilde{k}_i := \sqrt{\mu_i^2 - k_y^2 - k_z^2}. \tag{3.29}$$

We have the following expression

$$\tilde{\boldsymbol{\omega}}_i = \Re \begin{pmatrix} i\sqrt{k_y^2 + k_z^2}\tilde{\Psi}_i \\ -\bar{k}_y \tilde{\Psi}_i' - \mu_i \bar{k}_z \tilde{\Psi}_i \\ -\bar{k}_z \tilde{\Psi}_i' + \mu_i \bar{k}_y \tilde{\Psi}_i \end{pmatrix}. \tag{3.30}$$

where $f' := df/dx$. The vector potential of $\tilde{\boldsymbol{\omega}}_i$ is given by

$$\tilde{\boldsymbol{A}}_i = \Re\tilde{\Psi}_i \begin{pmatrix} i\mu_i/\sqrt{k_y^2+k_z^2} \\ -\bar{k}_z \\ \bar{k}_y \end{pmatrix}, \tag{3.31}$$

which belongs to $H^1(\Omega)$ and satisfies $\boldsymbol{n}\times\tilde{\boldsymbol{A}}_i = 0$, therefore, the condition we have imposed on $\tilde{\boldsymbol{A}}_i$ is satisfied. Note that $\tilde{\boldsymbol{A}}_i \notin H^1_{\Sigma\Sigma}(\Omega)$, therefore, it satisfies $\nabla\times\tilde{\boldsymbol{A}}_i = \tilde{\boldsymbol{\omega}}_i$ but not $\tilde{\boldsymbol{A}}_i = \tilde{\boldsymbol{\omega}}_i/\mu_i$.

We also have to check the condition imposed on $\tilde{\boldsymbol{V}} = (\tilde{\boldsymbol{P}}_\sigma - \mathcal{P}_\sigma\tilde{\boldsymbol{A}})/\delta_i$, that is, $\tilde{\boldsymbol{V}} \in H^1(\Omega)$. Inserting (3.26) into (3.25), we can calculate the jump of $\tilde{\boldsymbol{V}}$ at $x = x_r$ as

$$\begin{aligned}
[[\tilde{\boldsymbol{V}}]]_{x_r} &= \delta_i\left\{\alpha_1(\mu_1-\nu_1)[[\tilde{\boldsymbol{\omega}}_1]]_{x_r} + \alpha_2(\mu_2-\nu_1)[[\tilde{\boldsymbol{\omega}}_2]]_{x_r}\right\} \\
&= -\delta_i\left\{\alpha_1(\mu_1-\nu_1)[[\tilde{\psi}_1']]_{x_r} + \alpha_2(\mu_2-\nu_1)[[\tilde{\psi}_2']]_{x_r})\right\}\nabla\sin(k_y y + k_z z + \chi),
\end{aligned} \tag{3.32}$$

which must become zero. Otherwise, the derivative of $\tilde{\boldsymbol{V}}$ would produce the delta function, which is not an element of $L^2(\Omega)$. To satisfy this condition, we have to set the amplitudes α_1 and α_2 as

$$\alpha_1 = -\alpha(\mu_2-\nu_1)[[\tilde{\psi}_2']]_{x_r}, \quad \alpha_2 = \alpha(\mu_1-\nu_1)[[\tilde{\psi}_1']]_{x_r}, \tag{3.33}$$

where α is an arbitrary constant, and with which certainly $[[\tilde{\boldsymbol{V}}]]_{x_r} = 0$.

Remark 3.1.1. In the above, we did not use the canonical singular Casimir element C_ω because there is, in $U_{\mu_1,\mu_2}(\tilde{u})$, no term that would balance with C_ω. Although $|\nabla\times\tilde{\boldsymbol{A}}|^2$, the highest derivative term of $\tilde{\boldsymbol{A}}$ in (3.3), produces the term $[[\nabla x\times\tilde{\boldsymbol{B}}\cdot\tilde{\boldsymbol{A}}]]_{x_r}$ which can balance with the magnetic helical-flux Casimir C_j, $\tilde{\boldsymbol{P}}_\sigma\times(\nabla\times\tilde{\boldsymbol{P}}_\sigma)$, the highest derivative term of $\tilde{\boldsymbol{P}}_\sigma$ in (3.3) , does not produce such a term.

3.1.4 Criterion of tearing instability

Here we will estimate the energy (3.17) of the singular solution (tearing mode) obtained in the previous subsection.

Preliminarily, we calculate the following. From (3.30) and (3.31), we obtain

$$\tilde{\boldsymbol{\omega}}_i \times \tilde{\boldsymbol{A}}_j \cdot \nabla x = -\Re\tilde{\Psi}_i' \cdot \Re\tilde{\Psi}_j = -\tilde{\psi}_i'\tilde{\psi}_j \cos^2(k_y y + k_z z + \chi), \tag{3.34}$$

the jump of which can be calculated as

$$[[\tilde{\boldsymbol{\omega}}_i \times \tilde{\boldsymbol{A}}_j \cdot \nabla x]]_{x_r} = -[[\tilde{\psi}_i']]_{x_r} \cos^2(k_y y + k_z z + \chi), \tag{3.35}$$

where we have used $\tilde{\psi}_j(x_r) = 1$. Integrating it on the resonance surface Γ_r, we obtain

$$\int_{\Gamma_r} [[\tilde{\boldsymbol{\omega}}_i \times \tilde{\boldsymbol{A}}_j \cdot \nabla x]]_{x_r} dydz = -\frac{L_y L_z}{2}[[\tilde{\psi}_i']]_{x_r}. \tag{3.36}$$

Using this result, we can easily calculate the energy (3.17) of the tearing mode as

$$\begin{aligned} U_{\mu_1,\mu_2} &= \int_{\Gamma_r} [[\tilde{\boldsymbol{B}} \times \tilde{\boldsymbol{A}} \cdot \nabla x]]_{x_r} dydz \\ &= \int_{\Gamma_r} [[(\alpha_1\tilde{\boldsymbol{\omega}}_1 + \alpha_2\tilde{\boldsymbol{\omega}}_2) \times (\alpha_1\tilde{\boldsymbol{A}}_1 + \alpha_2\tilde{\boldsymbol{A}}_2) \cdot \nabla x]]_{x_r} dydz \\ &= -\frac{L_y L_z}{2}\left\{\alpha_1^2[[\tilde{\psi}_1']]_{x_r} + \alpha_1\alpha_2[[\tilde{\psi}_1']]_{x_r} + \alpha_1\alpha_2[[\tilde{\psi}_2']]_{x_r} + \alpha_2^2[[\tilde{\psi}_2']]_{x_r}\right\} \end{aligned} \tag{3.37}$$

In terms of $\Delta' := [[\tilde{\psi}'/\tilde{\psi}]]_{x_r}$, the criterion of the tearing instability, the energy (3.37) can be rewritten as

$$U_{\mu_1,\mu_2} = -\frac{L_y L_z}{2}\tilde{\psi}(x_r)^2\Delta', \tag{3.38}$$

which can be easily verified by estimating Δ' as follows:

$$\begin{aligned}
\Delta' &= [[\frac{\tilde{\psi}'}{\tilde{\psi}}]]_{x_r} = [[\frac{\tilde{\psi}\tilde{\psi}'}{\tilde{\psi}^2}]]_{x_r} \\
&= \frac{1}{\tilde{\psi}(x_r)^2}[[(\alpha_1\tilde{\psi}_1 + \alpha_2\tilde{\psi}_2)(\alpha_1\tilde{\psi}_1' + \alpha_2\tilde{\psi}_2')]]_{x_r} \\
&= \frac{1}{\tilde{\psi}(x_r)^2}[[\left\{\alpha_1^2\tilde{\psi}_1\tilde{\psi}_1' + \alpha_1\alpha_2\left(\tilde{\psi}_2\tilde{\psi}_1' + \tilde{\psi}_1\tilde{\psi}_2'\right) + \alpha_2^2\tilde{\psi}_1\tilde{\psi}_2'\right\}]]_{x_r} \\
&= \frac{1}{\tilde{\psi}(x_r)^2}\left\{\alpha_1^2[[\tilde{\psi}_1']]_{x_r} + \alpha_1\alpha_2[[\tilde{\psi}_1']]_{x_r} + \alpha_1\alpha_2[[\tilde{\psi}_2']]_{x_r} + \alpha_2^2[[\tilde{\psi}_2']]_{x_r}\right\}, \quad (3.39)
\end{aligned}$$

where the last equality follows from $\tilde{\psi}_1(x_r) = \tilde{\psi}_2(x_r) = 1$. Therefore, in the case of double-Beltrami fields, it is the energy-Casimir functional (magnetic and canonical helicities) that is directly related to the criterion of the tearing instability.

Let us examine the sign of (3.37) in more detail. Inserting (3.33), we obtain

$$\begin{aligned}
U_{\mu_1,\mu_2} &= -\alpha^2\frac{L_yL_z}{2}[[\tilde{\psi}_1']]_{x_r}[[\tilde{\psi}_2']]_{x_r}\Big[(\mu_2-\nu_1)^2[[\tilde{\psi}_2']]_{x_r} \\
&\quad -(\mu_1-\nu_1)(\mu_2-\nu_1)[[\tilde{\psi}_1']]_{x_r} - (\mu_1-\nu_1)(\mu_2-\nu_1)[[\tilde{\psi}_2']]_{x_r} + (\mu_1-\nu_1)^2[[\tilde{\psi}_1']]_{x_r}\Big] \\
&= -\alpha^2\frac{L_yL_z}{2}[[\tilde{\psi}_1']]_{x_r}[[\tilde{\psi}_2']]_{x_r}\Big[(\mu_2-\nu_1)(\mu_2-\mu_1)[[\tilde{\psi}_2']]_{x_r} + (\mu_1-\nu_1)(\mu_1-\mu_2)[[\tilde{\psi}_1']]_{x_r}\Big] \\
&= -\alpha^2\frac{L_yL_z}{2}(\mu_1-\mu_2)[[\tilde{\psi}_1']]_{x_r}[[\tilde{\psi}_2']]_{x_r}\Big[(\mu_1-\nu_1)[[\tilde{\psi}_1']]_{x_r} - (\mu_2-\nu_1)[[\tilde{\psi}_2']]_{x_r}\Big]. \quad (3.40)
\end{aligned}$$

Introducing $X_1 := \delta_i(\mu_1-\nu_1)[[\tilde{\psi}_1']]_{x_r}$ and $X_2 := \delta_i(\mu_2-\nu_1)[[\tilde{\psi}_2']]_{x_r}$, we can rewrite this as

$$U_{\mu_1,\mu_2} = -\frac{\alpha^2}{\delta_i}\frac{L_yL_z}{2}(\mu_1-\mu_2)X_1X_2\left(X_1-X_2\right), \quad (3.41)$$

where we have used the relation $\delta_i^2(\mu_1-\nu_1)(\mu_2-\nu_1) = 1$.

Without loss of generality, we can assume $\mu_1 > \mu_2$, therefore, the necessary and sufficient condition for the negative energy turns out to be

$$X_1 < 0 < X_2 \quad \text{or} \quad 0 < X_2 < X_1 \quad \text{or} \quad X_2 < X_1 < 0, \quad (3.42)$$

and thence, the necessary and sufficient condition for the positive energy is

$$X_2 < 0 < X_1 \quad \text{or} \quad 0 < X_1 < X_2 \quad \text{or} \quad X_1 < X_2 < 0. \tag{3.43}$$

3.2 Instability of double-Beltrami fields with sub/super-Alfvénic shear flow

Here, we examine how the value of U_{μ_1,μ_2} changes depending on Beltrami parameters μ_1 and μ_2. We focus on the parameter region of $\mu_1+\mu_2 \sim 0$, $\mu_1 \sim \mathcal{O}(1)$, and $\mu_2 \sim \mathcal{O}(1)$, where a flow is nearly Alfvénic, as shown later.

3.2.1 Double-Beltrami field with Beltrami parameters $\mu_1 + \mu_2 = 0$

First of all, we investigate the case of $\mu_1 + \mu_2 = 0$, that is, Beltrami parameters have the same amplitude but opposite signs. Let $\mu := \mu_1 = -\mu_2$, then we find

$$[[\tilde{\psi}_1']]_{x_r} = [[\tilde{\psi}_2']]_{x_r} = -\tilde{k}\left(\frac{\cos\tilde{k}(1-x_r)}{\sin\tilde{k}(1-x_r)} + \frac{\cos\tilde{k}x_r}{\sin\tilde{k}x_r}\right) = -\frac{\tilde{k}\sin\tilde{k}}{\sin\tilde{k}(1-x_r)\sin\tilde{k}x_r}, \tag{3.44}$$

where $\tilde{k} := \sqrt{\mu^2 - k_y^2 - k_z^2}$. We denote (3.44) by $[[\psi']]_{x_r}$, with which (3.40) is simplified as

$$U_{\mu_1,\mu_2} = -\alpha^2\frac{L_yL_z}{2}(\mu_1-\mu_2)^2[[\psi']]_{x_r}^3. \tag{3.45}$$

Thereby, if $[[\psi']]_{x_r} > 0$ the corresponding tearing mode has a negative energy, which implies the instability, on the other hand, if $[[\psi']]_{x_r} < 0$ the corresponding tearing mode has a positive energy. Because $0 < x_r < 1$, obviously $0 < \tilde{k}x_r < \tilde{k}$ and $0 < \tilde{k}(1-x_r) < \tilde{k}$. Therefore $\tilde{k} = \pi$ is the smallest value that makes $[[\psi']]_{x_r} = 0$ and we observe that $[[\psi']]_{x_r} < 0$ for $\tilde{k} < \pi$ and $[[\psi']]_{x_r} > 0$ for $\pi < \tilde{k} < \pi + \epsilon$, where ϵ is an appropriately small positive number.

Finally, we obtain the sufficient condition for the tearing mode ($k_y = m(2\pi/L_y)$ and $k_z = n(2\pi/L_z)$) to have a positive energy as follows:

$$\tilde{k} < \pi \Leftrightarrow \mu^2 < \pi^2 + k_y^2 + k_z^2 = \pi^2 + \left(m\frac{2\pi}{L_y}\right)^2 + \left(n\frac{2\pi}{L_z}\right)^2. \tag{3.46}$$

Obviously, as the value of the Beltrami parameter μ is increased, the lowest tearing mode, $(m,n) = (1,0)$ for $L_y > L_z$ or $(m,n) = (0,1)$ for $L_y < L_z$, gains the negative energy first.

To consider the relation between the energy of the tearing mode and the smallest eigenvalue of the curl operator $\mathcal{S}$, let us consider L_y and L_z such that $\pi^2 + (2\pi/L_y)^2 < (2\pi)^2$ and $L_z < L_y$. In this geometry, the smallest eigenvalue of $\mathcal{S}$ is $\lambda_1 = \sqrt{\pi^2 + (2\pi/L_y)^2}$. Then the condition for the positive energy of the lowest tearing mode $(m = 1, n = 0)$ is written as

$$\mu^2 < \pi^2 + \left(\frac{2\pi}{L_y}\right)^2 = \lambda_1^2. \tag{3.47}$$

Moreover, as soon as μ exceeds λ_1, the energy of the lowest tearing mode becomes negative. Therefore, it turns out that the smallest eigenvalue λ_1 gives the marginal value between positive and negative energy of the lowest tearing mode.

3.2.2 Double-Beltrami field with Beltrami parameters $\mu_1 + \mu_2 \sim 0$

Here, following the previous subsection, we investigate the case of $\mu_1 + \mu_2 \sim 0$. We assume that the resonance surface is at $x_r = 1/2$, by which $[[\tilde{\psi}_i']]_{x_r}$ $(i = 1, 2)$ is simplified as

$$[[\tilde{\psi}_i']]_{x_r} = -\tilde{k}_i \left(\frac{\cos\tilde{k}_i(1-x_r)}{\sin\tilde{k}_i(1-x_r)} + \frac{\cos\tilde{k}_i x_r}{\sin\tilde{k}_i x_r}\right) = -\frac{2\tilde{k}_i}{\tan(\tilde{k}_i/2)}. \tag{3.48}$$

Substituting (3.48) into (3.40), we obtain

$$U_{\mu_1,\mu_2} = \alpha^2 \frac{L_y L_z}{2}(\mu_1 - \mu_2)\frac{2\tilde{k}_1}{\tan(\tilde{k}_1/2)}\frac{2\tilde{k}_2}{\tan(\tilde{k}_2/2)} \left\{(\mu_1 - \nu_0)\frac{2\tilde{k}_1}{\tan(\tilde{k}_1/2)} - (\mu_2 - \nu_0)\frac{2\tilde{k}_2}{\tan(\tilde{k}_2/2)}\right\}, \quad (3.49)$$

which is a function of μ_1 and μ_2, fixing the mode number (m, n).

Fig.3.1 shows the contour of $U_{\mu_1,\mu_2}(\mu_1, \mu_2)$ of the lowest tearing mode $(m, n) = (1, 0)$ on the region $\pi < \mu_1 < 2\pi$ and $-2\pi < \mu_2 < -\pi$. On gray-colored regions and white-colored regions, the tearing mode has a negative and positive energy, respectively. It can be seen that there are three borders separating the negative and positive energy regions: two straight lines $\mu_1 = \lambda_1$ and $\mu_2 = -\lambda_1$ and a curved line.

First, let us consider the straight lines related to the smallest eigenvalue λ_1. In the previous study[15], it have been shown that the tearing mode without flow gains a negative energy when the absolute value of the Beltrami parameter $|\mu|$ exceeds the smallest eigenvalue λ_1. Therefore, it is natural to expect that the tearing mode would have a negative energy in the regions (1), (2), and (8) where both of $|\mu_1|$ and $|\mu_2|$ are larger than λ_1. On the other hand, it is also natural to expect that the tearing mode would have a positive energy in the regions (4), (5), and (6) where both of $|\mu_1|$ and $|\mu_2|$ are smaller than λ_1. Actually, however, we observe a positive energy in the region (2) and a negative energy in the region (6). Fig.3.2 shows $\tilde{\psi}_1$, $\tilde{\psi}_2$, and $\tilde{\psi} = \alpha_1\tilde{\psi}_1 + \alpha_2\tilde{\psi}_2$ of the tearing mode obtained in the region (2). It can be seen that, although each of $\tilde{\psi}_1$ and $\tilde{\psi}_2$ has the larger wavenumber than π (the criterion of the negative energy mode, see (3.46)), that of the total $\tilde{\psi}$ is smaller than λ_1. On the other hand, Fig.3.3 shows $\tilde{\psi}_1$, $\tilde{\psi}_2$, and $\tilde{\psi}$ of

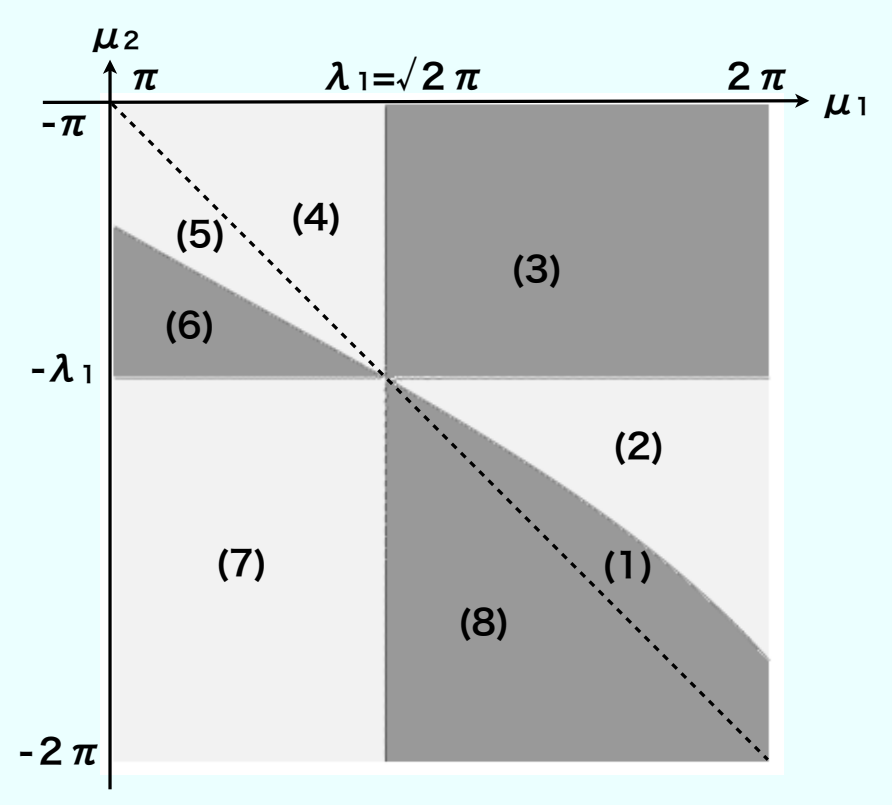

Figure 3.1: Contour of $U_{\mu_1,\mu_2}(\mu_1,\mu_2)$ of the tearing mode $(m,n)=(1,0)$ in the region $\pi<\mu_1<2\pi$ and $-2\pi<\mu_2<-\pi$. On gray-colored regions, the tearing mode has a negative energy. On white-colored regions, the tearing mode has a positive energy. $\lambda_1=\sqrt{2}\pi$ is the smallest eigenvalue of the curl operator. The parameters are set as below: $\delta_i=5\pi$, $\phi_{mz}=\sqrt{\delta_i}$, and $\phi_{my}=\phi_{cy}=\phi_{cz}=0$.

the tearing mode obtained in the region (6).Opposite to the case of (2), it can be seen that, although each of $\tilde{\psi}_1$ and $\tilde{\psi}_2$ has the smaller wavenumber than π, that of the total $\tilde{\psi}$ is larger than λ_1. These results show that the tearing stability of the double-Beltrami fields $\boldsymbol{B}_{\mu_1,\mu_2} = \boldsymbol{B}_{\mu_1} + \boldsymbol{B}_{\mu_2}$ can not be reduced to the sum of those of $\boldsymbol{B}_{\mu_1}$ and $\boldsymbol{B}_{\mu_2}$.

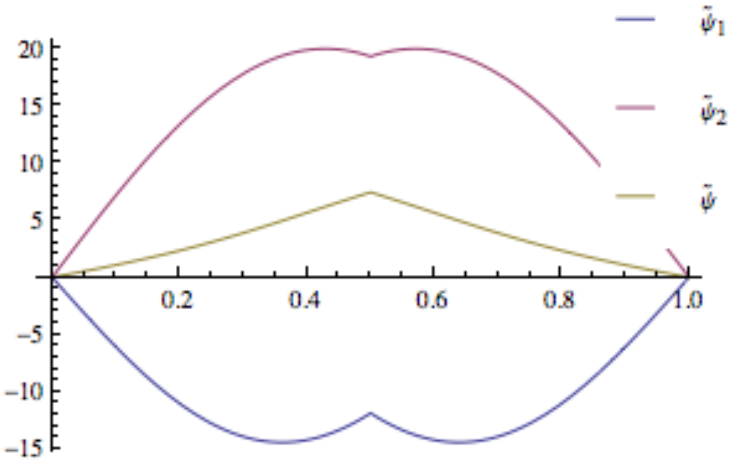

Figure 3.2: $\tilde{\psi}_1, \tilde{\psi}_2$, and $\tilde{\psi} = \alpha_1\tilde{\psi}_1 + \alpha_2\tilde{\psi}_2$ of the tearing mode obtained in the region (1).

Next, let us consider the curved line, which is possibly related to the flow amplitude and shear. The left of Fig.3.4 shows the contour plot of the energy of the tearing mode $(m, n) = (1, 0)$. The middle of Fig.3.4 shows the contour plot of the difference between the square amplitude of the magnetic field $\boldsymbol{B}$ and the flow field $\boldsymbol{V}$, that is, $B^2 - V^2$. In the white-colored region, the flow is sub-Alfvénic ($V^2 < B^2$). On the other hand, in the gray-colored region, the flow is super-Alfvénic ($V^2 > B^2$). The right of Fig.3.4 shows the ratio of the flow shear to the magnetic shear at the resonance surface $x_r = 1/2$, that is, $V_y(1/2)/B_y(1/2)$. In the white-colored region, the flow has sub-Alfvénic shear ($|V_y(1/2)| < |B_y(1/2)|$).

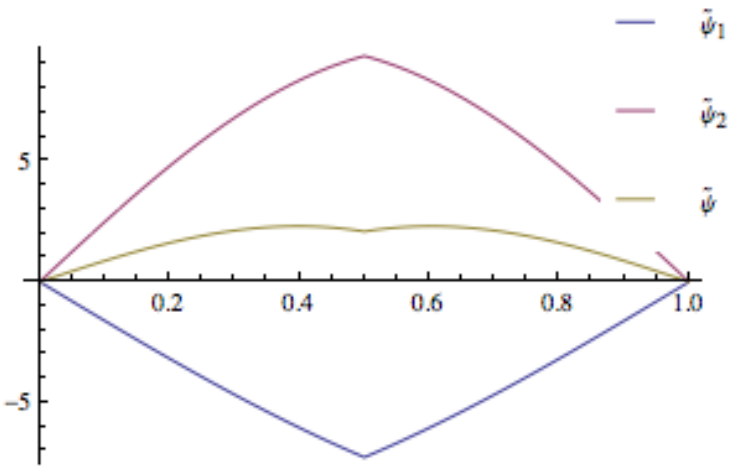

Figure 3.3: $\tilde{\psi}_1, \tilde{\psi}_2$, and $\tilde{\psi} = \alpha_1\tilde{\psi}_1 + \alpha_2\tilde{\psi}_2$ of the tearing mode obtained in the region (6).

On the other hand, in the gray-colored region, the flow has super-Alfvénic shear ($|V_y(1/2| > |B_y(1/2)|$). For all of contour plots shown in Fig.3.4, the ion-skin length parameter is set as $\delta_i = 1/5\pi$. Fig.3.5 is the $\delta_i = 1/31\pi$ version of Fig.3.4, namely, it shows the situation more close to the ideal MHD. As the situation approaches the ideal MHD ($\delta_i \to 0$), all of the curved line of the tearing mode energy contour, the boundary between sub- and super-Alfvénic flow, and the boundary between sub- and super-Alfvénic flow shear approach the line $\mu_1 + \mu_2 = 0$. Therefore, in the region of $\mu_1 + \mu_2 < 0$, the dominant instability mode changes from the tearing instability to the Kelvin-Helmholtz instability, which may causes the complexity of the contour of mode energy.

In Fig.3.6 and Fig.3.7, we plot the contours of the magnetic flux function and the stream function of an unstable tearing mode with zero canonical helicity, respectively. It can be seen that the flow is just shearing but not rotating. Fig.3.8 and Fig.3.9 are the finite canonical helicity version. In this occasion, the flow is not

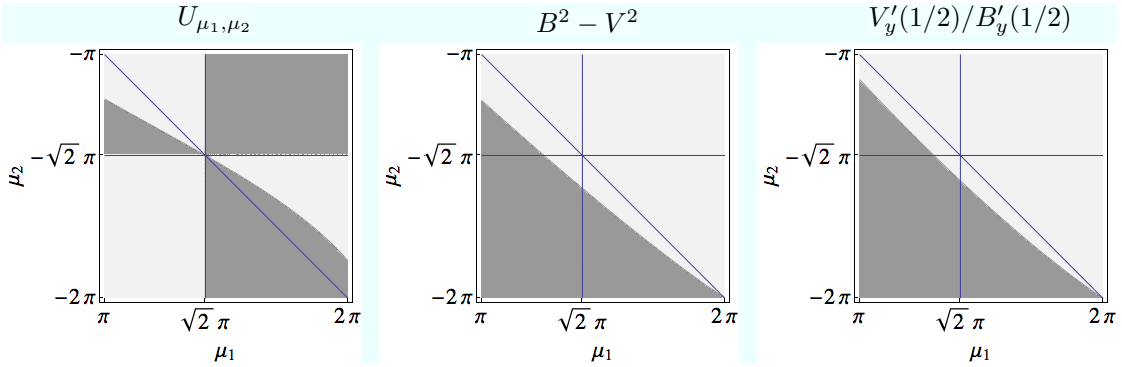

Figure 3.4: (Left) the energy U_{μ_1,μ_2} of the tearing mode $(m,n) = (1,0)$: in the gray colored region the tearing mode has negative energy $U_{\mu_1,\mu_2} < 0$ and in the white colored region positive energy $U_{\mu_1,\mu_2} > 0$. (Middle) the difference between the square amplitudes of the magnetic field $\boldsymbol{B}$ and the flow field $\boldsymbol{B}$: in the gray colored region the flow is super-Alfvénic $V^2 > B^2$ and in the white colored region sub-Alfvénic $V^2 < B^2$. (Right) the ratio of the flow shear $V_y'(1/2)$ to the magnetic shear $B_y'(1/2)$ on the resonance surface: in the gray colored region the flow shear is super-Alfvénic $|V_y'(1/2)| > |B_y'(1/2)|$ and in the white colored region sub-Alfvenic $|V_y'(1/2)| < |B_y'(1/2)|$. The parameter setting is the same as that of Fig.2.1. The ion-skin length $\delta_i = 1/5\pi$.

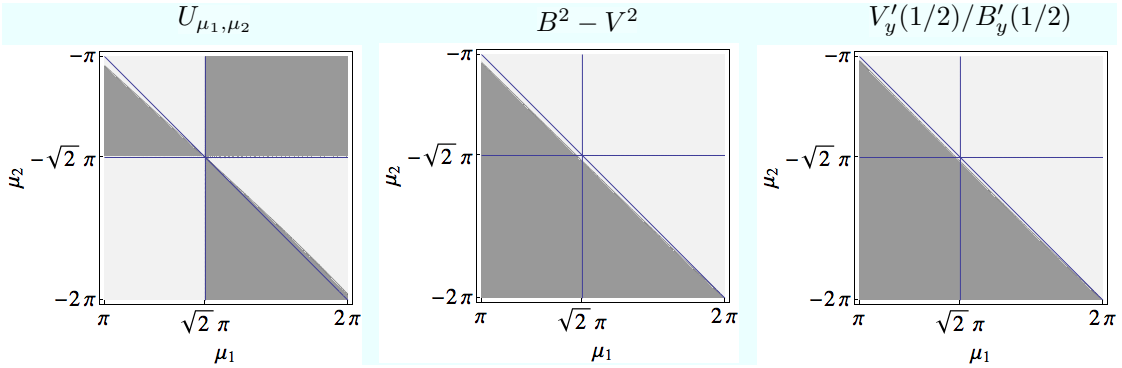

Figure 3.5: $\delta_i = 1/31\pi$ version of Fig.3.4.

only shearing but also rotating. Fig.3.10 and Fig.3.11 give the magnified views of Fig.3.8 and Fig.3.9, respectively. Although the magnetic flux function has strange "kinks", the stream function is smooth.

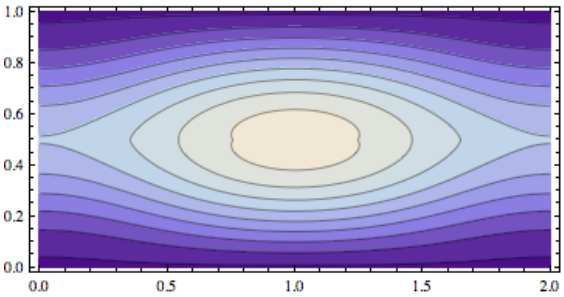

Figure 3.6: Contour plot of the magnetic flux function of the tearing mode that is obtained in the region (8) and has zero canonical helicity.

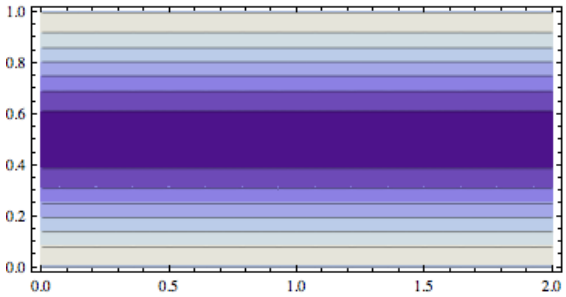

Figure 3.7: Contour plot of the strean function of the tearing mode that is obtained in the region (8) and has zero canonical helicity.

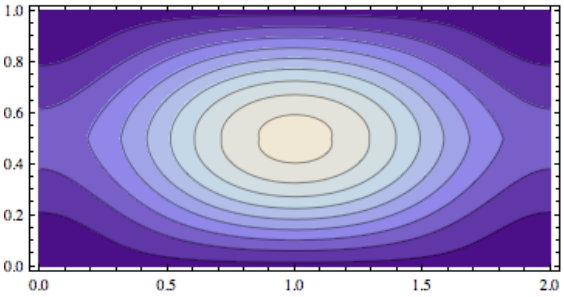

Figure 3.8: Contour plot of the magnetic flux function of the tearing mode that is obtained in the region (8) and has finite canonical helicity.

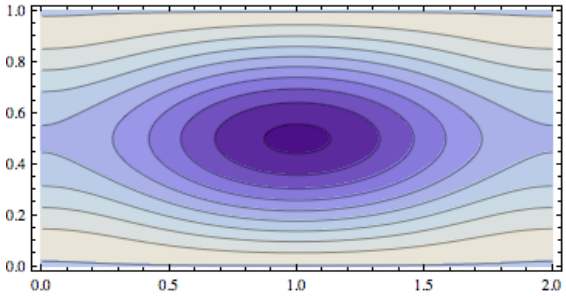

Figure 3.9: Contour plot of the strean function of the tearing mode that is obtained in the region (8) and has finite canonical helicity.

3.3 Summary and Discussion

Tearing mode of double-Beltrami fields have been shown to be characterized only by the helical-flux Casimir, as with the case of single-Beltrami fields[15], even in the presence of flow. However, there is a difference between previous and present

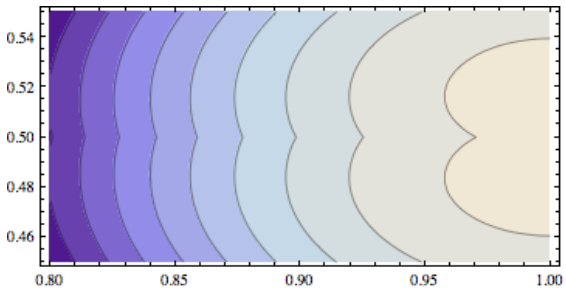

Figure 3.10: Magnified view of Fig.3.8.

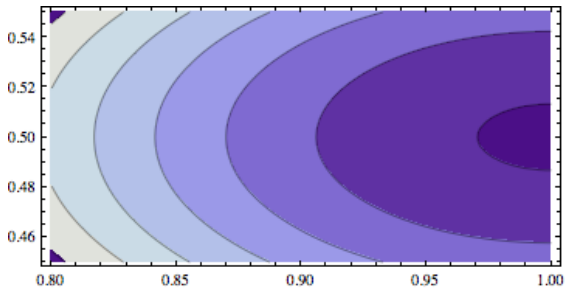

Figure 3.11: Magnified view of Fig.3.9.

tearing modes. In the previous theory, the tearing mode is represented by a singular eigenfunction of the curl operator $\mathcal{S}$. On the other hand, in the present theory, the tearing mode is given by superposition of 'two' singular eigenfunctions of the curl operator $\mathcal{S}$. As a result, the tearing instability criterion Δ' changes drastically, as shown in (3.40). We have shown that Δ' is directly related to the energy-Casimir functional U_{μ_1,μ_2}, obtained by combining the hamiltonian, the magnetic helicity, and the canonical helicity, through the equation $U_{\mu_1,\mu_2} = -(L_y L_z/2)\psi(x_r)^2\Delta'$. We observe that when the tearing mode $\tilde{u}^\dagger$ has the negative energy $U_{\mu_1,\mu_2}(\tilde{u}^\dagger) < 0$, its Δ' has the positive value $\Delta'(\tilde{u}^\dagger) > 0$, which implies the instability of the negative-energy mode in the presence of the finite resistivity η[29]. Thereby, in what follows, we regard the energy U_{μ_1,μ_2} of the tearing mode as the criterion of tearing instability. The possible scenario is that the symmetric equilibrium relaxes to the helical equilibrium that has the lower energy U_{μ_1,μ_2} than the symmetric one, through the tearing modes of $\Delta' > 0$.

Using the above obtained criterion U_{μ_1,μ_2}, we have investigated the tearing instability of double-Beltrami fields in the parameter region such that $\mu_1 + \mu_2 \sim 0$, $\mu_1 \sim \mathcal{O}(1)$, and $\mu_2 \sim \mathcal{O}(1)$. First, we have analyzed the simple case of $\mu_1 + \mu_2 = 0$ where the Beltrami parameters μ_1 and μ_2 of two Beltrami vortices, constituting a

double-Beltrami field, have the same amplitude $\mu = \mu_1 = -\mu_2$ but opposite signs. In this case, it has been shown that the tearing mode has the positive energy for $\mu < \lambda_1$, where λ_1 is the smallest eigenvalue of the curl operator, and gains the negative energy as soon as μ exceeds λ_1. This result is consistent with the theory of tearing instability without flow[15]. It is the smallest eigenvalue of the curl operator that determines the tearing instability.

However, in the region out of the line $\mu_1 + \mu_2 = 0$, the energy of the tearing mode U_{μ_1,μ_2} behaves complicatedly as shown in Fig.3.1. There are three lines separating positive and negative regions: the straight lines $\mu_1 = \lambda_1$ and $\mu_2 = -\lambda_1$ and the curved line. We have observed the negative energy tearing mode in the region (6) where both Beltrami vortices would have positive energies if there were no flow. On the other hand, we have observed the positive energy tearing mode in the region (2) where both Beltrami vortices would have negative energies if there were no flow.

One possibility is that we are observing not only the tearing instability but also the Kelvin-Helmholtz instability (the vortex-induced reconnection[39]). As plasma approaches the ideal MHD plasma ($\delta_i \to 0$), all of the curved line, the border between sub- and super-Alfvénic flow, and the border between sub- and super-Alfvénic shear on the resonance surface get close to the same line $\mu_1 + \mu_2 = 0$, as shown in Fig.3.5. Moreover, it is known that the double-Beltrami fields generally does not satisfy the sufficient condition for the Kelvin-Helmholtz stability in the region $\mu_1 + \mu_2 < 0$[49], where a double-Beltrami flow field is given by a combination of a sub-Alvénic vortex $\boldsymbol{V}_{\mu_1}$ with a larger structure ($\pi < \mu_1 < |\mu_2|$) and a super-Alfvénic vortex $\boldsymbol{V}_{\mu_2}$ with a smaller structure ($|\mu_2| > \mu_1$). Since in the

super-Alfvénic shear flow regime the tearing instability is replaced by the Kelvin-Helmholtz instability[40, 41], it is natural to suppose that the reconnected mode observed in the region $\mu_1 + \mu_2 < 0$ is not the tearing mode but the vortex-induced reconnection[39] due to the Kelvin-Helmholtz instability. Therefore, it would be considered that $U_{\mu_1,\mu_2} = -(L_y L_z/2)\psi(x_r)^2\Delta'$ ceases to be the criterion of the tearing instability in the region $\mu_1 + \mu_2 < 0$.

On the other hand, in the region $\mu_1 + \mu_2 > 0$, the tearing instability is still dominant. The negative-energy modes obtained from the regions (1) and (3) are intuitive results because, in those regions, the sub-Alfvénic Beltrami field has the Beltrami parameter μ_1 larger than λ_1 and it can be tearing-unstable. The positive-energy mode obtained from the region (4) is also intuitive because, in this region, both of Beltrami fields are tearing-stable in the absence of flow. The positive-energy mode obtained from the region (2) is an interesting result. In this region, the sub-Alfvenic Beltrami field may be unstable, although the super-Alfvénic Beltrami field is stable due to the super-Alfvénic shear flow[29]. Therefore, this positive energy possibly means the stabilizing effect due to the interaction between two Beltrami vortices.

On a final note, in Appendix B, it is shown that, in particular case, a double-Beltrami field is Lyapunov-stable on the line such that $\mu_1 + \mu_2 = 0$ and $\mu < \lambda_1$. This marginal value $\mu = \lambda_1$ is identical to that of tearing instability.

Chapter 4

Singular Casimir and Nonlinear tearing mode

The linear tearing-mode eigenfunction of the ideal MHD plasma was obtained in [15] and that of the Hall MHD was obtained in the previous section. Both of them, however, provide a somewhat strange structure of the island, that is, the magnetic surface "kinks" at the resonance surface, as shown in Fig.3.10. The reason of this may be because the linear theory neglects the second-order $\tilde{\boldsymbol{J}} \times \tilde{\boldsymbol{B}}$ force. As we have seen, the linear tearing mode has the singular current $\tilde{\boldsymbol{J}}$ described by the delta function, which violates the smallness of the corresponding force. Therefore, the neglect of the second-order term brings the strange kinks of the magnetic surface.

As we have already mentioned in the introduction, the resonance singularity $\boldsymbol{B}\cdot\nabla = 0$ may have relation to the extremal singularity stemming from the extremal of the magnetic flux function $\nabla\psi = 0$. Therefore, it is natural to expect that, by extending the notion of plateau singularity to extremal singularity, we can obtain a proper Casimir that characterizes the nonlinear tearing mode.

Here, we develop the notion of extremal singularity, based on the context of the nonlinear tearing mode in the ideal MHD.

4.1 Linear tearing mode and Resonance singularity

For comparison, here we concisely review the tearing mode theory of the ideal MHD developed in [15]. The linearized system around the single, constant density ($n = 1$), no-flow ($\boldsymbol{V} = 0$) Beltrami equilibrium $u_\mu = (1, 0, \boldsymbol{B}_\mu)$, where $\nabla \times \boldsymbol{B}_\mu = \mu \boldsymbol{B}_\mu$, is given by

$$\partial_t \tilde{u} = \mathcal{J}_\mu H_\mu \tilde{u}, \tag{4.1}$$

where $\tilde{u} = (\tilde{n}, \tilde{\boldsymbol{V}}, \tilde{\boldsymbol{B}})$ is the state vector, $\mathcal{J}_\mu$ is the Poisson operator evaluated at the fixed equilibrium point u_μ

$$\mathcal{J}_\mu :== \begin{pmatrix} 0 & -\nabla\cdot & 0 \\ -\nabla & 0 & (\nabla \times \circ) \times \boldsymbol{B}_\mu \\ 0 & \nabla \times (\circ \times \boldsymbol{B}_\mu) & 0 \end{pmatrix}, \tag{4.2}$$

where $\circ$ implies insertion of the function to the right of the operator, and H_μ is the linearized Hamiltonian

$$H_\mu := \begin{pmatrix} \varpi & 0 & 0 \\ 0 & 1 & 0 \\ 0 & 0 & 1 - \mu S^{-1} \end{pmatrix}. \tag{4.3}$$

ϖ is a positive coefficient by which $\varpi \tilde{n} = \tilde{h}$ evaluates the enthalpy perturbation, and S^{-1} is the inverse-curl operator which yields $\tilde{\boldsymbol{A}} = S^{-1}\tilde{\boldsymbol{B}}$.

In order for $(0, \boldsymbol{b})$ to be the member of $\mathrm{Ker}(\mathcal{J}_\mu)$, $\boldsymbol{b}$ must satisfy the condition

$$\boldsymbol{B}_\mu \times (\nabla \times \boldsymbol{b}) = 0. \tag{4.4}$$

In the slab geometry, we may write $\boldsymbol{B}_\mu = (0, B_y(x), B_z(x))$. To find a singular Casimir element, let us put

$$\boldsymbol{b} = \Re \begin{pmatrix} 0 \\ ik_y \vartheta(x) \\ ik_z \vartheta(x) \end{pmatrix} e^{i(k_y y + k_z z)}, \quad \nabla \times \boldsymbol{b} = \Re \begin{pmatrix} 0 \\ -ik_z \partial_x \vartheta(x) \\ ik_y \partial_x \vartheta(x) \end{pmatrix} e^{i(k_y y + k_z z)}, \tag{4.5}$$

with which (4.4) reduces to

$$(k_y B_y + k_z B_z)\, \partial_x \vartheta(x) = 0. \tag{4.6}$$

If there is a resonance surface $x = x_r$ satisfying the resonance condition

$$\boldsymbol{B}_\mu \cdot \boldsymbol{k} = B_y(x_r) k_y + B_z(x_r) k_z = 0, \tag{4.7}$$

(4.6) is solved by

$$\vartheta(x) = c_0 + c_1 Y(x - x^\dagger), \tag{4.8}$$

where $Y(\cdot)$ is the Heaviside step function, c_0, c_1 are complex constants.

Integrating the resulting $\boldsymbol{b}$, we obtain a helical-flux Casimir:

$$C_j(\tilde{u}) = C_j(\tilde{\boldsymbol{B}}) := \langle \tilde{\boldsymbol{B}}, \boldsymbol{b} \rangle = \int_\Omega \tilde{\boldsymbol{B}} \cdot \boldsymbol{b} d\boldsymbol{x}. \tag{4.9}$$

The energy-Casimir functional (without flow perturbation $\tilde{\boldsymbol{V}}$) is given by

$$\mathcal{F}_{\mu,\beta}(\tilde{\boldsymbol{B}}) := \frac{1}{2} \langle H_\mu \tilde{u}, \tilde{u} \rangle \Big|_{\tilde{\boldsymbol{V}}=0} - \beta C_j(\tilde{u}) = \frac{1}{2} \langle (S - \mu) S^{-1} \tilde{\boldsymbol{B}} - 2\beta \boldsymbol{b}, \tilde{\boldsymbol{B}} \rangle. \tag{4.10}$$

The tearing mode eigenfunction obtained from the Euler-Lagrange equation

$$\nabla \times \tilde{\boldsymbol{A}} - \mu \tilde{\boldsymbol{A}} = \beta P_\Sigma \boldsymbol{b}, \tag{4.11}$$

where P_Σ denotes the orthogonal projector from $L^2(\Omega)$ onto $L^2_\Sigma(\Omega)$.

4.2 Incompressible MHD with stream and flux functions

In this section, to reveal the relation between the resonance singularity and the extremal singularity and to find the singular Casimir element characterizing the nonlinear tearing mode, we will formulate the Hamiltonian formalism of the ideal MHD with the magnetic flux function.

Incompressible MHD can be written as

$$\partial_t \boldsymbol{V} = P_\sigma \left[-(\nabla \times \boldsymbol{V}) \times \boldsymbol{V} + (\nabla \times \boldsymbol{B}) \times \boldsymbol{B} \right], \tag{4.12}$$

$$\partial_t \boldsymbol{B} = \nabla \times (\boldsymbol{V} \times \boldsymbol{B}), \tag{4.13}$$

where P_σ denotes the orthogonal projector from $L^2(\Omega)$ onto $L^2_\Sigma(\omega)$.

We consider this equation in the slab geometry we introduced in Sec.2.2, and assume that all fields depend on only x and $\eta := \bar{k_y} y + \bar{k_z} z$ and have no dependence on $\zeta = \bar{k_y} z - \bar{k_z} y$. The dependent variables can be cast into the Clebsch-like form

$$\boldsymbol{V}(x,\eta) = \nabla\phi(x,\eta) \times \nabla\zeta + V_\zeta(x,\eta)\nabla\zeta, \tag{4.14}$$

$$\boldsymbol{B}(x,\eta) = \nabla\psi(x,\eta) \times \nabla\zeta + B_\zeta(x,\eta)\nabla\zeta, \tag{4.15}$$

where ϕ and ψ are stream and flux functions, V_ζ and B_ζ are ζ-component of $\boldsymbol{V}$ and $\boldsymbol{B}$. With this representation, we can rewrite the system of equations in the following form:

$$\partial_t \omega = [\omega, \phi] + [\psi, j], \tag{4.16}$$

$$\partial_t V_\zeta = [V_\zeta, \phi] + [\psi, B_\zeta], \tag{4.17}$$

$$\partial_t \psi = [\psi, \phi], \tag{4.18}$$

$$\partial_t B_\zeta = [B_\zeta, \phi] + [\psi, V_\zeta], \tag{4.19}$$

where $\omega := -\Delta\phi$ and $j := -\Delta\psi$ are the ζ-components of the vorticity and the current, and $[a, b] := -\nabla a \times \nabla b \cdot \nabla\zeta$ is the standard Poisson bracket.

With a new state vector $u = {}^t(\omega, V_\zeta, \psi, B_\zeta)$, the system of equations (4.16)-(4.19) is cast into the hamiltonian form (1.4) with a hamiltonian functional

$$\mathcal{H}(\omega, V_\zeta, \psi, B_\zeta) := \frac{1}{2} \int_\Omega \left(\phi\omega + V_\zeta^2 + j\psi + B_\zeta^2 \right) d\boldsymbol{x}, \quad \partial_u \mathcal{H} = (\phi, V_\zeta, j, B_\zeta), \tag{4.20}$$

and a Poisson operator

$$\mathcal{J}(u) := \begin{pmatrix} [\omega, \circ] & [V_\zeta, \circ] & [\psi, \circ] & [B_\zeta, \circ] \\ [V_\zeta, \circ] & 0 & 0 & [\psi, \circ] \\ [\psi, \circ] & 0 & 0 & 0 \\ [B_\zeta, \circ] & [\psi, \circ] & 0 & 0 \end{pmatrix}, \tag{4.21}$$

where $\circ$ implies insertion of the function to the right of the operator. Finally, the hamiltonian form of (4.16)-(4.19) is given by

$$\partial_t \begin{pmatrix} \omega \\ V_\zeta \\ \psi \\ B_\zeta \end{pmatrix} = \begin{pmatrix} [\omega, \circ] & [V_\zeta, \circ] & [\psi, \circ] & [B_\zeta, \circ] \\ [V_\zeta, \circ] & 0 & 0 & [\psi, \circ] \\ [\psi, \circ] & 0 & 0 & 0 \\ [B_\zeta, \circ] & [\psi, \circ] & 0 & 0 \end{pmatrix} \begin{pmatrix} \phi \\ V_\zeta \\ j \\ B_\zeta \end{pmatrix}. \tag{4.22}$$

The Poisson operator (4.21) has at least three Casimir elements. First of all, the cross helicity and magnetic helicity are inherited from the original MHD:

$$C_1 = \frac{1}{2}\int_\Omega \boldsymbol{A}\cdot\boldsymbol{B}d\boldsymbol{x} = \int_\Omega \psi B_\zeta d\boldsymbol{x}, \quad \partial_u C_1 = (0, 0, B_\zeta, \psi)\,. \tag{4.23}$$

$$C_2 = \int_\Omega \boldsymbol{V}\cdot\boldsymbol{B}d\boldsymbol{x} = \int_\Omega (\omega\psi + V_\zeta B_\zeta)\, d\boldsymbol{x}, \quad \partial_u C_2 = (\psi, B_\zeta, \omega, V_\zeta)\,. \tag{4.24}$$

The existence of the magnetic flux function (magnetic surface) gives the present system an additional Casimir element, which is the so-called flux-function Casimir:

$$C_F = \int_\Omega F(\psi) d\boldsymbol{x}, \quad \partial_u C_F = (0, 0, f(\psi), 0)\,, \tag{4.25}$$

where $F : \mathbb{R} \to \mathbb{R}$ is a real function and f is its derivative.

Let us invoke the magnetic helicity C_1 in an energy-Casimir functional:

$$\mathcal{H}_\mu := \mathcal{H} - \mu C_1. \tag{4.26}$$

The Euler-Lagrange equations are

$$j = \mu B_\zeta, \quad B_\zeta = \mu\psi, \tag{4.27}$$

which yields the Helmholtz equation

$$-\Delta\psi = \mu^2\psi. \tag{4.28}$$

This Helmholtz equation corresponds to the single-Beltrami equation (1.30).

Remark 4.2.1. In Eq. (4.22), it seems at first glance that the elements of Poisson operator $\mathcal{J}_{12}$ and $\mathcal{J}_{14}$ do not work, that is, they produce only zero result $[V_\zeta, V_\zeta] = 0$ and $[B_\zeta, B_\zeta] = 0$. However, these elements are necessary for the Poisson operator (4.21) to satisfy the Jacobi identity (1.3) and to possess the magnetic and cross helicities as Casimir elements. For example, we could consider another type of antisymmetric operator

$$\mathcal{J}'(u) = \begin{pmatrix} [\omega, \circ] & 0 & [\psi, \circ] & 0 \\ 0 & -[\phi, \circ] & 0 & [\psi, \circ] \\ [\psi, \circ] & 0 & 0 & 0 \\ 0 & [\psi, \circ] & 0 & -[\phi, \circ] \end{pmatrix}. \tag{4.29}$$

However, the poisson bracket defined by this operator $\mathcal{J}'(u)$ does not satisfy the Jacobi identity. Moreover, the magnetic and cross helicities are not Casimir elements of $\mathcal{J}'(u)$.

Remark 4.2.2. The cross and magnetic helicities are calculated as follows:

$$C_1 = \frac{1}{2}\int_\Omega \boldsymbol{A}\cdot\boldsymbol{B}d\boldsymbol{x} = \int_{\partial\Omega}\psi\boldsymbol{n}\cdot\nabla\Psi d\boldsymbol{x} + \int_\Omega (\psi B_z)\, d\boldsymbol{x}, \tag{4.30}$$

$$C_2 = \int_\Omega \boldsymbol{V}\cdot\boldsymbol{B}d\boldsymbol{x} = \int_{\partial\Omega}\psi\boldsymbol{n}\cdot\nabla\phi d\boldsymbol{x} + \int_\Omega (\omega\psi + V_z B_z)\, d\boldsymbol{x}, \tag{4.31}$$

where $\Psi := \Delta^{-1}B_z$. Therefore, we have to take $\psi \in H_0^1(\Omega)$.

4.3 Linear tearing mode theory and Extremal singularity

In this section, first, we rewrite the linear tearing mode theory [15] in terms of the magnetic flux function by using the formulation obtained in the previous

section, and then, we reveal the relation between the resonance singularity ($\boldsymbol{B}_\mu \cdot \nabla = 0$) and the plateau singularity ($\nabla\psi_\mu = 0$).

4.3.1 Linear tearing mode and Extremal singularity

The linearized system around the Beltrami equilibrium $u_\mu = (0, 0, \psi_\mu, \mu\psi_\mu)$ satisfying (4.27) is given by

$$\partial_t \tilde{u} = \mathcal{J}_\mu H_\mu \tilde{u}, \tag{4.32}$$

where $\tilde{u} = {}^t(\tilde{\omega}, \tilde{V_\zeta}, \tilde{\psi}, \tilde{B_\zeta})$ is the state vector, $\mathcal{J}_\mu$ is the Poisson operator evaluated at the fixed equilibrium point u_μ

$$\mathcal{J}_\mu := \mathcal{J}(u_\mu) = \begin{pmatrix} 0 & 0 & [\psi_\mu, \circ] & [\mu\psi_\mu, \circ] \\ 0 & 0 & 0 & [\psi_\mu, \circ] \\ [\psi_\mu, \circ] & 0 & 0 & 0 \\ [\mu\psi_\mu, \circ] & [\psi_\mu, \circ] & 0 & 0 \end{pmatrix}, \tag{4.33}$$

and H_μ is the linearized Hamiltonian

$$H_\mu = \begin{pmatrix} -\Delta^{-1} & 0 & 0 & 0 \\ 0 & 1 & 0 & 0 \\ 0 & 0 & -\Delta & -\mu \\ 0 & 0 & -\mu & 1 \end{pmatrix}. \tag{4.34}$$

In order for $(0, 0, f, 0)$ to be the member of $\mathrm{Ker}(\mathcal{J}_\mu)$, f must satisfy the condition

$$[\psi_\mu, f] = \nabla\psi_\mu \times \nabla f \cdot \nabla\zeta = 0 \tag{4.35}$$

To find a singular Casimir element, let us put

$$f = \Re\left(i\sqrt{k_y^2 + k_z^2} e^{i(k_y y + k_z z)} \vartheta(x)\right), \tag{4.36}$$

with which (4.35) reduces to

$$i(k_y^2 + k_z^2)\vartheta(x) e^{i(k_y y + k_z z)} \partial_x \psi_\mu = 0. \tag{4.37}$$

When there is a extremal point $x = x_r$ satisfying

$$\partial_x \psi_\mu(x_r) = 0, \tag{4.38}$$

(4.37) is solved by

$$\vartheta(x) = c_1 \delta(x - x_r), \tag{4.39}$$

where $\delta(\cdot)$ is the delta function and c_1 is a complex constant.

Integrating the resulting f, we obtain a singular magnetic flux Casimir

$$C_f(\tilde{\psi}) := \int_\Omega \Re\left(ic_1\sqrt{k_y^2+k_z^2}e^{i(k_y y+k_z z)}\delta(x-x_r)\right)\tilde{\psi}d\boldsymbol{x}. \tag{4.40}$$

Invoking this singular Casimir element, we construct the energy-Casimir functional (without flow perturbation)

$$\begin{aligned}\mathcal{F}_{\mu,\beta}(\tilde{\psi},\tilde{B}_\zeta) &:= \frac{1}{2}(\tilde{u}, H_\mu \tilde{u})\Big|_{\tilde{\boldsymbol{V}}=0} - \beta C_F \\ &= \int_\Omega \Big\{\frac{1}{2}\tilde{j}\tilde{\psi} + \frac{1}{2}\tilde{B}_\zeta{}^2 - \mu\tilde{\psi}\tilde{B}_\zeta \\ &\qquad -\beta\,\Re\left(ic_1\sqrt{k_y^2+k_z^2}e^{i(k_y y+k_z z)}\delta(x-x_r)\right)\tilde{\psi}\Big\}\,d\boldsymbol{x}\end{aligned} \tag{4.41}$$

The equilibrium points are determined by the Euler-Lagrange equation

$$\tilde{j} - \mu\tilde{B}_\zeta = \beta\Re\left(ic_1\sqrt{k_y^2+k_z^2}e^{i(k_y y+k_z z)}\right)\delta(x-x_r), \quad \tilde{B}_\zeta - \mu\tilde{\psi} = 0, \tag{4.42}$$

which are combined to

$$-\Delta\tilde{\psi} = \mu^2\tilde{\psi} + \beta\Re\left(ic_1\sqrt{k_y^2+k_z^2}e^{i(k_y y+k_z z)}\right)\delta(x-x_r). \tag{4.43}$$

It is the last term of the right-hand side of (4.43), we call it as the *delta function term*, that allows $\partial_x\tilde{\psi}$ to jump across the extremal line $x = x_r$ and produces the singular current on the line.

4.3.2 Relation between Resonance and Extremal singularities

Here, we see the relation between the extremal singularity and the resonance singularity. By using the magnetic fluc function ψ_μ, the Beltrami field can be rewritten as

$$\boldsymbol{B}_\mu = \nabla\psi_\mu(x) \times \nabla\zeta + \mu\psi_\mu(x)\nabla\zeta. \tag{4.44}$$

Let us substitute (4.44) into (4.7),

$$\begin{aligned} \boldsymbol{k}\cdot\boldsymbol{B}_\mu &= \sqrt{k_y^2+k_z^2}\nabla\eta\cdot(\nabla\psi_\mu\times\nabla\zeta+\mu\psi_\mu\nabla\zeta) \\ &= -\sqrt{k_y^2+k_z^2}\nabla x\cdot\nabla\psi_\mu \\ &= -\sqrt{k_y^2+k_z^2}\partial_x\psi_\mu(x), \end{aligned} \tag{4.45}$$

which shows that the extremal condition (4.38) is nothing but the resonance condition (4.7), that is,

$$\boldsymbol{k}\cdot\boldsymbol{B}_\mu(x) = 0 \Leftrightarrow \partial_x\psi_\mu(x) = 0. \tag{4.46}$$

Moreover, the equations (4.42) correspond to the linear tearing mode equation (4.11). To confirm this relation, let us take the curl of (4.11), and we obtain

$$\nabla\times\tilde{\boldsymbol{B}} - \mu\tilde{\boldsymbol{B}} = \beta\nabla\times\boldsymbol{b}. \tag{4.47}$$

Substituting $\tilde{\boldsymbol{B}} = \nabla\tilde{\psi}\times\nabla\zeta + \tilde{B}_\zeta\nabla\zeta$ into the above equation, we obtain

$$\left(\tilde{j}-\mu\tilde{B}_\zeta\right)\nabla\zeta + \nabla\left(\tilde{B}_\zeta-\mu\tilde{\psi}\right)\times\nabla\zeta = \beta\Re\left(ic_1\sqrt{k_y^2+k_z^2}e^{i(k_y y+k_z z)}\right)\delta(x-x_r)\nabla\zeta, \tag{4.48}$$

which is equivalent to Eqs.(4.42).

Therefore, at least in the linear theory, the tearing mode is related to the extremal singularity of the Poisson operator. In the next section, we will study the relation between the nonlinear tearing mode and the extremal singularity.

4.4 Nonlinear tearing mode theory

Here, we will develop the nonlinear tearing mode theory generalizing the linear theory mentioned above.

4.4.1 Nonlinear tearing mode equation and Delta function term

We start by ascertaining what kind of Casimir element we need. For convenience, let us rewrite Eq.(4.43) in a simpler form by adjusting the coefficient of the delta function term,

$$-\Delta\tilde{\psi} = \mu^2\tilde{\psi} + \beta\Re e^{i(k_y y + k_z z)}\delta(x - x_r). \tag{4.49}$$

In the linear theory, the delta function term $\Re e^{i(k_y y + k_z z)}\delta(x - x_r)$, obtained from the singular Casimir element, gives a boundary condition on the resonance surface, by which we can obtain a tearing mode solution. However, on this occasion, the coefficient of the delta function term $\Re e^{i(k_y y + k_z z)}$ is artificially given, which causes the singular current inside the island and results in the strange kinks of magnetic field lines on the resonance surface.

Therefore, we expect ψ to determine the coefficient of the delta function by itself as below,

$$-\Delta\psi = \mu^2\psi - \beta f(\psi, \partial_x\psi)\delta(x - x_r), \tag{4.50}$$

where $f(\psi, \partial_x\psi)$ is some appropriate function of ψ and $\partial_x\psi$ (in general, it also may be a function of even higher derivatives of ψ). Moreover, we expect ψ to determine not only the coefficient but also the position where the delta function has its value. Eventually, we anticipate that the nonlinear tearing mode may be given by the following type of equation:

$$-\Delta\psi = \mu^2\psi - \beta f(\psi, \partial_x\psi)\delta(\psi(\boldsymbol{x}) - \psi_0), \tag{4.51}$$

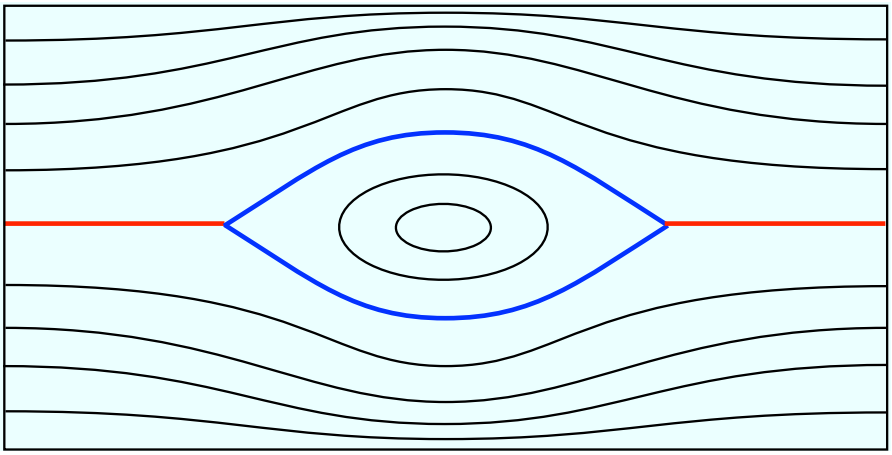

Figure 4.1: A cartoon of an anticipated nonlinear tearing mode.

where $\delta(\psi(\boldsymbol{x})-\psi_0)$ is a delta function that has its value at points where $\psi(\boldsymbol{x}) = \psi_0$.

What we want is a Casimir element such that its gradient gives the nonlinear delta function term $f(\psi, \partial_x\psi)\delta(\psi(\boldsymbol{x}) - \psi_0)$. In general, such a term may not be a member of the kernel of $\mathcal{J}_\psi(\psi) := \mathcal{J}_{13}(u) = [\psi, \circ]$. However, at the extremal of ψ where $\nabla\psi = 0$, $\mathcal{J}_\psi(\psi)$ is trivialized, i.e. $\mathcal{J}_\psi(\psi) = -\nabla\psi \times \nabla \circ \cdot\nabla\zeta = 0$. Therefore, if the coefficient $f(\psi, \partial_x\psi)$ is finite only at extremal, we can regard $\nabla\psi \times \nabla f(\psi, \partial_x\psi)\delta(\psi(\boldsymbol{x}) - \psi_0) = 0$. Fig.4.1 shows a cartoon of an anticipated nonlinear tearing mode. The red line indicates the position of extremal, where $\nabla\psi \times \nabla f(\psi, \partial_x\psi)\delta(\psi(\boldsymbol{x}) - \psi_0) = 0$ because of $\nabla\psi = 0$. On the blue line $\nabla\psi \neq 0$, here , we expect $f(\psi, \partial_x\psi) = 0$ so that $\nabla\psi \times \nabla f(\psi, \partial_x\psi)\delta(\psi(\boldsymbol{x}) - \psi_0) = 0$. Note that the connecting points of red and blue lines is the difficult problem. Although Fig.4.1 shows the T-shape connection, it may be actually the Y-shape connection. Fig.4.1 is just a cartoon.

4.4.2 Singular Casimir element producing Delta function term

Let us start by considering the following type of Casimir element[17], which has been introduced in Subsec.1.4.2,

$$C_G(\psi) := \int_\Omega G(\psi(\boldsymbol{x}))d\boldsymbol{x}, \tag{4.52}$$

where $G : \mathbb{R} \to \mathbb{R}$ is a Lipschitz continuous function. Then its gradient is given by $\tilde{\partial}_\psi C_G = g(\psi(\boldsymbol{x}))$, where $g := \tilde{\partial}_\xi G/$ is the Clarke gradient[16] of $G(\xi)$. When G has a "kink", a point where left-hand and right-hand derivative differ from each other, the resultant $g(\psi(\boldsymbol{x}))$ may no longer be a member of the domain of $\mathcal{J}_\psi(\psi) = [\psi, \circ]$. However, it is still a "hyperfunction solution" of $[\psi, \varphi] = 0$, since $\nabla g(\psi)$ is "parallel" to $\nabla\psi$.

Next, to generalize the above Casimir element, let us allow G to have a "step", that is, we consider the following functional

$$C_Y(\psi) := \int_\Omega Y(\psi(\boldsymbol{x}) - \psi_0)d\boldsymbol{x}, \tag{4.53}$$

where $Y(\psi - \psi_0)$ is the step function. Its gradient is formally given by the "delta function"

$$\partial_\psi C_Y(\psi) = \rho(\psi(\boldsymbol{x}) - \psi_0) := \frac{\delta(\boldsymbol{x} - \psi^{-1}(\psi_0))}{\boldsymbol{n} \cdot \nabla\psi}, \tag{4.54}$$

where $\delta(\boldsymbol{x} - \psi^{-1}(\psi_0))$ is defined as the two-dimensional delta function that has its value on the contour $\psi(\boldsymbol{x}) = \psi_0$, and $\boldsymbol{n}$ is the normal to the contour line $\psi(\boldsymbol{x}) = \psi_0$. We also regard this delta function $\rho(\psi(\boldsymbol{x}) - \psi_0)$ as a formal solution of $[\psi, \varphi] = 0$ in some hyperfunctional sense. Therefore, $C_Y(\psi)$ can be regarded as a Casimir element. It is, however, not the Casimir element we want because its gradient $\rho(\psi(\boldsymbol{x}) - \psi_0)$ has its value on the whole contour line $\psi = \psi_0$. We expect the delta function to have its value only on the extremal of ψ.

If the extremal line is "folded", the derivative there becomes multi-valued. To use this multi-valuedness, we introduce the following functionals

$$C_{fl}(\psi) := \int_\Omega f(\nabla\psi_l \cdot \nabla\psi_l) Y(\psi_l(\boldsymbol{x}) - \psi_0) d\boldsymbol{x}, \tag{4.55}$$

$$C_{fr}(\psi) := \int_\Omega f(\nabla\psi_r \cdot \nabla\psi_r) Y(\psi_r(\boldsymbol{x}) - \psi_0) d\boldsymbol{x}, \tag{4.56}$$

where $f : \mathbb{R} \to \mathbb{R}$ is a smooth function. ψ_l and ψ_r are basically identical with ψ but their derivatives at $x_0 = \psi^{-1}(\psi_0)$ (especially at the folded line) are differently defined. Let us see how to define their derivatives by using the one-dimensional example. First, we consider the case that ψ is 'folded' at x_0, as shown in Fig.4.2. We evaluate the derivative of ψ_l at x_0 by extending it from the left, as shown in Fig.4.3. In this one-dimensional example, this definition is equivalent to the left-hand derivative of ψ

$$\frac{d\psi_l}{dx}(x_0) := \lim_{\epsilon\to 0} \frac{d\psi}{dx}(x_0 - \epsilon). \tag{4.57}$$

In the same way, we evaluate the derivative of ψ_r by extending it from the right, which is, in the one-dimensional case, equivalent to the right-hand derivative

$$\frac{d\psi_r}{dx}(x_0) := \lim_{\epsilon\to 0} \frac{d\psi}{dx}(x_0 + \epsilon). \tag{4.58}$$

Next, we consider the case that ψ is smooth at $x_0 = \psi^{-1}(\psi_0)$, as shown in Fig.4.4. In this case, as Fig.4.5 shows, the extended ψ_l and ψ_r are equivalent to ψ, and therefore, $d\psi_l/dx = d\psi_r/dx = d\psi/dx$.

Eventually, the singular Casimir we want is constructed by taking difference between C_{fl} and C_{fr}, that is,

$$C_{fs}(\psi) := C_{fr}(\psi) - C_{fl}(\psi). \tag{4.59}$$

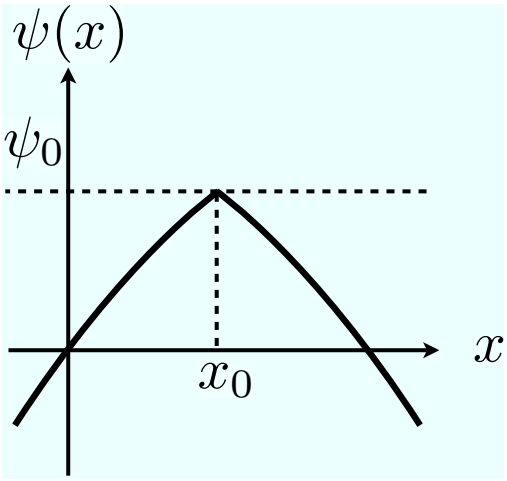

Figure 4.2: Magnetic flux function ψ with a folded extremal at x_0.

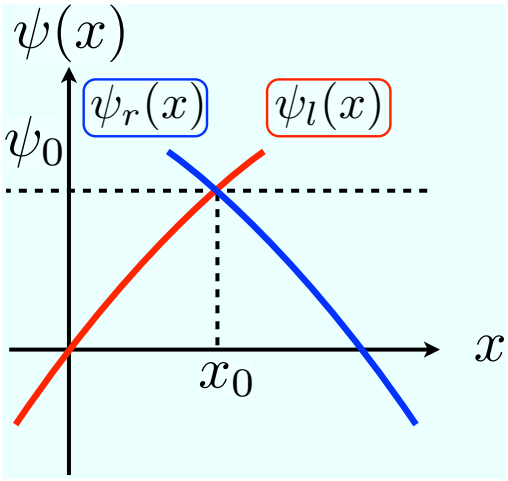

Figure 4.3: Left magnetic flux function ψ_l and Right magnetic flux function ψ_r.

To obtain the gradient of C_{fs}, first we calculate the variation of C_{fl} as follows:

$$
\begin{aligned}
& C_{fl}(\psi+\delta\psi) - C_{fl}(\psi) \\
= & \int_\Omega \Big[f(\nabla(\psi_l+\delta\psi)\cdot\nabla(\psi_l+\delta\psi)) Y(\psi_l+\delta\psi-\psi_0) \\
& \quad - f(\nabla\psi_l\cdot\nabla\psi_l) Y(\psi_l(\boldsymbol{x})-\psi_0) \Big] d\boldsymbol{x} \\
= & \int_\Omega \Big[f(\nabla\psi_l\cdot\nabla\psi_l)\big\{ Y(\psi_l+\delta\psi-\psi_0) - Y(\psi_l(\boldsymbol{x})-\psi_0)\big\} \\
& \quad + 2f'(\nabla\psi_l\cdot\nabla\psi_l)\nabla\delta\psi\cdot\nabla\psi_l Y(\psi_l(\boldsymbol{x})-\psi_0) + \mathcal{O}((\delta\psi)^2) \Big] d\boldsymbol{x} \\
= & \int_\Omega \Big[f(\nabla\psi_l\cdot\nabla\psi_l)\rho(\psi_l(\boldsymbol{x})-\psi_0)\delta\psi \\
& \quad - \nabla\cdot\big\{ 2f'(\nabla\psi_l\cdot\nabla\psi_l)\nabla\psi_l Y(\psi_l(\boldsymbol{x})-\psi_0)\big\}\delta\psi + \mathcal{O}((\delta\psi)^2) \Big] d\boldsymbol{x} \\
= & \int_\Omega \Big[f(\nabla\psi_l\cdot\nabla\psi_l)\rho(\psi_l(\boldsymbol{x})-\psi_0)\delta\psi - 2f'(\nabla\psi_l\cdot\nabla\psi_l)\nabla Y(\psi_l(\boldsymbol{x})-\psi_0)\cdot\nabla\psi_l\delta\psi \\
& \quad - \nabla\cdot\big\{ 2f'(\nabla\psi_l\cdot\nabla\psi_l)\nabla\psi_l\big\} Y(\psi_l(\boldsymbol{x})-\psi_0)\delta\psi + \mathcal{O}((\delta\psi)^2) \Big] d\boldsymbol{x} \\
= & \int_\Omega \Big[\big\{ f(\nabla\psi_l\cdot\nabla\psi_l) - 2f'(\nabla\psi_l\cdot\nabla\psi_l)\nabla\psi_l\cdot\nabla\psi_l\big\}\rho(\psi_l(\boldsymbol{x})-\psi_0)\delta\psi \\
& \quad - \nabla\cdot\big\{ 2f'(\nabla\psi_l\cdot\nabla\psi_l)\nabla\psi_l\big\} Y(\psi_l(\boldsymbol{x})-\psi_0)\delta\psi + \mathcal{O}((\delta\psi)^2) \Big] d\boldsymbol{x} \\
= & \int_\Omega \big\{ f(\nabla\psi_l\cdot\nabla\psi_l) - 2f'(\nabla\psi_l\cdot\nabla\psi_l)\nabla\psi_l\cdot\nabla\psi_l\big\}\rho(\psi_l(\boldsymbol{x})-\psi_0)\delta\psi d\boldsymbol{x} \\
& - \int_{\Omega_{\psi 0}} \nabla\cdot\big\{ 2f'(\nabla\psi\cdot\nabla\psi)\nabla\psi\big\}\delta\psi d\boldsymbol{x} + \mathcal{O}((\delta\psi)^2).
\end{aligned}
\tag{4.60}
$$

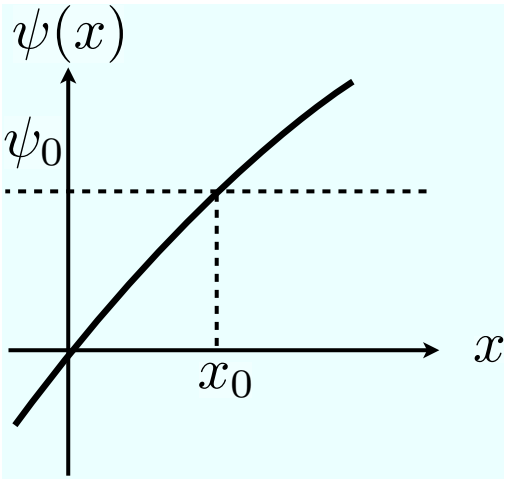

Figure 4.4: Magnetic flux function ψ being smooth at x_0.

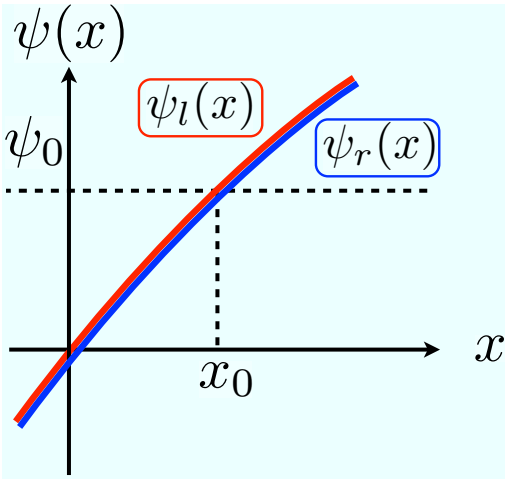

Figure 4.5: Left magnetic flux function ψ_l equals to Right magnetic flux function ψ_r.

$\Omega_{\psi 0}$ is the region where $\psi(\boldsymbol{x}) > \psi_0$ and therefore the derivatives of ψ_l and ψ_r are equivalent to that of ψ (remember that we distinguish ψ_l and ψ_r only by the difference bewteen their derivatives at $x_0 = \psi^{-1}(\psi_0)$). The third equality follows from the formal calculation

$$Y(\psi_l + \delta\psi - \psi_0) - Y(\psi_l(\boldsymbol{x}) - \psi_0) = \rho(\psi_l(\boldsymbol{x}) - \psi_0)\delta\psi + \mathcal{O}((\delta\psi)^2), \tag{4.61}$$

and the Stokes' theorem (note that $\delta\psi = 0$ on the boundary). In the fifth equality, we formally calculated $\nabla Y(\psi_l(\boldsymbol{x}) - \psi_0) = \rho(\psi_l(\boldsymbol{x}) - \psi_0)\nabla\psi_l$. In the same way, we calculate the variation of $C_{fr}(\psi)$ as

$$\begin{aligned} & C_{fr}(\psi + \delta\psi) - C_{fr}(\psi) \\ = & \int_\Omega \left\{ f(\nabla\psi_r \cdot \nabla\psi_r) - 2f'(\nabla\psi_r \cdot \nabla\psi_r)\nabla\psi_r \cdot \nabla\psi_r \right\} \rho(\psi_l(\boldsymbol{x}) - \psi_0)\delta\psi d\boldsymbol{x} \\ & - \int_{\Omega_{\psi 0}} \nabla \cdot \left\{ 2f'(\nabla\psi \cdot \nabla\psi)\nabla\psi \right\} \delta\psi d\boldsymbol{x} + \mathcal{O}((\delta\psi)^2). \end{aligned} \tag{4.62}$$

Subtracting (4.60) from (4.62), we obtain the variation of C_{fs}

$$\begin{aligned} & C_{fs}(\psi+\delta\psi) - C_{fs}(\psi) \\ = \; & \Big\langle \big\{ f(\nabla\psi_r\cdot\nabla\psi_r) - 2f'(\nabla\psi_r\cdot\nabla\psi_r)\nabla\psi_r\cdot\nabla\psi_r \big\}\rho(\psi_r(\boldsymbol{x})-\psi_0), \delta\psi \Big\rangle \\ & -\Big\langle \big\{ f(\nabla\psi_l\cdot\nabla\psi_l) - 2f'(\nabla\psi_l\cdot\nabla\psi_l)\nabla\psi_l\cdot\nabla\psi_l \big\}\rho(\psi_l(\boldsymbol{x})-\psi_0), \delta\psi \Big\rangle \\ & +\mathcal{O}((\delta\psi)^2), \end{aligned} \tag{4.63}$$

and therefore, the gradient of C_{fs} is given by

$$\begin{aligned} \partial_\psi C_{fs} &= -\Big[\Big[\big\{ f(\nabla\psi\cdot\nabla\psi) - 2f'(\nabla\psi\cdot\nabla\psi)\nabla\psi\cdot\nabla\psi \big\}\rho(\psi(\boldsymbol{x})-\psi_0)\Big]\Big] \\ &= -\left[\left[\frac{f(\nabla\psi\cdot\nabla\psi) - 2f'(\nabla\psi\cdot\nabla\psi)\nabla\psi\cdot\nabla\psi}{\boldsymbol{n}\cdot\nabla\psi}\right]\right]\delta(\boldsymbol{x}-\psi^{-1}(\psi_0)), \end{aligned} \tag{4.64}$$

where $[[g(\psi)]] := g(\psi_l) - g(\psi_r)$ and the second equality follows from (4.54). Obviously, the coefficient of this delta function term has finite value on the folded extremal line, where current sheet emerges (red lines in Fig.4.1), and becomes zero on the smooth line, corresponding to the edge of the island (blue line in Fig.4.1).

4.4.3 Singular Casimir element and Nonlinear tearing mode

Adding (4.59) to (4.26), we obtain a new energy-Casimir functional

$$\mathcal{F}_{\mu,\beta,f}(u) := \mathcal{H}(u) - \mu C_1(u) - \beta C_{fs}(u). \tag{4.65}$$

We can find equilibrium points by

$$\partial_u \mathcal{F}_{\mu,\beta,f}(u) = \partial_u\big[\mathcal{H}(u) - \mu C_1(u) - \beta C_{fs}(u)\big] = 0. \tag{4.66}$$

Note that $j = -\Delta\psi$ may include a delta function component. For convenience, we rewrite the term related to $j\psi$ as

$$\int_\Omega j\psi d\boldsymbol{x} = \int_\Omega \nabla\psi\cdot\nabla\psi d\boldsymbol{x} = \int_{\Omega\setminus\Gamma_{\psi_0}} j\psi d\boldsymbol{x} - \int_{\Gamma_{\psi_0}} [[\boldsymbol{n}\cdot\nabla\psi]]\psi dS, \tag{4.67}$$

where Γ_{ψ_0} is the line along which $\psi(\boldsymbol{x}) = \psi_0$. Then, we obtain the Euler-Lagrange equations in the following form: the Helmholtz equation

$$-\Delta\psi = \mu^2\psi \quad (\text{in } \Omega\backslash\Gamma_{\psi_0}), \tag{4.68}$$

and a Neumann type boundary condition

$$[[\boldsymbol{n}\cdot\nabla\psi]] = \beta\left[\left[\frac{f(\nabla\psi\cdot\nabla\psi) - 2f'(\nabla\psi\cdot\nabla\psi)\nabla\psi\cdot\nabla\psi}{\boldsymbol{n}\cdot\nabla\psi}\right]\right] \quad (\text{on } \Gamma_{\psi_0}). \tag{4.69}$$

This nonstandard boundary condition on Γ_{ψ_0} allows ψ to have folding lines, on which the singular current may emerge. Note that the boundary Γ_{ψ_0} is determined by ψ itself, which brings an additional Dirichlet type boundary condition

$$\psi = \psi_0 \quad (\text{on } \Gamma_{\psi_0}). \tag{4.70}$$

Note that the coexistence of boundary conditions (4.69) and (4.70) basically overdetermines the solution ψ. We solve this nonstandard boundary condition problem in two steps: first, we solve the Helmholtz equation (4.68) with the Dirichlet type boundary condition (4.70), then, we check whether or not it satisfies the Neumann type boundary condition (4.69).

In what follows, to examine what kind of solution there are, let us investigate specific cases of $f(\zeta) = 1$ and $f(\zeta) = \zeta$.

For $f(\zeta) = 1$, the boundary condition (4.69) becomes

$$[[\boldsymbol{n}\cdot\nabla\psi]] = \beta\Big[\Big[\frac{1}{\boldsymbol{n}\cdot\nabla\psi}\Big]\Big], \tag{4.71}$$

which may be written as

$$\{(\boldsymbol{n}\cdot\nabla\psi_l)(\boldsymbol{n}\cdot\nabla\psi_r) + \beta\}\,(\boldsymbol{n}\cdot\nabla\psi_l - \boldsymbol{n}\cdot\nabla\psi_r) = 0. \tag{4.72}$$

This condition demands that ψ is continuous on the contour line of $\psi = \psi_0$ or that the value of $(\boldsymbol{n} \cdot \nabla\psi_l)(\boldsymbol{n} \cdot \nabla\psi_r)$ is constant along the line $\psi = \psi_0$. Such a condition excludes the nonlinear tearing mode, like that shown in Fig.4.1, from the solution, because along the current sheet (red line in Fig.4.1) $(\boldsymbol{n} \cdot \nabla\psi_l)(\boldsymbol{n} \cdot \nabla\psi_r)$ may not be constant. However, we can obtain a symmetric current sheet solution with current sheet on $x = constant$ and without islands. For such a solution, $(\boldsymbol{n} \cdot \nabla\psi_l)(\boldsymbol{n} \cdot \nabla\psi_r)$ is constant along the current sheet because of its symmetry.

From the above example of $f(\zeta) = 1$, it is guessed that the solutions of this overdetermined system is considerably restricted and, in general, it does not have the nonlinear tearing mode solution. However, in the case of $f(\zeta) = \zeta$, the situation is totally different. In this case, the boundary condition (4.69) becomes

$$[[\boldsymbol{n} \cdot \nabla\psi]] = -\beta\Big[\Big[\frac{\nabla\psi \cdot \nabla\psi}{\boldsymbol{n} \cdot \nabla\psi}\Big]\Big] = -\beta[[\boldsymbol{n} \cdot \nabla\psi]]. \tag{4.73}$$

This condition holds only if $\beta = -1$ and, conversely, $\beta = -1$ trivializes this condition. Namely, in the case of $f(\zeta) = \zeta$, the Neumann type boundary condition (4.69) virtually disappears, and we can obtain the solution by solving the Helmholtz equation (4.68) under the Dirichlet type boundary condition (4.70). Fig.4.6 shows the cartoon of the symmetric nonlinear tearing mode solution which may be obtained by solving the above system (only the upper half region is described).

4.5 Summary and Discussion

We have formulated, by using stream and magnetic flux functions, the Hamiltonian formalism of the incompressible MHD with two independent variables and three dimensional vector fields. Then, we have rewrite the linear tearing mode theory[15] by using the above formalism. As a result, it has turned out to be

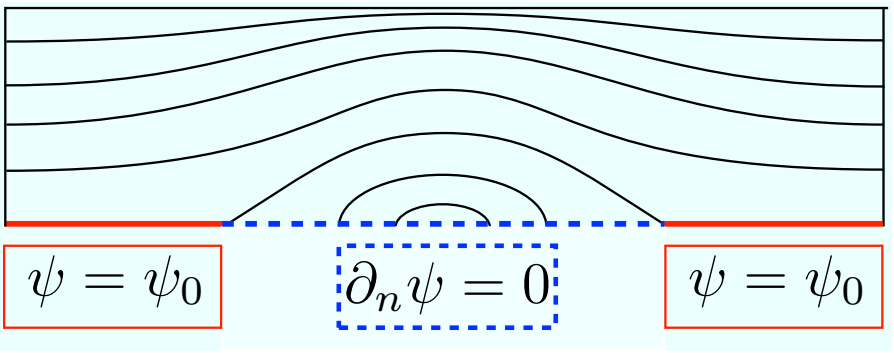

Figure 4.6: Cartoon of the symmetric nonlinear tearing mode on the upper half region.

that the resonance singularity $\boldsymbol{B}_\mu \cdot \boldsymbol{k} = 0$ is nothing but the extremal singularity $\nabla\psi_\mu = 0$.

In the linear theory, the singular Casimir element, obtained from the extremal singularity, produces the delta function term in the Euler-Lagrange equation, which allows an equilibrium solution to have the singular current. The problem of the linear theory is that the singular current exist even in the island of the tearing mode. To find a nonlinear, singular Casimir element that gives the singular current only on the extremal line of ψ, we have develop the notion of extremal singularity, extending the notion of plateau singularity. First, we have considered the Casimir element $C_Y(\psi)$ the integrand of which is given by $Y(\psi(\boldsymbol{x}) - \psi_0)$, where Y is the step function (see (4.53)). The gradient of $C_Y(\psi)$ is formally a member of the Poisson operator of the system. However, the delta function included in this gradient has its value not only on the extremal line of ψ but also on the edge of the island.

To obtain an appropriate singular Casimir element, we have to consider the speciality of the extremal line of ψ. Although we regard the value of $\nabla\psi$ on the

extremal line is zero (because the extremal singularity demands $[\psi, \circ] := \nabla\psi \times \nabla \circ \cdot\nabla\zeta = 0$), if the extremal line folds, we can also consider the left- and right-side derivatives of ψ from both sides of the extremal line $\psi = \psi_0$. To use this speciality on the "folded" extremal line, where the singular current emerges, we introduced the functionals C_{fl} (4.55) and C_{fr} (4.56), which are basically same functionals, but the gradient of them are differently defined by using the difference between left- and right-hand derivative of ψ. We have proposed the singular Casimir element C_{fs} (4.59) given by the difference of C_{fl} and C_{fr}, which detects the folding line on the contour of $\psi = \psi_0$. The gradient of C_{fs} (4.64) gives the delta function term that has a finite amplitude only on such a folded extremal line. The function f included in the definition of C_{fs} is arbitrary, which represents the fact that, on the extremal line, the operator $[\psi, \circ]$ is trivialized and, therefore, the gradient of C_{fs} can take arbitrary form there.

Using the above singular Casimir element, we have constructed the energy-Casimir functional $\mathcal{H} - \mu C_1 - \beta C_{fs}$, where C_1 is the magnetic helicity. The Euler-Lagrange equations of this functional gives the Helmholtz equation (4.68) with "nonstandard" boundary conditions (4.69) and (4.70). The word "nonstandard" means (1) the boundary (resonance surface) is determined by the solution itself and (2) both of the Neumann type and Dirichlet type boundary conditions are imposed on the same line. In terms of (2), this system is basically overdetermined. Therefore, although by choosing an appropriate β we can obtain the solution like the symmetric current sheet solution without island, in general, the nonlinear tearing mode solution may not be obtained. However, when we set $f(\zeta) = \zeta$, the situation drastically changes. In this special case, by choosing $\beta = -1$, the Neumann type boundary solution is removed, which allows the nonlinear tearing

mode solution with islands.

Chapter 5

Conclusion

At the beginning of the thesis, a question has been raised: How can we capture the identity of the vortex? This abstract question has been put into the context of the tearing mode theory and concretized as (1) Is there a Casimir element that characterizes the tearing mode with an ambient flow and (2) What kind of Casimir element characterizes the nonlinear tearing mode?

In Chap.2, in preparation for the theory of the tearing mode with flow, the bifurcation theory of double-Beltrami fields has been developed. It is Casimir elements and eigenvalues of the curl operator $\mathcal{S}$ that determines the bifurcation structure of double Beltrami fields. Namely, the magnetic and canonical helicities play the role of control parameters, and the magnetic and canonical fluxes work as the fixed parameters. Besides, bifurcation may occur at eigenvalues of the curl operator $\mathcal{S}$, if the geometry has symmetry.

In Sec.2.1, the sufficient and necessary condition of bifurcation has been proved in (Theorem 2 and Theorem 3), by which we can know what eigenvalue of $\mathcal{S}$ gives a bifurcation point. In Sec.2.2, a concrete example of bifurcation has been given, in a slab geometry. Fig.2.1 shows the magnetic and canonical helicity leaves projected onto the Beltrami parameter plane μ_1-μ_2. These leaves are "ripped" along the line where the orthogonality condition, given in Theorem 2 or Theorem 3, breaks down. On the rips, the helicity values diverge and the double-Beltrami fields

does not exist, as expected from Theorem 2 and Theorem 3. These rips basically due to the fixed fluxes. Namely, the motion is restricted onto the flux leaves and, on these flux leaves, the helicity leaves deform drastically. In this geometry, the symmetric double-Beltrami field gives the trunk solution, which is helically deformed by superposition of the helical solutions emerging from bifurcation points (eigenfunctions of $\mathcal{S}$), as shown in Fig.2.3.

In Chap.3, the linear theory of the tearing mode with flow has been developed on the framework of non-canonical Hamiltonian mechanics.

In Sec.3.1, it has been found that, even in the case of double-Beltrami fields and in the presence of an ambient flow, the tearing mode can be characterized as an equilibrium point only by the helical-flux Casimir element, which is surprisingly the same Casimir element characterizing the tearing mode without flow[15]. However, there is, of course, a difference between previous and present tearing modes. In the previous theory, the tearing mode is given by a singular eigenfunction of the curl operator $\mathcal{S}$. On the other hand, in the present theory, the tearing mode is given by superposition of two singular eigenfunctions. This difference is caused by the difference between the energy-Casimir functionals of single-Beltrami fields and double-Beltrami fields. The energy-Casimir functional of double-Beltrami fields includes the canonical helicity, in addition to the magnetic helicity which is included also in the energy-Casimir functional of single-Beltrami fields. It is this newly added Casimir element that has changed the structure of the tearing mode. Namely, the flow effect on the tearing mode is embedded in the canonical helicity characterizing the ambient flow fields. The standard criterion of the tearing instability Δ' has been shown to be directly related to the linearized energy-Casimir

functional U_{μ_1,μ_2} (3.17) through the equation $U_{\mu_1,\mu_2} = -(L_y L_z/2)\psi(x_r)^2\Delta'$.

In Sec.3.2, it has been examined how the sign of U_{μ_1,μ_2} changes depending on the values of Beltrami parameters μ_1 and μ_2, in the parameter region such that $\mu_1 + \mu_2 \sim 0$, $\mu_1 \sim \mathcal{O}(1)$, and $\mu_2 \sim \mathcal{O}(1)$. On the line $\mu_1 + \mu_2 = 0$, where both Beltrami parameters have the same amplitude $\mu = \mu_1 = |\mu_2|$ and the situation is close to that of single-Beltrami fileds, it has been observed that the tearing mode has positive energy for $\mu < \lambda_1$, where λ_1 is the smallest eigenvalue of $\mathcal{S}$, and gains negative energy as soon as μ exceeds λ_1. This result is consistent with that of [15]. It is the smallest eigenvalue of the curl operator that determines the tearing instability on this line $\mu_1 + \mu_2 = 0$. In Appendix B, the Lyapunov stability in the range $0 < \mu < \lambda_1$ is also proved for some specific case. However, in the region out of the line $\mu_1 + \mu_2 = 0$, the energy of the tearing mode U_{μ_1,μ_2} behaves complicatedly as shown in Fig.3.1. There are three lines separating positive and negative regions: the straight lines $\mu_1 = \lambda_1$ and $\mu_2 = -\lambda_1$ and the curved line. This curved line may be related to the border separating the region where the tearing instability is dominant and the region where the Kelvin-Helmholtz instability is dominant. In fact, as shown in Fig.3.5, in the ideal limit $\delta_i \to 0$ (δ_i is the ion-skin length), the curved line approaches the border between sub- and super-Alfvénic shear flow regimes (in the presence of super-Alfvénic shear flow, the tearing instability disappears and, instead, the Kelvin-Helmholtz instability becomes dominant[40, 41]).

In Chap.4, the notion of extremal singularity has been developed and applied to the nonlinear tearing mode theory. In Sec.4.2, the Hamiltonian formalism of the incompressible MHD, with two independent variables and three dimensional vector fields, has been formulated in terms of the stream and magnetic flux func-

tions ϕ and ψ. Then, in Sec.4.3, the relation between the resonance singularity $\boldsymbol{B}_\mu \cdot \boldsymbol{k} = 0$ and the extremal singularity $\nabla\psi_\mu = 0$ has been revealed.

In Sec.4.4, first, the Casimir element $C_Y(\psi)$ (4.53), the integrand of which is given by the step function $Y(\psi(\boldsymbol{x}) - \psi_0)$, has been considered. This Casimir element is the most natural generalization of the singular Casimir stemming from the plateau singularity, the integrand of which is given by the Lipschitz continuous but not smooth function. However, this newly considered Casimir element is not appropriate for the nonlinear tearing mode solution, because its gradient gives the delta function term that has its value even on the edge of island. For the nonlinear tearing mode, the delta function term is expected to have its value only on the "folded" extremal line of ψ, where the singular current emerges. Then, two functionals C_{fl} (4.55) and C_{fr} (4.56) have been introduced. They are basically same functionals, but the gradient of them are differently defined. The singular Casimir element C_{fs} (4.59) has been given by the difference of C_{fl} and C_{fr}. The gradient of C_{fs} gives the delta function that has its value only on the folding line of ψ. The Euler-Lagrange equations of the energy-Casimir functional $\mathcal{H} - \mu C_1 - \beta C_{fs}$ gives the Helmholtz equation (4.68) with the nonstandard boundary conditions: the Neumann type boundary condition (4.69) and the Dirichlet type boundary condition (4.70). The Neumann type boundary condition changes its form depending on the function f included in the definition of the singular Casimir element C_{fs}. Because these two boundary condition are imposed on the same line, this equation is basically overdetermined. However, with an appropriate choice of β, this system can have solutions. For example, in the case of $f(\zeta) = 1$, a symmetric singular current solution without islands is obtained. The case of $f(\zeta) = \zeta$ gives the special situation. In this case, for $\beta = -1$, the Neumann type boundary condition

is trivialized and disappears, which allows the nonlinear tearing mode solution with islands. Namely, $\beta = -1$ is the singularity of the Euler-Lagrange equations obtained from $\mathcal{H} - \mu C_1 - \beta C_{fs}$. (cf. an Alfvén wave in the ideal MHD is obtained as the Galilean-boosted Beltrami vortex, which stems from the singularity $\mu_2 = \pm 1$ of the Euler-Lagrange equation of $\mathcal{H} - \mu_1 C_1 - \mu_2 C_2$[11], see Subsec.1.3.2.)

In a theory of linear wave, a structure of a wave basically dues to a boundary condition, which is given from the outside. On the other hand, in the present theory, the boundary condition is given by the presence of the vortex itself, and at the same time, the boundary condition allows the vortex to exist as an equilibrium state. In that sense, the identity of the vortex is not the extrinsic one but the intrinsic. Therefore, it can be said that the vortex, which retains its identity for a long time once it makes its appearance, is the nonlinear, self-referential being that sustains its existence by being there.

Appendices

Appendix A

Singular kernel element of the plateau singularity

We consider the noncanonical symplectic operator

$$\mathcal{J}(\omega)\phi := \nabla\omega \times \nabla\phi \cdot \nabla z, \tag{A.1}$$

and the singular Casimir

$$C_G(\omega) := \int_\Omega G(\omega(\boldsymbol{x}))d\boldsymbol{x}, \quad G(\xi) := \begin{cases} 0 & (\xi \leq \omega_0) \\ \xi - \omega_0 & (\omega_0 < \xi) \end{cases}, \tag{A.2}$$

from which we obtain

$$\partial_\omega C_G(\omega) = g(\omega), \quad g(\xi) = \tilde{\partial}_\xi G = Y(\xi - \omega_0), \tag{A.3}$$

where $\tilde{\partial}_\xi$ is the Clarke gradient and $Y(\xi)$ is the filled step function.

For a singular point ω that has a plateau (or generally plateaus) on the region where $\omega(\boldsymbol{x}) = \omega_0$, we can choose a smooth $g(\omega) \in H^1(\Omega)$, therefore, the following equation is well-defined:

$$\mathcal{J}(\omega)\partial_\omega C_G(\omega) = \nabla\omega \times \nabla g \cdot \nabla z = 0. \tag{A.4}$$

If such a plateau shrinks into a line, $g(\omega)$ becomes

$$g(\omega(\boldsymbol{x})) = \begin{cases} 0 & (\boldsymbol{x} \in \Omega/\Omega_0) \\ 1 & (\boldsymbol{x} \in \Omega_0) \end{cases}, \tag{A.5}$$

where Ω_0 is the region where $\omega > \omega_0$, therefore, it becomes discontinuous on the line. For this g, ∇g may lose its meaning. However, we observe $\nabla\omega = 0$ on the

same line and thereby the equation (A.4) keeps its meaning on the whole. In the more general case that $\nabla\omega \neq 0$ on the region where $\omega = \omega_0$, we have to consider the equation (A.4) in $H^{-1}(\Omega)$, i.e., we consider the weak form:

$$(\nabla\omega \times \nabla g \cdot \nabla z, \phi) = 0 \quad \forall\phi \in H_0^1(\Omega). \tag{A.6}$$

We define the derivative of a distribution ∇f as follows:

$$(\nabla\omega \times \nabla f \cdot \nabla z, \phi) := (f, \nabla\phi \times \nabla\omega \cdot \nabla z). \tag{A.7}$$

Let us confirm that $g(\omega)$ defined as (A.5) satisfies the equation (A.6). Putting $g(\omega)$ into the left-hand side of (A.6), we obtain

$$\begin{aligned}
(\nabla\omega \times \nabla g \cdot \nabla z, \phi) &= (g, \nabla\phi \times \nabla\omega \cdot \nabla z) = \int_\Omega g\nabla\phi \times \nabla\omega \cdot \nabla z d\boldsymbol{x} \\
&= \int_{\Omega_0} \nabla\phi \times \nabla\omega \cdot \nabla z d\boldsymbol{x} = \int_{\Omega_0} \nabla \times (\phi\nabla\omega) \cdot \nabla z d\boldsymbol{x} \\
&= \int_{\partial\Omega_0} \phi\nabla\omega \cdot d\boldsymbol{l} = 0.
\end{aligned}$$

where the last equality follows because, from the definition of Ω_0, $\omega = \omega_0$ on the boundary $\partial\Omega_0$ and thereby $\nabla\omega \cdot d\boldsymbol{l} = 0$.

Summarizing the above discussions (and making an obvious generalization), we can say that the equation (A.4) holds as an equation in $H^{-1}(\Omega)$ for all $\omega \in C^{0,1}(\Omega)$.

Appendix B

Stability of double-Beltrami fields with longitudinal flow

If the coercivity condition

$$c\|\tilde{u}\|^2 \leq U_{\mu_1,\mu_2}(\tilde{u}) \tag{B.1}$$

holds (where c is a positive constant), the linearized energy-Casimir functional U_{μ_1,μ_2} plays the role of a Lyapunov function bounding the norm of $\tilde{u}$, i.e. the equilibrium u_{μ_1,μ_2} is stable[50]. In the case of single-Beltrami fields[15, 50], the Beltrami parameter μ smaller than the minimum eigenvalue of $\mathcal{S}$ guarantees the coercivity of its linearized energy-Casimir functional. On the other hand, in the case of double-Beltrami fields, the linearized energy-Casimir functional U_{μ_1,μ_2} does not satisfy the coercivity condition (B.1) because the highest order derivative term in the functional is not positive definite[45, 48, 51–53]. However, for a special class of flow proposed by Ohsaki et al.[48], we can construct a Lyapunov function, which guarantees the Lyapunov stability, by finding out an enstrophy order invariant.

In this appendix, we will improve the Lyapunov stability theory of double-Beltrami fields with 'longitudinal' flow[48].

B.1 Double Beltrami fields with longitudinal flow

In what follows, we consider perturbations depending only on $x, \eta = \bar{k}_y y + \bar{k}_z z$ and t. Then, using stream and flux functions, the perturbed fields $\tilde{\boldsymbol{B}}$ and $\tilde{\boldsymbol{V}}$

can be written in a Clebsch-like form

$$\tilde{\boldsymbol{B}} = \nabla\tilde{\psi}(x,\eta,t) \times \nabla\zeta + \tilde{B}_\zeta \nabla\zeta, \tag{B.2}$$

$$\tilde{\boldsymbol{V}} = \nabla\tilde{\phi}(x,\eta,t) \times \nabla\zeta + \tilde{V}_\zeta \nabla\zeta. \tag{B.3}$$

We can also rewritten the magnetic and flow fields $\boldsymbol{B}_{\mu_1,\mu_2}$ and $\boldsymbol{V}_{\mu_1,\mu_2}$ of the symmetric double-Beltrami equilibrium in the Clebsh-like form

$$\boldsymbol{B}_{\mu_1,\mu_2} = \nabla\psi_{\mu_1,\mu_2} \times \nabla\zeta + B_{\zeta,\mu_1,\mu_2}\nabla\zeta \tag{B.4}$$

$$\boldsymbol{V}_{\mu_1,\mu_2} = \nabla\phi_{\mu_1,\mu_2} \times \nabla\zeta + V_{\zeta,\mu_1,\mu_2}\nabla\zeta \tag{B.5}$$

Writing $\phi = \phi_{\mu_1,\mu_2} + \tilde{\phi}$, $\psi = \psi_{\mu_1,\mu_2} + \tilde{\psi}$, $V_\zeta = V_{\zeta,\mu_1,\mu_2} + \tilde{V}_\zeta$ and $B_\zeta = B_{\zeta,\mu_1,\mu_2} + \tilde{B}_\zeta$, (2.1) and (2.2) can be cast in a form of coupled nonlinear Liouville equations:

$$\begin{aligned}
\partial_t(-\Delta\phi) &= [-\Delta\psi, \phi] + [\psi, -\Delta\psi], && \text{(B.6)}\\
\partial_t V_z &= [V_z, \phi] + [\psi, B_z], && \text{(B.7)}\\
\partial_t \psi &= [\psi, \phi] - \delta_i[\psi, B_z], && \text{(B.8)}\\
\partial_t B_z &= [B_z, \phi] + [\psi, V_z] - \delta_i[\psi, \Delta\psi], && \text{(B.9)}
\end{aligned}$$

where $[f, g] := -\nabla f \times \nabla g \cdot \nabla\zeta$ is the standard Poisson bracket. Corresponding to (3.3),

$$G_0 = \|\nabla\tilde{\psi}\|^2 + \|\nabla\tilde{\psi}\|^2 + \|\tilde{B}_\zeta\|^2 + \|\tilde{V}_\zeta\|^2 - 2\nu_1\langle\tilde{\psi}, \tilde{B}_\zeta\rangle - 2\nu_2\langle\tilde{\psi} + \delta_i\tilde{V}_\zeta, \tilde{B}_\zeta - \delta_i\Delta\tilde{\phi}\rangle \tag{B.10}$$

is a constant of motion of the nonlinear equations (B.6)-(B.9) and its linearized equations.

Let us consider the case that the equilibrium flow $\boldsymbol{V}_{\mu_1,\mu_2}$ has only a longitudinal component, that is, $\phi_{\mu_1,\mu_2} = 0$. Using (2.30), (2.89) and (2.90), we can

show that the condition $\phi_{\mu_1,\mu_2} = 0$ holds when we set the Beltrami parameters and the magnetic and canonical fluxes as

$$\mu_1 + \mu_2 = 0, \quad \boldsymbol{\Omega}_{\mathbf{H}} \cdot \nabla\eta = 0, \quad (\boldsymbol{\Omega}_H - \boldsymbol{B}_H) \cdot \nabla\zeta = 0, \tag{B.11}$$

where the last equation also can be viewed as

$$\nabla \times \boldsymbol{V}^H \cdot \nabla\zeta = 0. \tag{B.12}$$

Here, we introduce μ and represent the Beltrami parameters as

$$\mu := \mu_1 = -\mu_2. \tag{B.13}$$

As shown in [48], in this special case, we can obtain an additional constants of motion

$$G_1 = \|\tilde{\psi} + \delta_i \tilde{V}_\zeta\|^2, \tag{B.14}$$

and

$$G_2 = \|\nabla(\tilde{\psi} + \delta_i \tilde{V}_\zeta)\|^2. \tag{B.15}$$

In [48], where δ_i is set to be unity, it is shown that we can construct a Lyapunov function, which guarantees the stability of the equilibrium, by combining the constants of motion G_0, G_1, and G_2 if the Beltrami parameter μ satisfy the following inequality

$$\mu^2 < \lambda_1^2 - 1, \tag{B.16}$$

where λ_1 is the smallest eigenvalue (in absolute value) of the curl operator $\mathcal{S}$. However, writing explicitly δ_i in the above inequality, we obtain

$$\mu^2 < \lambda_1^2 - \frac{1}{\delta_i^2}, \tag{B.17}$$

which is too strict condition, that is, the right-hand side of this inequality becomes negative for a small δ_i and there is no μ satisfying it.

B.2 Sufficient condition for Lyapunov stability

Here, by improving the estimation of inequality in [48], we will find a better stability condition. The most important point to improve the estimation of inequality is rewriting the constant of motion G_0, using (2.35), as

$$\begin{aligned} G_0 &= \|\nabla\tilde{\psi}\|^2 + \|\nabla\tilde{\phi}\|^2 + \|\tilde{B_\zeta}\|^2 + \|\tilde{V_\zeta}\|^2 \\ &\quad +2\delta_i^2\mu^2\nu_2\langle\tilde{\psi},\tilde{B_\zeta}\rangle - 2\nu_2\langle\delta_i\tilde{V_\zeta},\tilde{B_\zeta}\rangle - 2\nu_2\langle\tilde{\psi}+\delta_i\tilde{V_\zeta},-\delta_i\Delta\tilde{\phi}\rangle. \end{aligned} \tag{B.18}$$

Then, using

$$\langle\tilde{\psi},\tilde{B_\zeta}\rangle \le \frac{1}{\alpha_1}\|\tilde{\psi}\|^2 + \alpha_1\|\tilde{B_\zeta}\|^2 \quad (\forall\alpha_2>0), \tag{B.19}$$

$$\langle\delta_i\tilde{V_\zeta},\tilde{B_\zeta}\rangle \le \frac{\delta_i^2}{\alpha_2}\|\tilde{V_\zeta}\|^2 + \alpha_2\|\tilde{B_\zeta}\|^2 \quad (\forall\alpha_2>0), \tag{B.20}$$

$$\langle\tilde{\psi}+\delta_i\tilde{V_\zeta},-\delta_i\Delta\tilde{\phi}\rangle \le \frac{1}{\alpha_3}\|\nabla(\tilde{\psi}+\delta_i\tilde{V_\zeta})\|^2 + \delta_i^2\alpha_3\|\nabla\tilde{\phi}\|^2 \quad (\forall\alpha_3>0), \tag{B.21}$$

we observe

$$\begin{aligned} G_0 \ge\ & \|\nabla\tilde{\psi}\|^2 + \|\nabla\tilde{\phi}\|^2 + \|\tilde{B_\zeta}\|^2 + \|\tilde{V_\zeta}\|^2 - \delta_i^2\mu^2|\nu_2|\left(\frac{1}{\alpha_1}\|\tilde{\psi}\|^2 + \alpha_1\|\tilde{B_\zeta}\|^2\right) \\ & -|\nu_2|\left(\frac{\delta_i^2}{\alpha_2}\|\tilde{V_\zeta}\|^2 + \alpha_2\|\tilde{B_\zeta}\|^2\right) - |\nu_2|\left(\frac{1}{\alpha_3}\|\nabla(\tilde{\psi}+\delta_i\tilde{V_\zeta})\|^2 + \delta_i^2\alpha_3\|\nabla\tilde{\phi}\|^2\right). \end{aligned} \tag{B.22}$$

In a bounded domain, we have the following Poincaré-type inequality

$$\|\nabla\tilde{\psi}\|^2 \ge \lambda_1^2\|\tilde{\psi}\|^2. \tag{B.23}$$

Using (B.15) and (B.23), we can rearrange (B.22) to

$$\begin{aligned} G_0 + \frac{|\nu_2|}{\alpha_3}G_2 \ge\ & \left(1 - \frac{\delta_i^2\mu^2|\nu_2|}{\alpha_1\lambda_1^2}\right)\|\nabla\tilde{\psi}\|^2 + \left(1-\delta_i^2|\nu_2|\alpha_3\right)\|\nabla\tilde{\phi}\|^2 \\ & + \left(1-\delta_i^2\mu^2|\nu_2|\alpha_1 - |\nu_2|\alpha_2\right)\|\tilde{B_\zeta}\|^2 + \left(1-\frac{\delta_i^2|\nu_2|}{\alpha_2}\right)\|\tilde{V_\zeta}\|^2. \end{aligned} \tag{B.24}$$

If all the coefficients of the right-hand side of (B.24) are positive, the left-hand side of (B.24) works as a Lyapunov function bounding the energy associated with the magnetic and flow fluctuations. To make the first, second, and fourth coefficients positive, we must choose α_1, α_2 and α_3 as

$$\alpha_1 > \frac{\delta_i^2 \mu^2 |\nu_2|}{\lambda_1^2}, \quad \alpha_2 > \delta_i^2 |\nu_2|, \quad 0 < \alpha_3 < \frac{1}{\delta_i^2 |\nu_2|}. \tag{B.25}$$

Using (B.25), we can estimate the third coefficient as

$$1 - \delta_i^2 \mu^2 |\nu_2| \alpha_1 - |\nu_2| \alpha_2 > 1 - \frac{\delta_i^4 \mu^4 |\nu_2|^2}{\lambda_1^2} - \delta_i^2 |\nu_2|^2 = \frac{\delta_i^2 \mu^2}{\lambda_1^2 (\delta_1^2 \mu^2 + 1)} (\lambda_1^2 - \mu^2), \tag{B.26}$$

where the last equality follows from (2.34). Thereby, the sufficient condition for the Lyapunov stability can be written as

$$\mu^2 < \lambda_1^2, \tag{B.27}$$

which is improved by $-1/\delta_i^2$ compared to (B.17).

Bibliography

[1] Z. Yoshida and Y. Giga. Remarks on spectra of operator rot. *Mathematische Zeitschrift*, **204**:235–245, 1990.

[2] L. Woltjer. A theorem on force-free magnetic fields. *Proceedings of the National Academy of Sciences*, **44**:489–491, 1958.

[3] J. B. Taylor. Relaxation of toroidal plasma and generation of reverse magnetic fields. *Physical Review Letters*, **33**:1139–1141, 1974.

[4] J. B. Taylor. Relaxation and magnetic reconnection in plasmas. *Reviews of Modern Physics*, **58**:741–763, 1986.

[5] S. M. Mahajan and Z. Yoshida. Double curl beltrami flow: Diamagnetic structures. *Physical Review Letters*, **81**:4863–4866, 1998.

[6] Z. Yoshida and S. M. Mahajan. Simultaneous beltrami conditions in coupled vortex dynamics. *Journal of Mathematical Physics*, **40**:5080–5091, 1999.

[7] Z. Yoshida, S. M. Mahajan, S. Ohsaki, M. Iqbal, and N. Shatashvili. Beltrami fields in plasmas: High-confinement mode boundary layers and high beta equilibria. *Physics of Plasmas*, **8**:2125–2131, 2001.

[8] S. Ohsaki, N. L. Shatashvili, Z. Yoshida, and S. M. Mahajan. Magnetofluid coupling: Eruptive events in the solar corona. *The Astrophysical Journal*, **559**:L61–L65, 2001.

[9] S. Ohsaki, N. L. Shatashvili, Z. Yoshida, and S. M. Mahajan. Energy transformation mechanism in the solar atmosphere associated with magnetofluid coupling: Explosive and eruptive events. *The Astrophysical Journal*, **570**:395–407, 2002.

[10] D. Kagan and S. M. Mahajan. Application of double beltrami states to solar eruptions. *Monthly Notices of the Royal Astronomical Society*, **406**:11401145, 2010.

[11] Z. Yoshida. Nonlinear Alfvn/Beltrami waves—An integrable structure built around the casimir. *Communications in Nonlinear Science and Numerical Simulation*, **17**:2223–2232, 2012.

[12] S. Emoto and Z. Yoshida. Irregular modulation of non-linear Alfvn/Beltrami wave coupled with an ion-sound wave. *Communications in Nonlinear Science and Numerical Simulation*, **19**:53–59, 2014.

[13] P. J. Morrison. Hamiltonian description of the ideal fluid. *Reviews of Modern Physics*, **70**:467–521, 1998.

[14] H. P. Furth, J. Killeen, and M. N. Rosenbluth. Finite - Resistivity instabilities of a sheet pinch. *Physics of Fluids*, **6**:459–484, 1963.

[15] Z. Yoshida and R. L. Dewar. Helical bifurcation and tearing mode in a plasma—a description based on casimir foliation. *Journal of Physics A: Mathematical and Theoretical*, **45**:365502, 2012.

[16] F. H. Clarke. Generalized gradients and applications. *Transactions of the American Mathematical Society*, **205**:247–262, 1975.

[17] Z. Yoshida, P. J. Morrison, and F. Dobarro. Singular casimir elements of the euler equation and equilibrium points. *Journal of Mathematical Fluid Mechanics*, pages 1–17, 2013.

[18] E. Hameiri. The complete set of casimir constants of the motion in magnetohydrodynamics. *Physics of Plasmas*, **11**:3423–3431, 2004.

[19] Y. Kawazura and E. Hameiri. The complete set of casimirs in hall-magnetohydrodynamics. *Physics of Plasmas*, **19**:082513–082513–7, 2012.

[20] Z. Yoshida and E. Hameiri. Canonical hamiltonian mechanics of hall magnetohydrodynamics and its limit to ideal magnetohydrodynamics. *Journal of Physics A: Mathematical and Theoretical*, **46**:335502, 2013.

[21] Z. Yoshida. Singular casimir elements: Their mathematical justification and physical implications. *Procedia IUTAM*, **7**:141–150, 2013.

[22] D. Biskamp. *Magnetic Reconnection in Plasmas*. Cambridge University Press, 2005. ISBN 9780521020367.

[23] M. Yamada, R. Kulsrud, and H. Ji. Magnetic reconnection. *Reviews of Modern Physics*, **82**:603–664, 2010.

[24] Z. Yoshida and S. Mahajan. Perturbation theory for the alfven wave. *International Journal of Modern Physics B*, **9**:2857–2898, 1995.

[25] P. H. Rutherford. Nonlinear growth of the tearing mode. *Physics of Fluids*, **16**:1903–1908, 1973.

[26] R. B. White, D. A. Monticello, M. N. Rosenbluth, and B. V. Waddell. Saturation of the tearing mode. *Physics of Fluids (1958-1988)*, **20**:800–805, 1977.

[27] T. S. Hahm and R. M. Kulsrud. Forced magnetic reconnection. *Physics of Fluids*, **28**:2412–2418, 1985.

[28] R. L. Dewar, A. Bhattacharjee, R. M. Kulsrud, and A. M. Wright. Plasmoid solutions of the HahmKulsrudTaylor equilibrium model. *Physics of Plasmas*, **20**:082103–082103–7, 2013.

[29] X. L. Chen and P. J. Morrison. Resistive tearing instability with equilibrium shear flow. *Physics of Fluids B: Plasma Physics (1989-1993)*, **2**:495–507, 1990.

[30] L. Ofman, P. J. Morrison, and R. S. Steinolfson. Nonlinear evolution of resistive tearing mode instability with shear flow and viscosity. *Physics of Fluids B: Plasma Physics (1989-1993)*, **5**:376–387, 1993.

[31] J. H. Li and Z. W. Ma. Nonlinear evolution of resistive tearing mode with sub-alfvenic shear flow. *Journal of Geophysical Research: Space Physics*, **115**:A09216, 2010.

[32] D. Chandra, A. Sen, P. Kaw, M. P. Bora, and S. Kruger. Effect of sheared flows on classical and neoclassical tearing modes. *Nuclear Fusion*, **45**:524, 2005.

[33] T. Terasawa. Hall current effect on tearing mode instability. *Geophysical Research Letters*, **10**:475478, 1983.

[34] A. Fruchtman and H. R. Strauss. Modification of short scale-length tearing modes by the hall field. *Physics of Fluids B: Plasma Physics*, **5**:1408, 1993.

[35] L. Ofman, X. L. Chen, P. J. Morrison, and R. S. Steinolfson. Resistive tearing mode instability with shear flow and viscosity. *Physics of Fluids B: Plasma Physics (1989-1993)*, **3**:1364–1373, 1991.

[36] R. Coelho and E. Lazzaro. Effect of sheared equilibrium plasma rotation on the classical tearing mode in a cylindrical geometry. *Physics of Plasmas*, **14**:012101, 2007.

[37] A. Sen, D. Chandra, and P. Kaw. Tearing mode stability in a toroidally flowing plasma. *Nuclear Fusion*, **53**:053006, 2013.

[38] R. J. La Haye, D. P. Brennan, R. J. Buttery, and S. P. Gerhardt. Islands in the stream: The effect of plasma flow on tearing stability. *Physics of Plasmas*, **17**:056110, 2010.

[39] Z. X. Liu and Y. D. Hu. Local magnetic reconnection caused by vortices in the flow field. *Geophysical Research Letters*, **15**:752755, 1988.

[40] Q. Chen, A. Otto, and L. C. Lee. Tearing instability, kelvin-helmholtz instability, and magnetic reconnection. *Journal of Geophysical Research: Space Physics*, **102**:151161, 1997.

[41] D. A. Knoll and L. Chacn. Magnetic reconnection in the two-dimensional kelvin-helmholtz instability. *Physical Review Letters*, **88**:215003–215003–4, 2002.

[42] J. H. Li and Z. W. Ma. Roles of super-alfvenic shear flows on KelvinHelmholtz and tearing instability in compressible plasma. *Physica Scripta*, **86**:045503, 2012.

[43] J. P. Goedbloed and S. Poedts. *Principles of Magnetohydrodynamics: With Applications to Laboratory and Astrophysical Plasmas*. Cambridge University Press, 2004. ISBN 9780521626071.

[44] Z. Yoshida, S. M. Mahajan, and S. Ohsaki. Scale hierarchy created in plasma flow. *Physics of Plasmas*, **11**:3660–3664, 2004.

[45] D. D. Holm. Hall magnetohydrodynamics: Conservation laws and lyapunov stability. *Physics of Fluids*, **30**:1310–1322, 1987.

[46] Z. Yoshida. Discrete eigenstates of plasmas described by the chandrasekharkendall functions. *Progress of Theoretical Physics*, **86**:45–55, 1991.

[47] Z. Yoshida. Eigenfunction expansions associated with the curl derivatives in cylindrical geometries: Completeness of ChandrasekharKendall eigenfunctions. *Journal of Mathematical Physics*, **33**:1252–1256, 1992.

[48] S. Ohsaki and Z. Yoshida. Lyapunov function of relaxed states in two-fluid plasmas: Stability of double-beltrami flows. *Physics of Plasmas*, **10**:3853–3857, 2003.

[49] A. Ito, Z. Yoshida, T. Tatsuno, S. Ohsaki, and S. M. Mahajan. Kelvin-Helmholtz instability in beltrami fields. *Physics of Plasmas*, **9**:4856–4862, 2002.

[50] Z. Yoshida, S. Ohsaki, A. Ito, and S. M. Mahajan. Stability of beltrami flows. *Journal of Mathematical Physics*, **44**:2168–2178, 2003.

[51] Z. Yoshida and S. M. Mahajan. Variational principles and self-organization in two-fluid plasmas. *Physical Review Letters*, **88**:095001, 2002.

[52] S. Ohsaki and Z. Yoshida. Variational principle with singular perturbation of hall magnetohydrodynamics. *Physics of Plasmas*, **12**:064505–064505–4, 2005.

[53] S. Ohsaki. Variational principle of hall magnetohydrodynamics. *Journal of Fusion Energy*, **26**:135–137, 2006.

Acknowledgments

I would like to express my deepest gratitude to my supervisor Professor Zensho Yoshida. I came to this laboratory with interest in self-organization phenomena but no idea how to deal with this subject. He taught me how to view the world from the perspective of physics and gave me an interesting motif of vortex. Recently, I am interested in vortex not only in terms of physics but also of philosophy, folklore, or cognitive science. So, the vortex will continue to be my motif even after my graduation.

I also thank Associate Professor Masaru Furukawa, Dr. Haruhiko Saito, and Associate Professor Masaki Nishiura. Before Associate Professor Furukawa went to Tottori University, he taught me the plasma physics and English. Before Mr. Saito went to Max Planck Institute, he always encouraged me. And after Associate Professor Nishiura came to our Lab, he encouraged me, too. Moreover they taught me a plasma viewed from experiments.

I am also grateful to Professor Robert Leith Dewar in Australian National University for helpful advices and discussions during his stay in our Lab. Moreover, he taught me about important papers of the tearing mode theory.

I appreciate Dr. Yoshihisa Yano and Dr. Yohei Kawazura. Dr. Yano is always in a calm way as senior member of our Lab, which relaxed me. Dr. Kawazura helped me in many problems, in many ways, and in many times. Without these helps, I could not have finished my thesis.

I express my thank to Ms. Kitayama. She always helped me do paperworks

and took care of me in my laboratory life. I also appreciate student members of our Lab. I was able to enjoy my student life due to conversations with them.

Finally, I express my sincere appreciation my parents, my sister, her husband, and relatives for their support and encouragement during my study.

Publications

[1] S. Emoto and Z. Yoshida:

"Irregular modulation of non-linear Alfvén/Beltrami wave coupled with an ion-sound wave"

Communications in Nonlinear Science and Numerical Simulation

Vol. 19, Issue 1, (2014) Pages 53-59.